Transtensional deformation of the western Moncton Sub-basin, southern New Brunswick

by

Jared Kugler

A thesis submitted in partial fulfillment of the requirements for the degree of

Master of Science

Department of Earth and Atmospheric Sciences

University of Alberta

Abstract

The Maritimes Basin of Atlantic Canada contains deformed late Paleozoic sedimentary rocks. Major dextral strike-slip deformation produced complex structural geometries and stratigraphic relationships. Large strike-slip faults separate smaller sub-basins from basement uplifts; these sub-basins display similar stratigraphy and deformation histories. The Moncton Sub-basin in southern New Brunswick contains the unconformity-bounded, Late Devonian to Early Mississippian Horton Group. The Albert Formation within this group is host to the productive onshore McCully gas field, roughly 2.5 km below the surface. This member is up to 800 m thick and comprises interbedded sandstone, siltstone, and mudstone rocks. Wellbore and 2- and 3-dimensional seismic data from the McCully gas field was combined with outcrop data to investigate the 3D geometry of the Horton Group in the western Moncton Sub-basin. Kinematic parameters were calculated using the geometrical observations of faults and folds that deform the Frederick Brook and Hiram Brook members. At McCully, the subsurface data display large curved ESE-WNW-striking extensional faults within the upper Horton Group, with less common contractional faults and folds. Vertical seismic sections perpendicular to the normal faults show horizontal extension in the range of 12 to 16%, contrasted with vertical seismic sections parallel to the extensional faults that show smaller amounts of horizontal shortening. Analogous outcrop-scale structures are observed within the Albert Formation, 13 km from the seismic data location, along the general strike of the structural pattern. 3-dimensional outcrop mapping reveals a complex relationship of these structures. Relative orientations between extensional and contractional structures, as well as the orientations of the structures relative to the Kennebecasis Fault, indicates that major dextral strike-slip deformation has produced significant clockwise rotation of structures (upwards of 60° for extensional faults). Subsurface measurements, combined with outcrop observations, of the bulk strain suggest that the basin deformed in a transtensional setting with a large angle of divergence (59°) early in its history; however, variations in the apparent stretch and orientation of the faults across the shear zone indicate that the basin deformed heterogeneously in space and time, in addition to asynchronous development of structural

features. Towards the SE, the apparent stretch decreases and the orientation of the faults relative to the shear zone boundary increases, resulting in a gradual decrease in α across the shear zone. It is possible to explain the SW-directed concave curvature of the extensional faults by using these variations in the kinematic parameters.

Preface

Chapter 1 introduces the thesis and provides a roadmap of the sections that follow.

Chapter 2 of this thesis is intended as a basis for a publication by J.C. Kugler, J.W.F. Waldron, and M. Duvall. It will be submitted in a structural geology journal. I collected and analyzed the data and composed the manuscript. J.W.F. Waldron assisted with data collection and provided manuscript edits. M. Duvall assisted in data collection and preliminary interpretation.

Chapter 3 of this thesis will be submitted as a paper to be authored by J.C. Kugler, J.W.F. Waldron, and P. Durling. It will be submitted in the Journal of Structural Geology. I was responsible for data collection and interpretation and the composition of the manuscript. J.W.F. Waldron assisted with interpretation and provided manuscript edits. P. Durling provided preliminary interpretation of the seismic reflection data and provided expertise on the McCully gas field.

Chapter 4 provides a summary of the main conclusions of Chapter 2 and 3 and makes suggestions for future work.

Acknowledgements

I would like to thank my supervisor, John W.F. Waldron, for not only the opportunity to work with him, but also his for guidance and patience. His commitment to research and his love for geoscience was both inspirational and motivational.

I would like to thank my friends at the University of Alberta who offered their support and kindness, especially everyone in the Structural Geology and Tectonics Research Group. Thank you to Michael Duvall for being an outstanding field assistant and friend.

Costs were supported by an NSERC Discovery Grant held by John Waldron and by a teaching assistantship at the Department of Earth and Atmospheric Sciences, University of Alberta. Presentations of the results were supported by a University of Alberta Graduate Students' Association travel grant.

Subsurface data were provided by Corridor Resources Inc. We thank them for this support and for assistance in the field. Special thanks are due to Paul Durling for sharing his expertise on the McCully area. Steven Hinds and Adrian Park of the New Brunswick Department of Natural Resources are thanked for sharing their great knowledge of southern New Brunswick geology.

Petrel seismic interpretation software was provided by Schlumberger Inc. Photogrammetric analysis of outcrop data was carried out using an educational license for AgiSoft Photoscan Professional software.

I thank my family for their encouragement through this process, especially my wife, Katie, for her unconditional support. My dogs, Milton and Meghan, are thanked for their undeniable stress-relieving abilities.

Table of Contents

Abstract ii

Preface iv

Acknowledgements v

Chapter 1: Introduction 1

1.1. Maritimes Basin 1

1.2. Objectives of study 4

1.3. Strike-slip tectonics 6

1.4. Study area 9

1.5. Dataset description 20

1.6. Roadmap of thesis 20

1.7. References 21

Chapter 2: 3D outcrop mapping of Horton Group sedimentary rocks in the western Moncton Sub-basin, New Brunswick 27

2.1. Introduction 27

2.2. Methods 36

2.3. Stratigraphy 42

2.4. Faults 53

2.5. Folds 56

2.6. Unconformity 58

2.7. Discussion 58

2.8. Conclusion 65

2.9. References 65

Chapter 3: Fault development and the role of strike-slip deformation at the McCully gas field, New Brunswick, Canada 69

3.1. Introduction 70

3.2. Subsurface data 80

3.3. Outcrop objectives and methods 97

3.4. Discussion 101

3.5. Conclusions 116

3.6. References 118

Chapter 4: Conclusion and recommendations 122

Bibliography 127

Appendix A: Orthophotographs and interpretations of road outcrops along Highway 1 133

List of Figures

Figure 1.1. Regional maps of the Maritimes Basin and the Moncton Sub-basin. 2

Figure 1.2. Definitions of simple shear, transtension, and transpression. 5

Figure 1.3. Typical structures found in simple-shear dextral strike-slip settings. 5

Figure 1.4. Extensional faults and the Albion Syncline in the Stellarton Sub-basin, Nova Scotia. 10

Figure 1.5. Diagrammatic representation of strike-slip block faulting. 11

Figure 1.6. Stratigraphic chart of the western Moncton Sub-basin. 12

Figure 1.7. Geologic map and cross-section of the McCully area. 17

Figure 2.1. Typical structures found in simple-shear dextral strike-slip settings. 29

Figure 2.2. Regional maps of the Maritimes Basin and the Moncton Sub-basin. 30

Figure 2.3. Geologic map of the Sussex area. 32

Figure 2.4. Stratigraphic chart of the western Moncton Sub-basin. 34

Figure 2.5. Block diagram of a dipping bed offset by a dextral strike-slip-dominated fault. 37

Figure 2.6. Schematic diagram of 3 folded beds. 37

Figure 2.7. A screen capture from AgiSoft Photoscan Professional showing the aligned cameras. 39

Figure 2.8. An example of a pre-processed photograph used in the 3D model created in AgiSoft Photoscan Professional. 39

Figure 2.9. A screen capture of a 3D model of a small portion of the northern roadcut. 40

Figure 2.10. A small portion of a vertical orthomosaic photograph of the northern roadcut. 40

Figure 2.11. Top down orthomosaic photographs overlain on a satellite photograph. 41

Figure 2.12. Generalized stratigraphic log of units 1-5 at the study area. 45

Figure 2.13. Geologic map of four roadcuts along Highway 1, roughly 3 km SW of the City of Sussex, New Brunswick. ..... pocket

Figure 2.14. Interpreted vertical sections of the four roadcuts along Highway 1. 47

Figure 2.15. Structures observed in Units 3 and 4. 52

Figure 2.16. Equal-area projected stereoplots of poles to the fault planes at the four roadcuts along Highway 1. 54

Figure 2.17. Calcite mineral lineations on fault surfaces. 55

Figure 2.18. Interpreted outcrop photograph illustrating the complex relationship between extensional and contractional faults. 55

Figure 2.19. Close-up interpretations of heavily deformed areas. 57

Figure 2.20. Equal-area projected stereoplots of poles to bedding, poles to axial surfaces, and fold axes at the four roadcuts along Highway 1. 59

Figure 2.21. The expected initial and present-day observed orientations of structures relative to one another at the study location, in a simple-shear environment. 61

Figure 2.22. Simple-shear kinematic models illustrating the rotation of structures within a shear zone. 63

Figure 3.1. Typical structures found in simple-shear dextral strike-slip settings. 71

Figure 3.2. Definition of the transtensional α-angle. 72

Figure 3.3. Regional maps of the Maritimes Basin and the Moncton Sub-basin. 73

Figure 3.4. Geologic map of the McCully area. 75

Figure 3.5. Stratigraphic chart of the western Moncton Sub-basin. 79

Figure 3.6. Interpreted seismic sections from the 3D volume showing the major stratigraphic units and faults, displayed in two-way travel time. 81

Figure 3.7. Subsurface time structure contour maps of the top Windsor salt, Sussex unconformity, and the top Frederick Brook shale horizons. 89

Figure 3.8. Illustration of a typical fault pick in the Horton Group within the 3D seismic data. 90

Figure 3.9. Structural dip map of the Frederick Brook shale at McCully. 91

Figure 3.10. Equal-area stereoplots of fault data from the study area. 92

Figure 3.11. Subsurface time structure contour map of the top of the Fredrick Brook shale horizon. 93

Figure 3.12. Map of the northernmost roadcut at the study location along Highway 1. 98

Figure 3.13. Interpreted orthomosaic photo of the Highway 1 roadcut. 100

Figure 3.14. Field photographs of the Highway 1 roadcuts. 103

Figure 3.15. Diagrammatic representation of strike-slip block faulting. 109

Figure 3.16. Kinematic parameters of the Moncton Sub-basin at the Frederick Brook shale horizon. 111

Figure 3.17. Reconstruction of the top of the Frederick Brook shale-fault intersection lines. 113

Figure 4.1. Geologic map of four roadcuts along Highway 1, roughly 3 km SW of the City of Sussex, New Brunswick. pocket

Figure 4.2. Subsurface time structure contour map of the Fredrick Brook shale horizon. 125

Figure 4.3. Reconstruction of the Frederick Brook shale-fault intersection lines. 126

List of Symbols and Abbreviations

SZB	shear zone boundary
°	degrees
γ	shear strain
ψ	shear angle
α	angle of divergence from simple shear
w	width of fault block
h	fault heave
θ	original orientation of extensional faults relative to the SZB
θ'	present day orientation of extensional faults relative to the SZB
S'	apparent shortening
S^*	apparent stretch
T	displacement gradient parallel to the SZB
S	displacement gradient perpendicular to the SZB

Chapter 1: Introduction

1.1. Maritimes Basin

The late Paleozoic Maritimes Basin (Figure 1.1; Roliff, 1962) is the largest intermontane basin in the Appalachian Orogen, covering an area of nearly 150,000 km^2 across parts of New Brunswick, Nova Scotia, Prince Edward Island, Newfoundland, Québec, and extending beneath the Gulf of St. Lawrence (Williams, 1974). It contains late Paleozoic sedimentary rocks that rest on early Paleozoic and older rocks both onshore and offshore Atlantic Canada (Gibling et al., 2009). The basin formed during the final stages of the formation of Pangea (Gibling et al., 2009). Appalachian (NE-SW) and Minas (E-W) fault trends, which dissect the majority of the basin, have been interpreted to record significant dextral strike-slip components of movement (Waldron et al., 2015). Many tectonic models for basin development have been proposed, which include rift models (Belt, 1968; McCutcheon and Robinson, 1987), continental collision and loading subsidence models (Gussow, 1953), and major strike-slip models (Bradley, 1982; Hibbard and Waldron, 2009). Recent models that involve major strike slip deformations along Appalachian and Minas fault trends (Hibbard and Waldron, 2009; Murphy et al., 2011; Waldron et al., 2015) suggest that strike-slip tectonism played a large role in the development of the Maritimes Basin, though contributions from other tectonic processes is possible. Broadly speaking, the basin can be split into two phases separated by an unconformity at the Mississippian – Pennsylvanian boundary that extends basin wide (Bradley, 1982; St. Peter, 2006). Recent work by Waldron et al. (2013) suggests that the unconformity represents a major change in tectonism from transtension to transpression as a consequence of a change from dextral movement along the Appalachian-trend faults to dextral movement along the Minas-trend faults.

The Maritimes Basin comprises many smaller sub-basins, which are separated by uplifts and major bounding faults (Howie and Barss, 1975; St. Peter, 1993). Because of similarities of the basal stratigraphic units the sub-basins have been interpreted to have comparable tectonic histories

Figure 1.1. Regional maps of the Maritimes Basin and the Moncton Sub-basin.

(a) Map of North America. The black box shows the location of (b). (b) Regional map of the Eastern Canada showing the extent of the late Paleozoic Maritimes Basin and major faults. Modified from Waldron et al. (2013). Abbreviations: BIF, Belleisle fault zone; CBF, Cabot fault; CCHF, Caledonia – Clover Hill fault zone; HF, Hollow fault; MFZ, Minas fault zone. (c) Geological map of southern New Brunswick, Canada. Faults are shown in red. Modified from Waldron et al. (2015). The white star indicates the location of the studied road outcrops along Highway 1. Abbreviation: F = Fault.

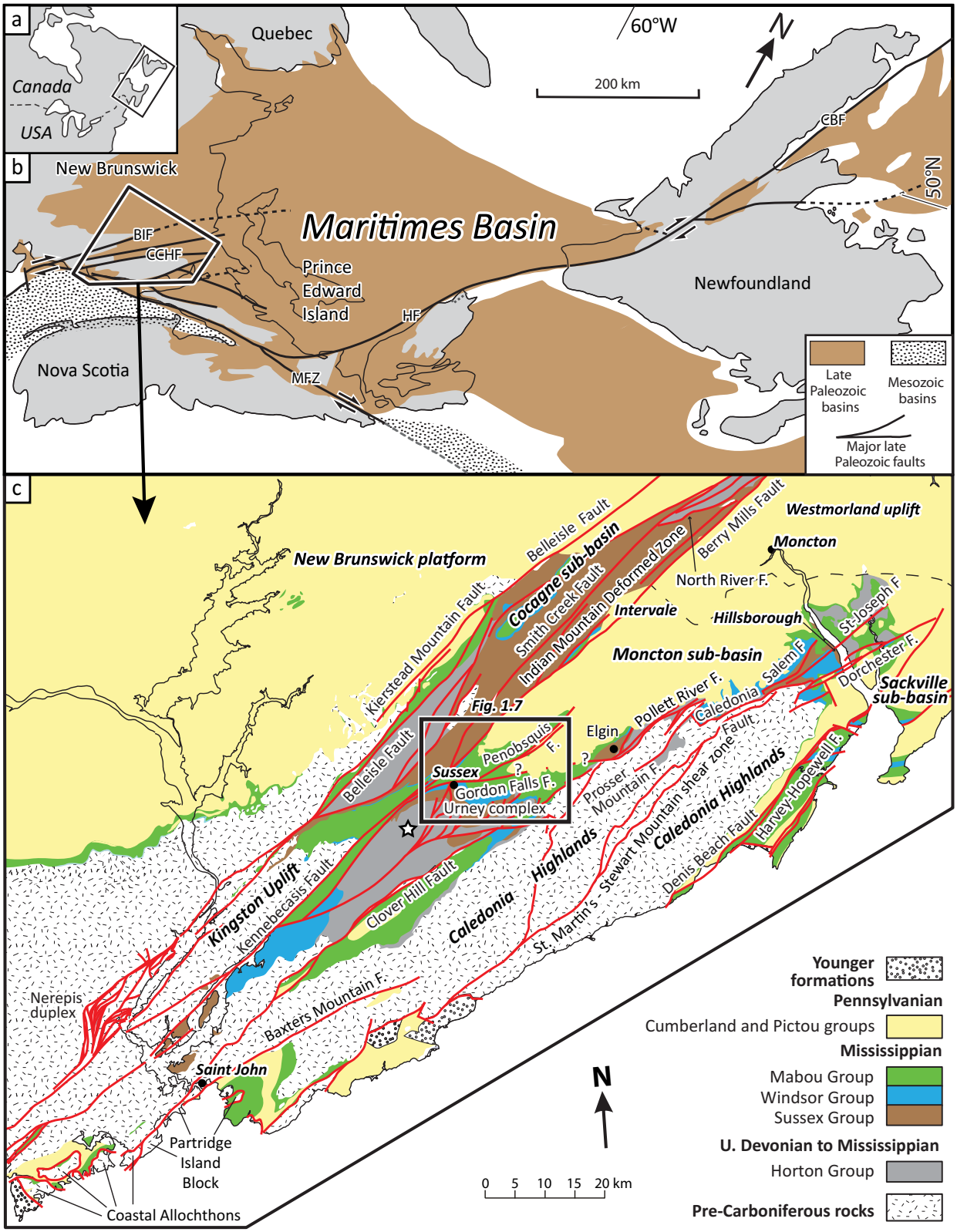
a
Canada
USA
Quebec
60°W
N
200 km
b
New Brunswick
Maritimes Basin
BIF
CCHF
Prince
Edward
Island
HF
CBF
50°N
Newfoundland
Nova Scotia
MFZ
Late
Paleozoic
basins
Mesozoic
basins
Major late
Paleozoic faults
c
New Brunswick platform
Belleisle Fault
Westmorland uplift
Moncton
Berry Mills Fault
Cocagne sub-basin
Smith Creek Fault
Indian Mountain Deformed Zone
North River F.
Intervale
Hillsborough
St-Joseph F.
Moncton sub-basin
Salem F.
Dorchester F.
Sackville
sub-basin
Kierstead Mountain Fault
Fig. 1.7
Pollett River F.
Caledonia
Fault
Elgin
Penobsquis
F.
Sussex
Gordon Falls F.
Urney complex
Belleisle Fault
Prosser
Mountain F.
Caledonia Highlands
Harvey-Hopewell F.
Denis Beach Fault
St. Martin's - Stewart Mountain shear zone
Kingston Uplift
Kennebecasis Fault
Clover Hill Fault
Caledonia
Highlands
Nerepis
duplex
Baxters Mountain F.
Saint John
Partridge
Island
Block
Coastal Allochthons
N
0 5 10 15 20 km
Younger
formations
Pennsylvanian
Cumberland and Pictou groups
Mississippian
Mabou Group
Windsor Group
Sussex Group
U. Devonian to Mississippian
Horton Group
Pre-Carboniferous rocks

(Bradley, 1982); however, active deposition in the Maritimes Basin may have changed locations through time due to variations in major fault movement (St. Peter and Johnson, 2009; Waldron et al., 2015). These sub-basins are characterized by times of rapid subsidence and deposition alternating with intervals of contraction, inversion, and uplift (Bradley, 1982; St. Peter, 1993).

The vast size of the Maritimes Basin alone has intrigued resource explorationists for decades. Many economic deposits of salt, petroleum, coal, and ores are found on the onshore portions of many sub-basins (St. Peter and Johnson, 2009); however, because majority of the basin is offshore (~70%), exploration is limited and expensive.

1.2. Objectives of study

This thesis presents and interprets high quality outcrop and subsurface data from the McCully area (Figure 1.1). Previous work on basin formation and fault kinematics (e.g. Wilson, 2005; Wilson and White, 2006) was limited to lesser quality, 2D seismic and wellbore data. The 3D seismic data used here fill the blanks between the 2D seismic lines, allow more accurate interpretations of the geometry of the 3D structure of the subsurface of the Moncton Sub-basin, and provide the ability to make enhanced interpretations on basin development and fault kinematics.

Dextral strike-slip movement has been recognized along the major faults that bound the Moncton Sub-basin (Park et al., 2007; Waldron et al., 2015). However, the amount of subsidence attributed to strike-slip, transtension, and extension during the formation of the Moncton Sub-basin is not fully understood. The focus of this project is to show the relationship between oblique deformation and the development of normal faults during the Late Devonian to Early Mississippian in the Moncton Sub-basin. A solid understanding of the geometry and kinematics of fault movement is critical for understanding the tectonic system, and for further exploration for resources in the Moncton Sub-basin, the greater Maritimes Basin, and similar basins worldwide.

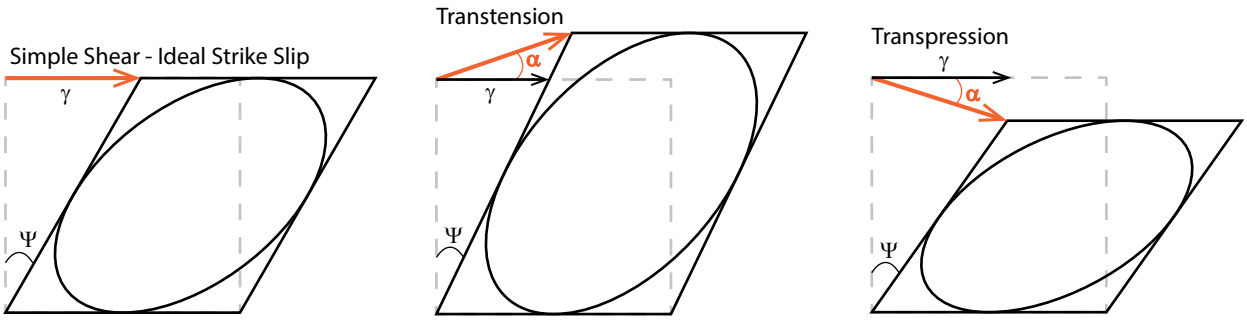

Figure 1.2. Definitions of simple shear, transtension, and transpression.

The red arrows represent the displacement vector of particles in the shear zone. Symbols: α = angle of divergence (transtension or transtension angle); ψ = angle of shear; γ = shear strain; e = instantaneous extension direction.

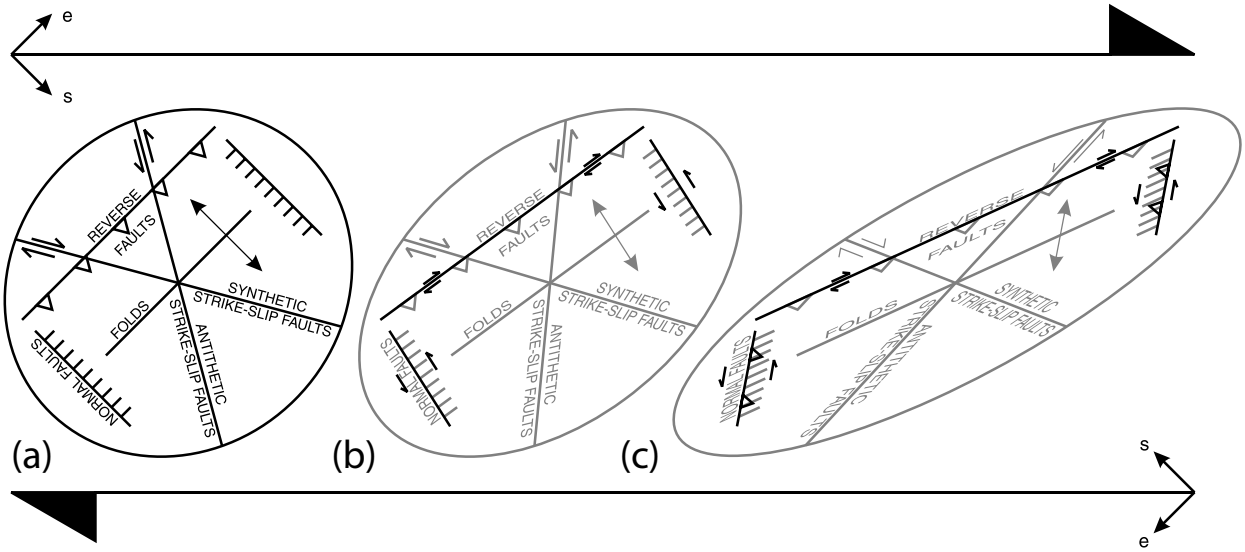

Figure 1.3. Typical structures found in simple-shear dextral strike-slip settings.

Symbols: *s* represents the instantaneous shortening direction; *e* represents the instantaneous extension direction. (a) Geometry of the structures found in strike-slip settings where there has been little strike-slip movement along the shear zone boundary, after Harding (1974). (b) and (c) Modification of (a) showing how structures rotate and change with continued movement along the shear zone boundary (Waldron, 2005).

1.3. Strike-slip tectonics

Because of the importance of strike-slip faults in the evolution of the Maritimes Basin, a brief review of strike-slip tectonics in provided here.

1.3.1. Definitions

Strike-slip deformation laterally displaces adjacent blocks of crust (Wilcox et al., 1973; Sylvester, 1988); such an environment is often referred to as a wrench tectonic regime (Wilcox et al., 1973; Fossen, 2016). Wrench regimes are either right-lateral (dextral) or left-lateral (sinistral; Sylvester, 1988; Fossen, 2016). Strike-slip deformation zones in many cases are near-vertical and consequently are linear features in map view (Sylvester, 1988; Fossen, 2016). Deformation within a strike-slip shear zone is complicated by the presence of both horizontal shortening and horizontal extension processes (Fossen et al., 1994) acting simultaneously in different directions. Shear zones involving strike slip can be split into three categories based on the overall deformation (Figure 1.2): (1) simple-shear ideal strike slip; (2) transtension (strike slip plus vertical shortening and horizontal extension); and (3) transpression (strike slip plus vertical extension and horizontal shortening; Wilcox et al., 1973; Sylvester, 1988; Dewey et al., 1998).

Simple shear is a deformation which deforms rocks such that the area is conserved and all displacement vectors are parallel to the shear zone boundary (SZB; Ramsay and Huber, 1983). Ideal strike-slip zones experience simple shear; the instantaneous stretching direction and instantaneous shortening direction are 45° degrees from the SZB and are perpendicular to one another (Fossen et al., 1994). In a dextral situation the horizontal instantaneous shortening direction is clockwise from the SZB and the horizontal instantaneous stretching direction is counter-clockwise (vice-versa for sinistral; Harding, 1974; Sylvester, 1988). Ideal strike-slip shear zones often contain both extensional and shortening structures; extensional structures form perpendicular to the instantaneous extension axis and shortening structures form perpendicular to the instantaneous shortening axis (Wilcox et al., 1973; Sylvester, 1988; Fossen and Tikoff, 1998). Displacements within this setting are predominantly parallel to the SZB with no vertical

displacement (Wilcox et al., 1973; Sylvester, 1988).

Transtension refers to deformation that is a combination of strike-slip movement, horizontal extension, and vertical shortening (Dewey et al., 1998; Fossen and Tikoff, 1998). Transtensional zones are typically found at releasing bends in strike-slip faults and in oblique rifts (Fossen, 2016). This tectonic setting is a departure from simple shear and produces a prolate bulk strain ellipsoid (Dewey et al., 1998). The horizontal extension component induces an increase in area, volume being conserved by vertical thinning (Dewey et al., 1998). The instantaneous stretching direction and instantaneous shortening direction are no longer at 45° from the SZB; the instantaneous stretching direction is at an angle larger than 45° from the SZB and the instantaneous shortening direction is at an angle smaller than 45° (Sanderson and Marchini, 1984; Dewey et al., 1998; Fossen and Tikoff, 1998). The symbol alpha (α) is used in strike-slip tectonics to indicate the amount of divergence from simple shear (Figure 1.2), in a range of 0° to 90° (Tikoff and Teyssier, 1994; Dewey et al., 1998). Simple-shear zones have an α-value of 0° (Tikoff and Teyssier, 1994; Dewey et al., 1998). When $\alpha < 20°$, the shortening axis is horizontal and simple-shear strike-slip dominates, whereas when $\alpha > 20°$, the shortening axis is vertical and pure-shear extension dominates (Dewey et al., 1998).

Transpression refers to deformation that is a combination of strike-slip movement, horizontal shortening, and vertical extension (Dewey et al., 1998; Fossen and Tikoff, 1998). Transpressional zones are typically found at restraining bends in strike-slip faults and in orogens undergoing oblique convergence (Fossen, 2016). This also is a deviation from simple shear and creates an oblate strain ellipsoid (Dewey et al., 1998; Fossen and Tikoff, 1998). Area is decreased by the horizontal shortening, but volume is conserved through the extrusion of material (Dewey et al., 1998). As with transtension, the instantaneous stretching and shortening directions are no longer at 45° degrees from the SZB. The instantaneous stretching direction is at an angle smaller than 45° and the instantaneous shortening direction is at an angle larger than 45° (Sanderson and Marchini, 1984; Dewey et al., 1998; Fossen and Tikoff, 1998). α is used to indicate the amount

of divergence from simple shear in transpressional settings (Figure 1.2). When $\alpha < 20°$, the extending axis is horizontal and simple-shear strike-slip dominates, whereas when $\alpha > 20°$, the extending axis is vertical and pure-shear shortening dominates (Dewey et al., 1998).

1.3.2. Strike-slip sedimentary basins and associated structures

Strike-slip basins are typically deep but have a small surface area and are elongated in a direction parallel to the SZB (Nilsen and Sylvester, 1995). A basin may form in a large, broad shear zone developed between strike-slip faults or in a releasing bend of a single strike-slip fault, forming a pull-apart basin (Aydin and Nur, 1982; Nilsen and Sylvester, 1995). Pronounced vertical shortening in transtension leads to the typical development of deep sedimentary basins, in contrast to settings characterized by transpression or ideal strike-slip. Structures found in strike-slip sedimentary basins include normal faults, reverse faults, strike-slip faults, and folds (Figure 1.3; Harding, 1974). Basins formed in transtensional settings are dominated by extensional features; *en echelon* normal faults typically accommodate the horizontal extensional component of deformation (Allen et al., 1998; Waldron, 2005).

Although the instantaneous strains acting on the structures within shear zones may remain constant (Figure 1.3a), the orientations of the structures change with every increment of deformation (Figure 1.3b; 1.3c). As illustrated in Figure 1.3, structures formed in strike-slip basins progressively rotate towards the orientation of the SZB with continued deformation (Garfunkel and Ron, 1985; Waldron, 2005). Structures rotate clockwise in dextral settings and counter-clockwise in sinistral settings (Garfunkel and Ron, 1985). Faults transition from dip-slip to strike-slip as cumulative rotation occurs. Normal faults may rotate sufficiently to become inverted (Figure 1.3c; Waldron, 2005). This occurs when the shear angle exceeds 45°, which causes the normal faults to pass perpendicularity to the SZB (Figure 1.3c) into a field of shortening (Waldron, 2005). The progressive rotation of structures in strike-slip zones makes it difficult to understand initial basin configurations.

The Stellarton Sub-basin in Nova Scotia (Figure 1.4) is an excellent example of a strike-slip

sub-basin in the greater Maritimes Basin. In this sub-basin, sedimentary rocks are extended by N – S normal faults and perpendicularly shortened by the E-plunging Albion Syncline (Figure 1.4). Waldron (2005) developed a model that used the structural geometries in the Stellarton Sub-basin to make inferences about the kinematics. Simply explained, the model's concept is as follows. Progressive deformation of the shear zone results in an increase shear strain and causes fault blocks (structural features) to rotate (Figure 1.3). Both of these effects result in the development of fault heaves along extensional faults (Figure 1.5). Waldron recognized a relationship between the apparent stretch (S^*), the apparent shortening (S'), and the orientation of the faults (θ') that can be used to estimate the angle of divergence of the basin (α) and to quantify the amount of rotation that the structures have undergone in both ideal strike-slip and transtensional settings. Values of 1.14 for S^*, 0.9 for S', and 48° for θ' calculated for the Stellarton Sub-basin result in an α-angle of 6° and a total fault rotation of 7° clockwise (Waldron, 2005).

1.4. Study area

The Moncton Sub-basin, in southern New Brunswick (Figure 1.1), is filled with late Paleozoic terrestrial clastic and marine carbonate rocks (Gussow, 1953; Gibling et al., 1992; St. Peter, 1993; St. Peter and Johnson, 2009). The sub-basin trends NE-SW, has a length of ~100 km, and a width of ~10 km in the SW that increases gradually to ~35 km in the NE. Accumulations of hydrocarbons occur within the Albert Formation at the Stoney Creek oil and gas field (St. Peter, 2001) and the McCully gas field (Durling and Martel, 2003). Potash and rock salt have been mined from the Carboniferous strata in the Moncton Sub-basin; the largest mine is the Penobsquis Mine (Wilson et al., 2006). Sediment-hosted copper-silver, copper-manganese, lead-zinc, uranium deposits, fault-related barite, and sulphide mineralization deposits have been explored throughout the Moncton Sub-basin (St. Peter and Johnson, 2009).

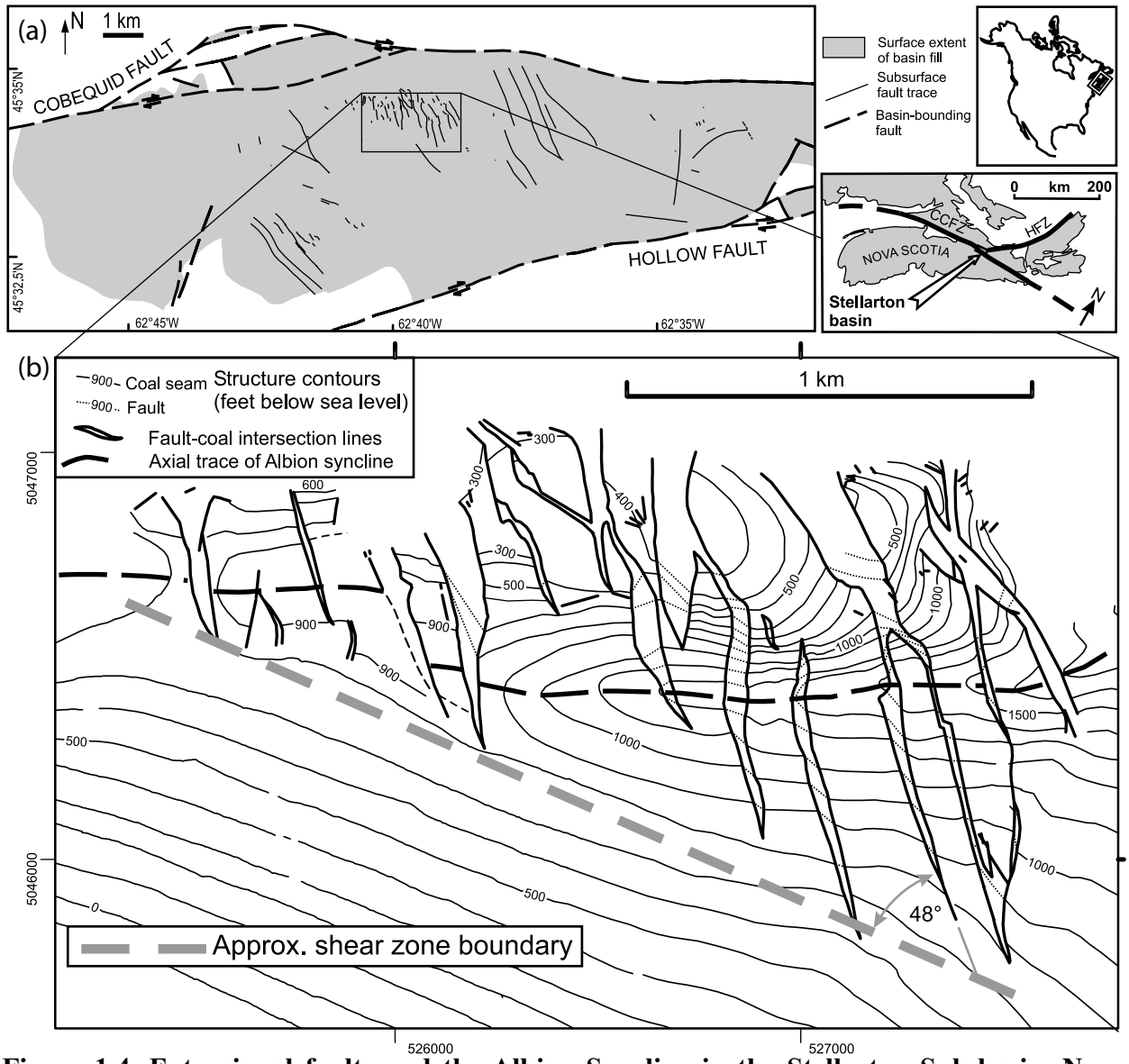

Figure 1.4. Extensional faults and the Albion Syncline in the Stellarton Sub-basin, Nova Scotia.

Modified from Waldron (2005). Abbreviations: CCFZ = Cobequid-Chedabucto Fault Zone; HFZ = Hollow Fault Zone. (a) A simplified map of the Stellarton Sub-basin showing fault traces. The inset map shows the location of the sub-basin in Atlantic Canada. (b) Enlarged subsurface structure map of a coal seam cut by en echelon extensional faults.

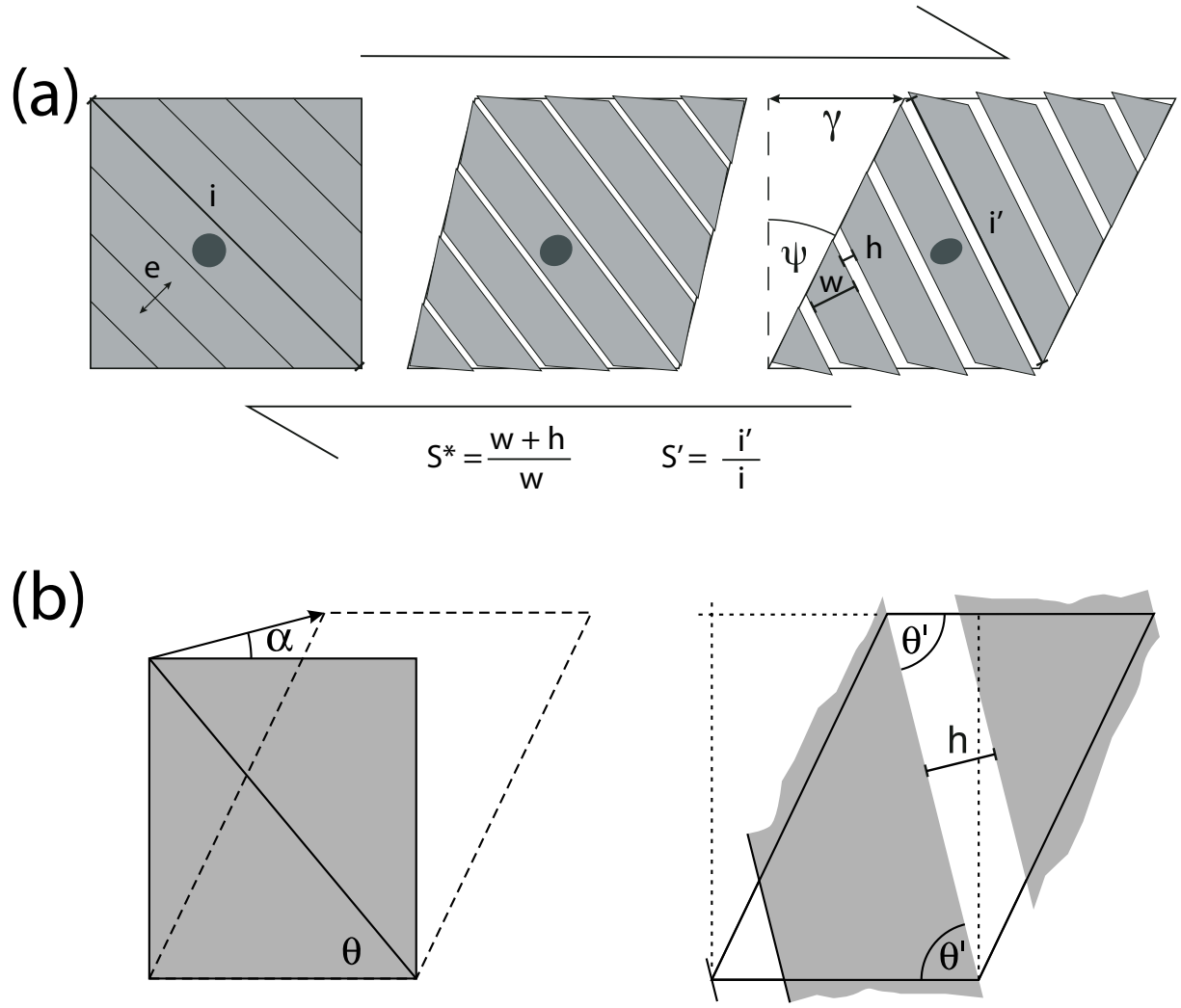

Figure 1.5. Diagrammatic representation of strike-slip block faulting.

Modified from Waldron (2005). α represents the angle of divergence (transtension or transtension angle); ψ represents the angle of shear; γ represents the shear strain; θ represents the initial orientation of faults; θ' represents the final orientation of faults. (a) Simple shear ideal strike-slip case. As progressive strike-slip deformation occurs, the combined effect of increasing shear strain and rotation of fault blocks results in increased fault heaves (*h*). (b) Transtensional case drawn for a rectangle. In this scenario, extensional faults form at greater angles to the SZB due to the horizontal extensional component perpendicular to the SZB.

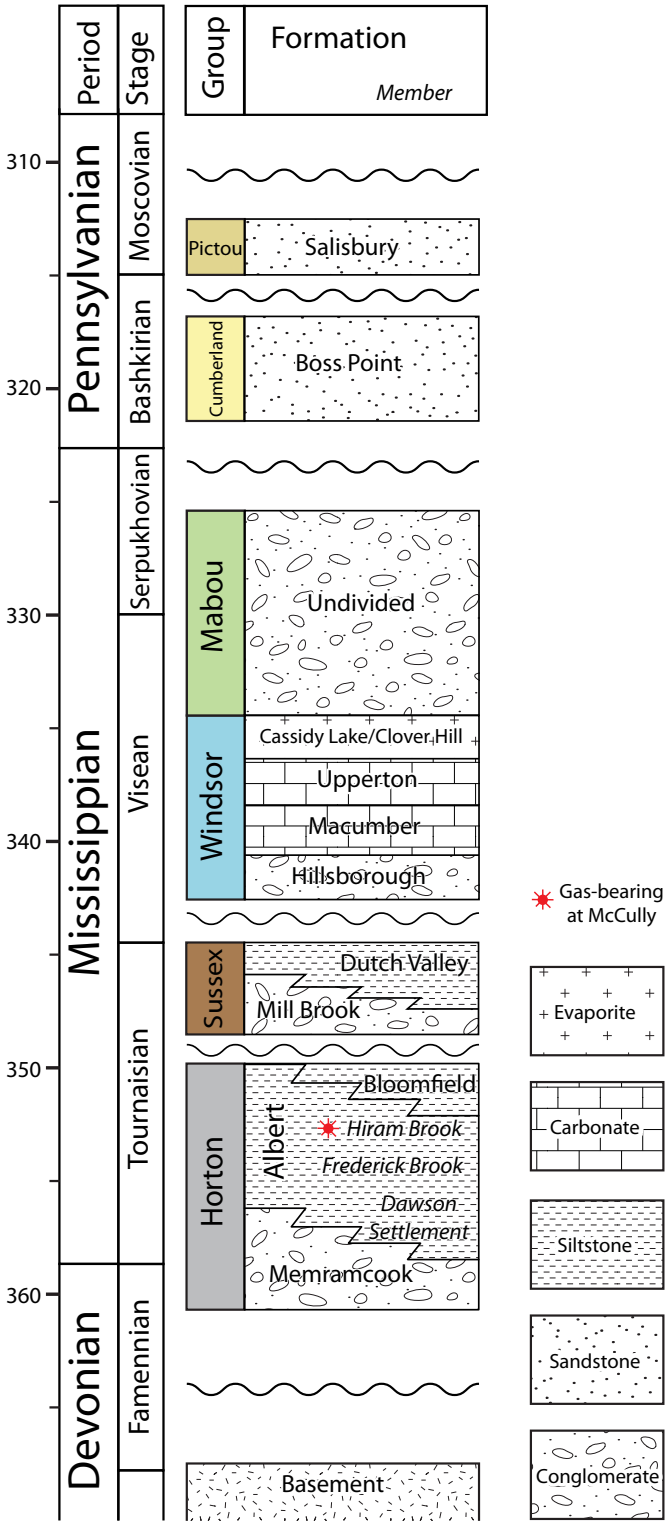

Figure 1.6. Stratigraphic chart of the western Moncton Sub-basin.

After Wilson and White (2006) and St. Peter and Johnson (2009). Dominant lithologies are shown. Ages and stages are from Davydov et al. (2012).

1.4.1. Stratigraphy

The Moncton Sub-basin contains terrestrial clastic and marine carbonate rocks that are divided into six successions (Gussow, 1953; Gibling et al., 1992; St. Peter, 1993; St. Peter and Johnson, 2009). In ascending order, these successions are the Horton, Sussex, Windsor, Mabou, Cumberland, and Pictou Groups (Figure 1.6). Five major surfaces of erosion or nondeposition have been identified: (1) the Horton – Sussex unconformity, (2) the Sussex – Windsor unconformity, (3) the Mabou – Cumberland unconformity, (4) the Cumberland – Pictou unconformity, and (5) an unconformity related to the latest contraction phase (Gussow, 1953; McCutcheon, 1981; Gibling et al., 1992; St. Peter, 1993, 2002; Wilson and White, 2006; St. Peter and Johnson, 2009).

The Horton Group, the focus of this study, comprises terrestrial fine- to coarse-grained, red to grey clastic units. In the western Moncton Sub-basin it has been split into the Memramcook, Albert, and Bloomfield formations (Hinds, 2008a, 2008b, 2008c, 2008d; Keighley, 2008; St. Peter and Johnson, 2009). The Albert Formation contains an internal petroleum system and has further been subdivided into the Dawson Settlement, Frederick Brook (source/seal), and the Hiram Brook (reservoir) members (Wilson, 2005; St. Peter and Johnson, 2009). The trapping mechanism for the gas field is a combined anticline – unconformity trap. Many authors have interpreted the Horton Group to represent an alluvial fan to lacustrine environment (Gussow, 1953; Carter and Pickerill, 1985b; St. Peter, 1993; Keighley, 2008; St. Peter and Johnson, 2009).

The Sussex Group has similar characteristics to the Horton Group and is not recognized as a distinct unit in other sub-basins in the Maritimes Basin (Gibling et al., 2009). The two groups are separated by an angular unconformity (St. Peter, 2002) that formed as a result of post-Horton Group inversion of the Moncton Sub-basin (St. Peter et al., 2005; St. Peter and Johnson, 2009). In the east the Sussex Group includes the Round Hill, the Gautreau, and the Weldon formations and in the west it consists of the Mill Brook and Dutch Valley formations (Wilson and White, 2006; St. Peter and Johnson, 2009).

The Windsor Group includes the only marine rocks found in the Maritimes Basin (Gibling et al., 2009). The group consists largely of carbonate, evaporite, and shale deposits throughout the Maritimes Basin (Schenk, 1969; Giles, 1981) with minor coarse-grained clastics in the Moncton Sub-basin (McCutcheon, 1981). The Windsor Group consists of the Hillsborough, the Gays River / Macumber, the Upperton, and the Cassidy Lake / Clover Hill formations in the Moncton Sub-Basin (Figure 1.6; McCutcheon, 1981; Wilson, 2005; St. Peter, 2006; St. Peter and Johnson, 2009). The group has been interpreted to have been deposited throughout the Maritimes Basin in shallow to deep marine environments (Giles, 1981; McCutcheon, 1981; St. Peter and Johnson, 2009).

The overlying Mabou Group is largely undivided in the Moncton Sub-basin but has been separated in places into an underlying, unnamed unit of fine-grained redbeds and overlying coarse-grained clastics of the Hopewell Cape Formation (Wilson, 2005; St. Peter and Johnson, 2009). These nonmarine rocks were likely deposited in an alluvial environment (St. Peter and Johnson, 2009). The uppermost Cumberland and Pictou groups primarily comprise mature mudstone and quartzose sandstone with varying amounts of coal, interpreted to have been deposited in a fluvial channel system to alluvial plain environment (St. Peter and Johnson, 2009).

1.4.2. Basin structure

The Moncton Sub-basin is dominated by NE-SW striking faults (Figure 1.1), known as Appalachian-trend faults (Waldron et al., 2015), and also includes some E-W and NW-SE striking faults (Park and St. Peter, 2005; Wilson and White, 2006; Park et al., 2007). The sub-basin is bounded by the Kennebecasis – Berry Mills and Clover Hill – Caledonia fault zones to the N and S, respectively (St. Peter, 1993). Movement along the NE-SW striking faults is thought to be the main control on the geologic structure and subsidence of the Moncton Sub-basin (St. Peter and Johnson, 2009). Inversion of the basin-bounding faults (discussed in more detail below), likely a consequence of dextral movement along Minas trend faults, occurred throughout the Carboniferous, resulting in uplift and erosion (Wilson and White, 2006).

The Clover Hill – Caledonia Fault Zone separates the Moncton sub-basin from the Caledonia Uplift and the Sackville Sub-basin in the south (Park et al., 2007). In the west, near the town of Sussex (Figure 1.1), the Clover Hill Fault is near vertical; however, to the east, by Hillsborough, the Caledonia Fault dips gently northwest (Park et al., 2007). Park et al. (2007) and Waldron et al. (2015) interpreted the fault zone to have undergone substantial dextral strike-slip displacement (up to 30 km) in the west and normal, reverse, and strike-slip displacements in the east. Reverse-sense reactivation of the normal faults is seen throughout the fault zone (Wilson and White, 2006; Park et al., 2007).

The Kennebecasis – Berry Mills Fault Zone separates the Moncton Sub-basin from the Kingston Uplift and the Indian Mountain Deformed Zone towards the north (St. Peter, 1993; St. Peter and Johnson, 2009). Faults in this zone are typically steep and likely dip southeast (Park and St. Peter, 2009). Park and St. Peter (2009) interpreted the Berry Mills Fault to be either extensional or transtensional with more than 800 m of dip-slip movement. Waldron et al. (2015) interpreted the deformation along the Kennebecasis – Berry Mills Fault Zone and associated splays to have occurred over different times, including a total dextral strike-slip motion of up to 60 km. Splays from the Kennebecasis – Berry Mills Fault Zone that strike east to southeast into the Moncton Sub-basin, such as the Gordon Falls Fault (Figure 1.1), link it with the Clover Hill – Caledonia Fault Zone (Park et al., 2007).

1.4.3. Previous work on sub-basin development and deformation

Several authors (Gussow, 1953; Howie and Barss, 1975; McCutcheon, 1981; Carter and Pickerill, 1985; St. Peter, 1993, 2002; Wilson and White, 2006; Park and St. Peter, 2009; St. Peter and Johnson, 2009) have presented ideas on how the Moncton Sub-basin formed and deformed through time. It is widely understood that the basin has a complex history that includes many periods of subsidence and deposition separated by times of inversion of basin-bounding faults, uplift, and erosion.

Detailed observations and interpretations of seismic lines by Wilson (2005) and Wilson and

White (2006) show that the basin likely initiated in the latest Devonian to middle Tournaisian along the Gordon Falls and Clover Hill faults. Thick successions of Horton Group are observed in the hanging walls of these faults but little to no Horton Group is seen in the footwalls. Many authors have identified an unconformity between the Horton and Sussex Groups (Gussow, 1953; Howie and Barss, 1975; Carter and Pickerill, 1985; St. Peter, 1993, 2002; St. Peter and Johnson, 2009) as well as ENE-WSW striking thrust faults within the Horton Group that do not reach the Sussex Group (Wilson, 2005; Wilson and White, 2006). This has led to the interpretation that a middle Tournaisian post-Horton, pre-Sussex inversion event occurred (St. Peter, 1993; Wilson, 2005; Wilson and White, 2006; St. Peter and Johnson, 2009).

The Sussex Group was deposited on top of the inverted Horton Group half-grabens during the late Tournaisian to early Visean (St. Peter, 1993; Wilson, 2005; Wilson and White, 2006). Accommodation space was created due to renewed extension along northeast-striking normal faults, as seen on seismic interpretations by Wilson (2005) and Wilson and White (2006). Furthermore, these authors interpreted thrust faults within the Sussex Group that do not reach the Windsor Group, suggesting that basin shortening occurred prior to the deposition of the Windsor sediments. An unconformity between the Sussex and Windsor groups in the Moncton Sub-basin has been attributed to this syn- to post-Sussex Group contraction event (Wilson, 2005; Wilson and White, 2006; St. Peter and Johnson, 2009). Following this contraction episode, a marine transgression drowned the majority of the Moncton Sub-basin which led to the deposition of the Windsor Group limestones and evaporites during the early Visean (McCutcheon, 1981; St. Peter, 1993; Wilson and White, 2006; St. Peter and Johnson, 2009).

Subsequent regression led to the deposition of the terrestrial Mabou Group during the middle Visean to early Namurian (St. Peter, 1993; St. Peter and Johnson, 2009). Wilson and White (2006) identified Mabou Group reflections in seismic profiles that climb onto a triangle zone located southeast of the Berry Mills Fault. These authors interpreted the climbing Mabou reflectors to have been deposited whilst southeast-directed thrusting formed the triangle zone. Furthermore,

Figure 1.7. Geologic map and cross-section of the McCully area.

(a) The subsurface data locations are shown. The black box shows the extent of the 3D seismic reflection data volume and the bold black lines are the 2D seismic reflection data lines. The bottom-hole locations of 49 vertical to slightly deviated wells used in subsurface interpretation are displayed. Modified from Hinds (2008a, 2008b, 2008c, 2008d, 2008e) and Hinds and St. Peter (2008). (b) Cross-section A-A' in (a). Modified from Hinds and St. Peter (2005).

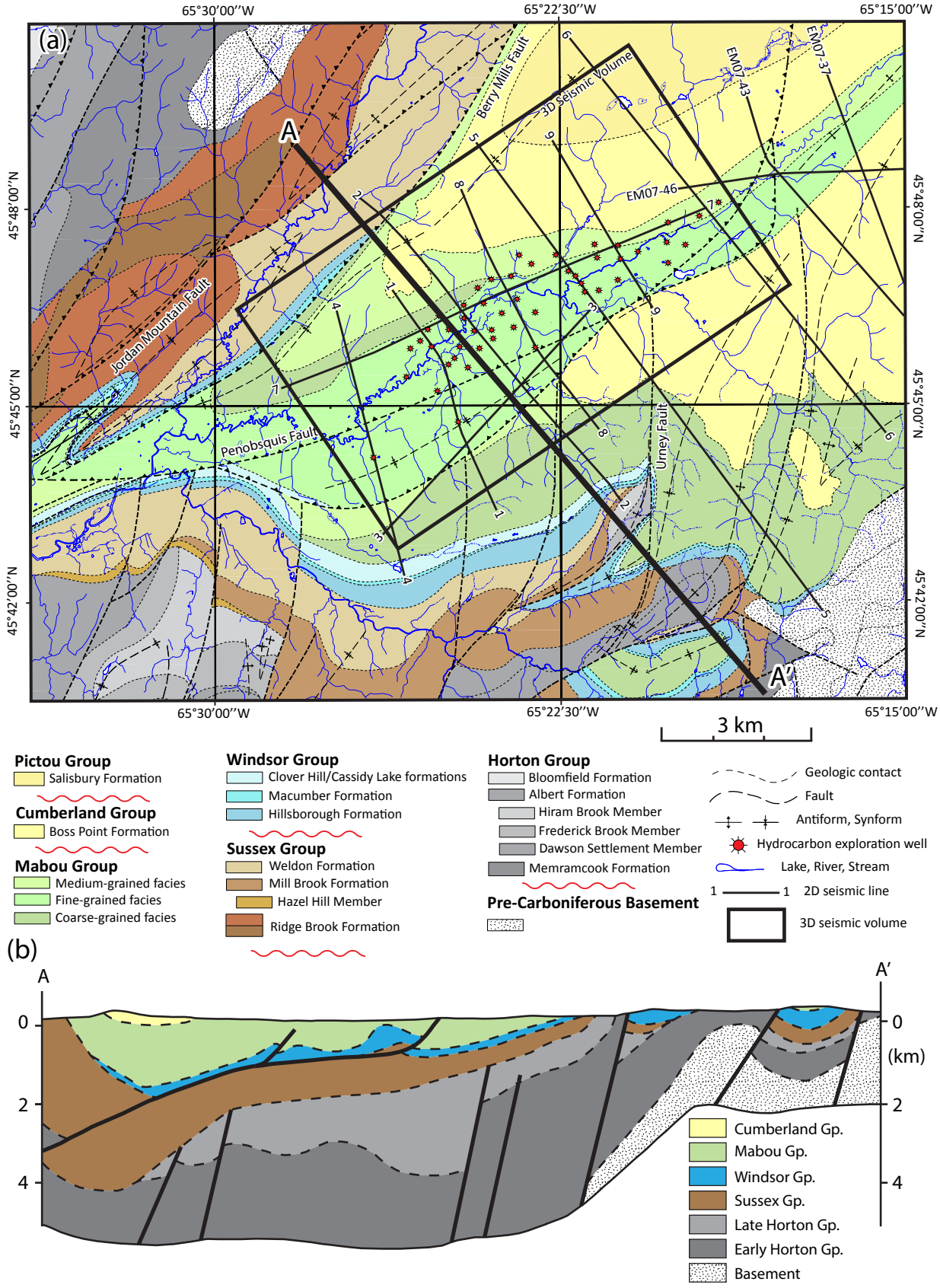
(a)
65°30′00″W
65°22′30″W
65°15′00″W
45°48′00″N
45°45′00″N
45°42′00″N
A
A′
Berry Mills Fault
3D Seismic Volume
EM07-37
EM07-43
EM07-46
Jordan Mountain Fault
Penobsquis Fault
Urney Fault
3 km
Pictou Group
Salisbury Formation
Cumberland Group
Boss Point Formation
Mabou Group
Medium-grained facies
Fine-grained facies
Coarse-grained facies
Windsor Group
Clover Hill/Cassidy Lake formations
Macumber Formation
Hillsborough Formation
Sussex Group
Weldon Formation
Mill Brook Formation
Hazel Hill Member
Ridge Brook Formation
Horton Group
Bloomfield Formation
Albert Formation
Hiram Brook Member
Frederick Brook Member
Dawson Settlement Member
Memramcook Formation
Pre-Carboniferous Basement
Geologic contact
Fault
Antiform, Synform
Hydrocarbon exploration well
Lake, River, Stream
2D seismic line
3D seismic volume
(b)
A
A′
0
2
4
(km)
Cumberland Gp.
Mabou Gp.
Windsor Gp.
Sussex Gp.
Late Horton Gp.
Early Horton Gp.
Basement

observed reverse displacement of the Mabou Group but not the Cumberland Group along the Gordon Falls Fault supports pre-Cumberland contraction (Wilson and White, 2006).

Bradley (1982) suggested there was a distinct transition in subsidence mechanism in the Maritimes Basin from a strike-slip- and transtension-dominated subsidence, during the deposition of the Horton, Sussex, Windsor, and Mabou Groups, to thermal sag during the deposition of the Cumberland and Pictou Groups (early Bashkirian to early Moscovian). However, more recent work (e.g. Waldron et al., 2013, 2015) shows that large amounts of subsidence in the Maritimes Basin can be attributed to salt expulsion and that there was thrusting in the Pennsylvanian Period. The Bashkirian Boss Point Formation of the Cumberland Group is the first regionally distributed unit throughout the entire Maritimes Basin, indicating that sub-basins were no longer acting as individual depocenters (Gibling et al., 1992), although localized halotectonics may have controlled deposition between sub-basins (Waldron and Rygel, 2004).

Wilson and White (2006) seismically identified folded and reverse faulted Cumberland Group, and in some areas Pictou Group, in the Moncton Sub-basin. Furthermore, they suggested that some folds and faults which affect the Cumberland Group are related to salt movement (i.e. Penobsquis Fault and salt structure) leading to the interpretation that the halotectonism occurred after deposition of the Cumberland Group. However, work elsewhere in the Maritimes Basin (Waldron and Rygel, 2005; Waldron et al., 2013) suggest that salt movement began during deposition of the Mabou Group or earlier. Wilson (2005), Wilson et al. (2006), and Waldron et al. (2015) have interpreted salt movement to be linked with a regional WNW – ESE contraction, possibly a result of dextral movements along the Minas Fault Zone. The unconformity between the two groups (St. Peter, 1993; St. Peter and Johnson, 2009) also suggests that the deposition of the Cumberland and Pictou Groups did not occur during a single thermal sag event, as suggested by Bradley (1982), but that Pennsylvanian tectonism was more complex.

1.5. Dataset description

Corridor Resources Inc. provided a 3D prestack migrated seismic volume and twelve 2D seismic lines covering the McCully gas field (Figure 1.7). The 3D volume has a surface area of roughly 13.5 by 8 km. The inline and crossline spacing of the data is 30 m, with the inlines oriented NW-SE and the crosslines oriented NE-SW. The 2D lines have a combined length of 113 km. Ten 2D lines are oriented NW-SE and 2 are oriented NE-SW (Figure 1.7). The vertical resolution for the 3D dataset is roughly 40 m, whereas the 2D dataset has a vertical resolution of roughly 30 m. The seismic data image up to 3 s of TWT (two-way traveltime), however, reflections below ~1.75 s are faint and difficult to interpret. The polarity of the seismic data are positive. Wellbore data from 59 vertical to slightly deviated wells containing varying amounts of wireline data were also made available by Corridor Resources. 54 of the wells lie within the 3D volume (Figure 1.7). Corridor provided well top picks for stratigraphic boundaries and tied 49 wells to the seismic data.

Subsurface data were complemented by surface outcrop data along Highway 1, roughly 13 km to the SW of the McCully area (Figure 1.1) Sandstone, siltstone, and mudstone rocks of the Albert Formation are present at this location. The Albert Formation is at surface in this location because the outcrops are located within the footwall of the large normal Gordon Falls fault, whereas the McCully area is in the hanging-wall. At this location four roadcuts, two on the SW-bound lanes and two on the NE-bound lanes, were examined. The subsurface and outcrop data locations are interpreted to lie along depositional strike from each other, so major variations in thickness or facies variations are not expected.

1.6. Roadmap of thesis

This thesis is presented in paper format. It contains two manuscripts that use the observed outcrop and subsurface structural geometries to make kinematic interpretations for the early development of the western Moncton Sub-basin.

Following this introduction (Chapter 1), Chapter 2 focusses on the 3D geometry of faults and folds in four roadcuts located 3 km SW of the City of Sussex, New Brunswick. Here, sedimentary rocks of the Albert Formation display an intricate relationship between faults and folds. AgiSoft Photoscan Professional software was used to make 3D models of the outcrops for high mapping precision. A geologic map of the roadcuts is presented. These results are used to constrain the likely amount of deformation at sub-seismic scale in Chapter 3.

Chapter 3 concentrates on the 3D subsurface structural geometry of the Horton and Sussex groups at the McCully gas field. Interpretations on high-quality 2D and 3D seismic reflection data show the complex relationship between faults and folds. Observations on fault separations and orientations allow the estimation of kinematic parameters of the early Moncton Sub-basin, using methods developed by Waldron (2005), to describe the early deformation of the Moncton Sub-basin.

Chapter 4 is a summary of the major conclusions of the research into the geometry and kinematics of the Moncton Sub-basin and provides insight into future work on this topic.

1.7. References

Allen, M.B., Macdonald, D.I., Xun, Z., Vincent, S.J., Brouet-Menzies, C., 1998. Transtensional deformation in the evolution of the Bohai Basin, northern China. Geological Society, London, Special Publications 135, 215–229.

Aydin, A., Nur, A., 1982. Evolution of pull-apart basins and their scale independence. Tectonics 1, 91–105.

Belt, E.S., 1968. Post-Acadian rifts and related facies, eastern Canada. In: Zen, E., White, W.S., Hadley, J.. (Eds.), Studies of Appalachian Geology, Northern and Maritime. Wiley Interscience, New York, 95–113.

Bradley, D.C., 1982. Subsidence in late Paleozoic basins in the northern Appalachians. Tectonics 1, 107–123.

Carter, D.C., Pickerill, R.K., 1985. Lithostratigraphy of the Late Devonian–Early Carboniferous Horton Group of the Moncton Subbasin, southern New Brunswick. Maritime Sediments and Atlantic Geology 21, 11–24.

Claerbout, J.F., 1985. Imaging the Earth's Interior. Blackwell Sci. Publ., London.

Davydov, V.I., Korn, D., Schmitz, M.D., Gradstein, F.M., Hammer, O., 2012. The Carboniferous Period. In: Gradstein, F.M., Ogg, J.G., Schmidtz, M., Ogg, G. (Eds.), The Geologic Time Scale 2012. Elsevier, 603–651.

Dewey, J.F., Holdsworth, R.E., Strachan, R.A., 1998. Transpression and transtension zones. In: Dewey, J.F., Holdsworth, R.E., Strachan, R.A. (Eds.), Continental Transpressional and Transtensional Tectonics, Geological Society of London Special Publication. 1–14.

Durling, P., Martel, A.T., 2003. The McCully gas field: A proven resource with high exploration potential. Geological Society of America Abstracts with Programs 35, 81.

Fossen, H., 2016. Structural Geology, 2nd ed. Cambridge University Press.

Fossen, H., Tikoff, B., 1998. Extended models of transpression and transtension, and application to tectonic settings. In: Holdsworth, R.E., Strachan, R.A., Dewey, J.F. (Eds.), Continental Transpressional and Transtensional Tectonics, Geological Society of London Special Publication. 15–33.

Fossen, H., Tikoff, B., Teyssier, C.T., 1994. Strain modelling of transpressional and transtensional deformation. Norsk Geologisk Tidsskrift 74, 134–145.

Garfunkel, Z., Ron, H., 1985. Block rotation and deformation by strike-slip faults. Journal of Geophysical Research 90, 8589–8602.

Gibling, M.R., Calder, J.H., Ryan, R., Van de Poll, H.W., Yeo, G.M., 1992. Late Carboniferous and early Permian drainage patterns in Atlantic Canada. Canadian Journal of Earth Sciences 29, 338–352.

Gibling, M.R., Culshaw, N., Rygel, M.C., Pascucci, V., 2009. The Maritimes Basin of Atlantic Canada: Basin Creation and Destruction in the Collisional Zone of Pangea. In: Miall, A. (Ed.), Sedimentary Basins of the World. 211–244.

Giles, P.S., 1981. Major Transgressive-Regressive Cycles in Middle to Late Visean Rocks of Nova Scotia, Nova Scotia Department of Mines and Energy Branch, Paper.

Gussow, W.C., 1953. Carboniferous stratigraphy and structural geology of New Brunswick, Canada. The American Association of Petroleum Geologists Bulletin 37, 1713–1816.

Harding, T.P., 1974. Petroleum traps associated with wrench faults. American Association of Petroleum Geologists Bulletin 58, 1290–1304.

Hibbard, J., Waldron, J.W.F., 2009. Truncation and translation of Appalachian Promontories: Mid-Paleozoic strike-slip tectonics and basin initiation. Geology 37, 487–490. https://doi.org/10.1130/G25614A.1

Hinds, S., 2008a. Geology of the Apohaqui area (NTS 21 H/12h), Kings County, New Brunswick., New Brunswick Department of Natural Resources: Minerals, Policy, and Planning Division, Plate 2008-10 (revised 2009). ed.

Hinds, S., 2008b. Geology of the Sussex Corner area (NTS 21 H/11e), Kings County, New Brunswick., New Brunswick Department of Natural Resources: Minerals, Policy, and Planning Division, Plate 2008-7 (revised 2009). ed.

Hinds, S., 2008c. Geology of the Cedar Camp area (NTS 21 H/11f), Kings County, New Brunswick., New Brunswick Department of Natural Resources: Minerals, Policy, and Planning Division, Plate 2008-08 (revised 2009). ed.

Hinds, S., 2008d. Geology of the Jordan Mountain area (NTS 21 H/14d), Kings County, New Brunswick., New Brunswick Department of Natural Resources: Minerals, Policy, and Planning Division, Plate 2008-13 (revised 2009). ed.

Hinds, S., 2008e. Geology of the Crockets Corner area (NTS 21 H/14c), Kings County, New Brunswick., New Brunswick Department of Natural Resources: Minerals, Policy, and Planning Division, Plate 2008-12 (revised (2009). ed.

Hinds, S., St. Peter, C.J., 2008. Geology of the Summerfield area (NTS 21 H/13a), Kings County, New Brunswick., New Brunswick Department of Natural Resources: Minerals, Policy, and Planning Division, Plate 2008-11 (revised 2009). ed.

Hinds, S., St. Peter, C., 2005. The McCully gas field project. New Brunswick Department of Natural Resources: Geological surveys division.

Howie, R.D., Barss, M.S., 1975. Upper Paleozoic rocks of the Atlantic provinces, Gulf of St. Lawrence, and adjacent continental shelf. In: Van Der Linden, W.J.M., Wade, J.A. (Eds.), Offshore Geology of Eastern Canada, Volume 2 - Regional Geology, Geological Survey of Canada, Paper. 35–50.

Keighley, D., 2008. A lacustrine shoreface succession in the Albert Formation, Moncton Basin, New Brunswick. Bulletin of Canadian Petroleum Geology 56, 235–258.

McCutcheon, S.R., 1981. Stratigraphy and paleogeography of the Windsor Group in southern New Brunswick. New Brunswick Department of Natural Resources; Mineral Resources Branch Open File Report 81-31, 210.

McCutcheon, S.R., Robinson, P.T., 1987. Geological constraints on the genesis of the Maritimes Basin, Atlantic Canada. In: Beaumont, C., Tankard, A.J. (Eds.), Sedimentary Basins and Basin-Forming Mechanism, Canadian Society of Petroleum Geologists, Memoir. 287–297.

Murphy, J.B., Waldron, J.W.F., Kontak, D., Pe-Piper, G., Piper, D.J.W., 2011. Minas Fault Zone: Late Paleozoic history of an intra-continental orogenic transform fault in the Canadian Appalachians. Journal of Structural Geology 33, 312–328.

Nilsen, T.H., Sylvester, A.G., 1995. Strike-slip basins. Tectonics of Sedimentary Basins 425–457.

Oldenburg, D.W., Scheuer, T., Levy, S., 1983. Recovery of acoustic impedance from reflection seismology. Geophysics 48, 1318–1337.

Park, A.F., St. Peter, C.J., 2009. Stratigraphy and structure of the Indian Mountain Deformed Zone, Maritimes Basin, Westmorland County, Southeastern New Brunswick, New Brunswick Department of Natural Resources; Minerals, Policy and Planning Division, Mineral Resources Report.

Park, A.F., St. Peter, C.J., 2005. Deformation of Lower Carboniferous rocks in the Rosevale to Saint-Joseph area, Albert and Westmorland counties, southeastern New Brunswick. In: Martin, G.L. (Ed.), Geological Investigations in New Brunswick for 2004, New Brunswick Department of Natural Resources; Minerals, Policy and Planning Division, Mineral Resources Report. 45–98.

Park, A.F., St. Peter, C.J., Keighley, D.G., 2007. Structural styles in Late Devonian – early Carboniferous rocks along the southern margin of the Moncton Subbasin: Caledonia Mountain to Elgin, southeastern New Brunswick. In: Martin, G.L. (Ed.), Geological Investigations in New Brunswick for 2006, New Brunswick Department of Natural Resources, Mineral Resources Report. 87–125.

Ramsay, J.G., Huber, M.I., 1983. The Techniques of Modern Structural Geology. Volume 1: Strain Analysis. Academic Press, London.

Roliff, W.A., 1962. The Maritimes Carboniferous Basin of Eastern Canada. Geological Association of Canadian Proceedings 14, 21–44.

Sanderson, D.J., Marchini, W.R.D., 1984. Transpression. Journal of Structural Geology 6, 449–458.

Schenk, P.E., 1969. Carbonate-sulfate-redbed facies and cyclic sedimentation of the Windsorian Stage (middle Carboniferous), Maritime Provinces. Canadian Journal of Earth Sciences 6, 1037–1066.

St. Peter, C.J., 2006. Geological relationship between the Cocagne Subbasin and the Indian Mountain deformed zone, Maritimes basin, New Brunswick. In: Martin, G.L. (Ed.), Geological Investigations in New Brunswick for 2005, New Brunswick Department of Natural Resources, Mineral Resources Report. 103-183.

St. Peter, C.J., 2002. Bedrock geology of the McCully natural gas field area, Moncton Subbasin (parts of 21 H/11, 12, 13 and 14), New Brunswick., New Brunswick Department of Natural Resources and Energy; Minerals and Energy Division, Plate 2002-33 (revised 2004). ed.

St. Peter, C.J., 2001. Petroleum geology in the Carboniferous of southeastern New Brunswick. In: Guidebook to Field Trips in New Brunswick and western Maine, R.K. Pickerill and

D.R. Lentz (editors). New England Intercollegiate Geological Conference, 93rd Annual Meeting.

St. Peter, C.J., 1993. Maritimes Basin evolution: key geologic and seismic evidence from the Moncton Subbasin of New Brunswick. Atlantic Geology 29, 233–270.

St. Peter, C.J., Johnson, S.C., 2009. Stratigraphy and structural history of the late Paleozoic Maritimes Basin in southeastern New Brunswick, Canada, New Brunswick Department of Natural Resources, Memoir.

St. Peter, C.J., Johnson, S.C., Barr, S.M., White, C.E., 2005. Bedrock Geology of the Hillsborough area (NTS 21 H/15), Albert and Westmorland Counties, New Brunswick., New Brunswick Department of Natural Resources and Energy, Plate.

Sylvester, A.G., 1988. Strike-slip faults. Geological Society of America Bulletin 100, 1666–1703.

Tikoff, B., Teyssier, C., 1994. Strain modeling of displacement-field partitioning in transpressional orogens. Journal of Structural Geology 16, 1575–1588.

Vestrum, R., Gittins, J., 2009. Technologies from foothills seismic imaging: replacements or complements? First Break 27, 61–66.

Waldron, J.W.F., 2005. Extensional fault arrays in strike-slip and transtension. Journal of Structural Geology 27, 23–34.

Waldron, J.W.F., Barr, S.M., Park, A.F., White, C.E., Hibbard, J.P., 2015. Late Paleozoic strike-slip faults in Maritime Canada and their role in the reconfiguration of the northern Appalachian orogen. Tectonics 34, 1661–1684. https://doi.org/10.1002/2015TC003882

Waldron, J.W.F., Rygel, M.C., 2005. Role of evaporite withdrawal in the preservation of a unique coal-bearing succession: Pennsylvanian Joggins Formation, Nova Scotia. Geology 33, 337–340.

Waldron, J.W.F., Rygel, M.C., 2004. Salt tectonism and sedimentation patterns in the Cumberland Basin, Nova Scotia: new insights from Devon Canada's seismic reflection profiles. Abstracts, Canadian Society of Petroleum Geologists Convention, Calgary AB.

Waldron, J.W.F., Rygel, M.C., Gibling, M.R., Calder, J.H., 2013. Evaporite tectonics and the late Paleozoic stratigraphic development of the Cumberland basin, Appalachians of Atlantic Canada. Geological Society of America Bulletin 125, 945–960.

Wilcox, R.E., Harding, T.P., Seely, D.R., 1973. Basic wrench tectonics. AAPG Bulletin 57, 74–96.

Williams, E.P., 1974. Geology and petroleum possibilities in and around Gulf of St. Lawrence. AAPG Bulletin 58, 1137–1155.

Wilson, P., 2005. Stratigraphy, structural geology, and tectonic history of the McCully area, Moncton Subbasin, southeastern New Brunswick. New Brunswick Department of Natural Resources; Minerals, Policy and Planning Division Mineral Resource Report 2005-5, 104.

Wilson, P., White, J.C., 2006. Tectonic evolution of the Moncton Basin, New Brunswick, Eastern Canada; new evidence from field and sub-surface data. Bulletin of Canadian Petroleum Geology 54, 319–336. https://doi.org/10.2113/gscpgbull.54.4.319

Wilson, P., White, J.C., Roulston, B.V., 2006. Structural geology of the Penobsquis salt structure: late Bashkirian inversion tectonics in the Moncton Basin, New Brunswick, eastern Canada. Canadian Journal of Earth Sciences 43, 405–419. https://doi.org/10.1139/e05-116

Yilmaz, O., 2001. Seismic Data Analysis, Investigations in Geophysics. Society of Exploration Geophysicists.

Chapter 2: 3D outcrop mapping of Horton Group sedimentary rocks in the western Moncton Sub-basin, New Brunswick

The transtensional Moncton Sub-basin contains deformed late Paleozoic sedimentary rocks. Roadcuts along Highway 1 in southern New Brunswick provide excellent exposures of Horton Group rocks, allowing detailed outcrop-scale mapping of primary and secondary structures. Four roadcuts, ranging in length between 250 to 300 m, located 3 km southwest of the City of Sussex contain sandstone, siltstone, and mudstone beds, likely belonging to the Hiram Brook Member of the Albert Formation, which is host to the productive McCully gas field only 13 km to the northeast. Observations of structures likely formed by soft-sediment deformation, such as convolute bedding directly overlain or truncated by flat laminae and sandstone dykes that follow fault planes, and an unconformity suggest that the sub-basin was deformed early in its history. Detailed outcrop mapping was combined with a 3-dimensional outcrop model to make an accurate geologic map of the outcrops, which illustrates the complex relationship between extensional and contractional structures. Initial orientations of these structures are predicted to be perpendicular in ideal strike slip; however, at the study area, the orientation of a set of conjugate extensional faults is only ~30° from that of the contractional faults, suggesting that a large amount of clockwise rotation has occurred as a result of major dextral strike-slip movement along the sub-basin-bounding faults.

2.1. Introduction

Basins that develop in strike-slip tectonic regimes contain complex structures that make it difficult to achieve a solid understanding of their geometries and kinematics. The complexity is attributable to the concurrent extension and shortening strains that such basins experience as they are deformed. Typical structures in strike slip basins include extensional faults, contractional faults, strike-slip faults, and folds (Figure 2.1; Harding, 1974). Transtensional basins, in which strike slip is combined with horizontal extension and vertical shortening, contain more

extensional features than contractional features. The transtensional Moncton Sub-basin in southern New Brunswick (Figure 2.2), which formed in a zone of major strike-slip motion during the late Paleozoic (Waldron et al., 2015), is an exceptional basin in which to study strike-slip geometries and kinematics. Furthermore, a series of roadcuts along the divided Highway 1 near the City of Sussex (Figure 2.3) provide excellent exposures of sedimentary rocks that were deformed early in the basin history. These outcrops provide the opportunity to document the detailed geometry of faults and folds at a scale smaller than the resolution of subsurface seismic data. (An extensive subsurface dataset, including well logs and 3D seismic data, is available for the McCully gas field.) It is important to understand the geometries and kinematics of such transtensional basins to allow improved characterization of resource potential and exploitation.

2.1.1. Regional geologic setting

The late Paleozoic Maritimes Basin (Roliff, 1962; Gibling et al., 2009) in Atlantic Canada has an area of nearly 150,000 km^2 and is the largest intermontane basin in the Appalachian Orogen (Figure 2.2; Williams, 1974). A period of transtension after the Acadian orogeny formed this basin, which now contains a sedimentary fill (up to 12 km thick) that sits on Proterozoic and early Paleozoic basement (Williams, 1974; Hibbard and Waldron, 2009; Waldron et al., 2015). The Maritimes Basin comprises many smaller structures, referred to as sub-basins, which typically trend NE to E and are separated by uplifts and major sub-basin-bounding faults (Figure 2.2; Howie and Barss, 1975; St. Peter, 1993; Gibling et al., 2009). These sub-basins have complex deformation histories which include varying amounts of subsidence, inversion, faulting, folding, erosion, and salt tectonism at different times during their development (Wilson and White, 2006; Gibling et al., 2009; St. Peter and Johnson, 2009; Waldron et al., 2015).

2.1.1.1. Bounding structures of the Moncton sub-basin

The Moncton Sub-basin (St. Peter, 1993) trends NE, extending roughly 100 km NE to SW and 10 – 35 km NW to SE and is bounded by basement uplifts and long (tens of kilometres)

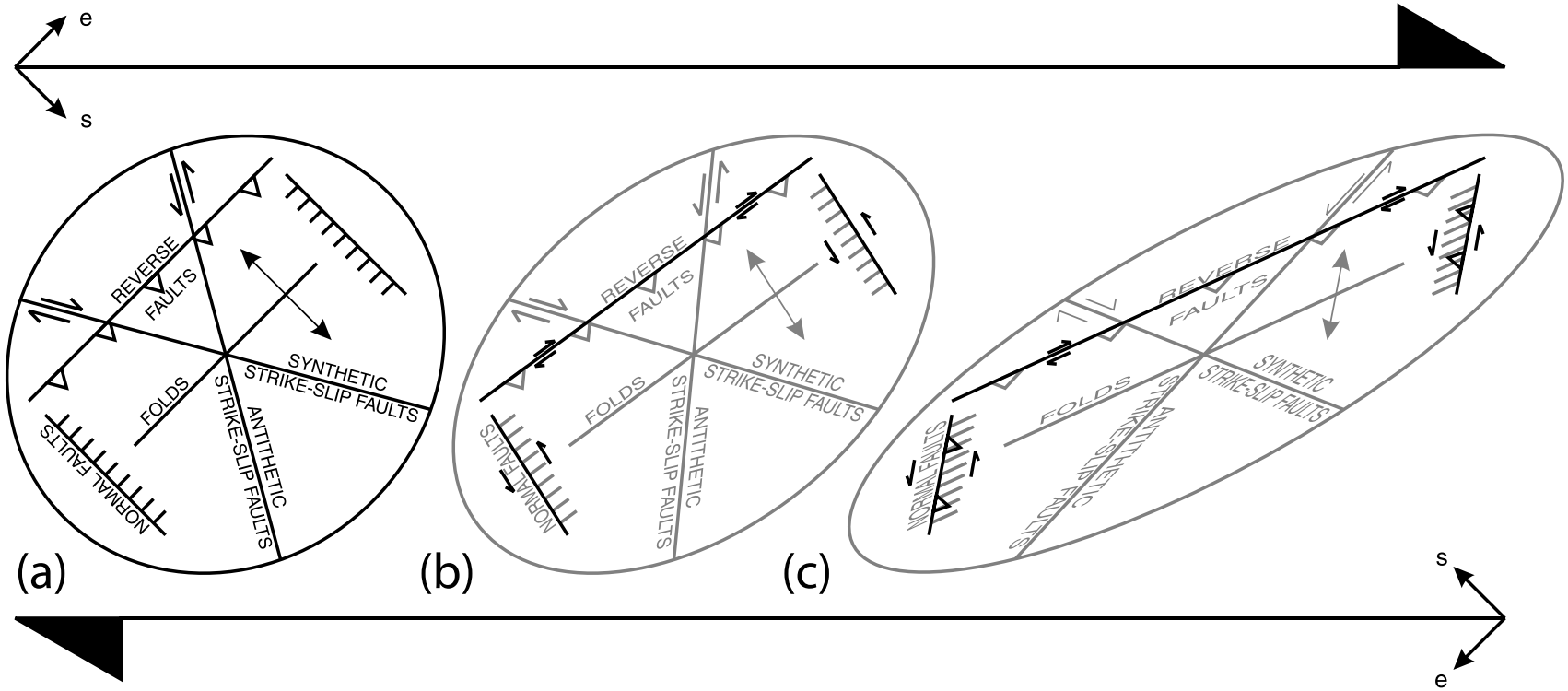

Figure 2.1. Typical structures found in simple-shear dextral strike-slip settings.

Symbols: *s* represents the instantaneous shortening direction; *e* represents the instantaneous extension direction. (a) Geometry of the structures found in strike-slip settings where there has been little strike-slip movement along the shear zone boundary, after Harding (1974). (b) and (c) Modification of (a) showing how structures rotate and change with continued movement along the shear zone boundary (Waldron, 2005).

Figure 2.2. Regional maps of the Maritimes Basin and the Moncton Sub-basin.

(a) Map of North America. The black box shows the location of (b). (b) Regional map of the Eastern Canada showing the extent of the late Paleozoic Maritimes Basin and major faults. Modified from Waldron et al. (2013). Abbreviations: BIF, Belleisle fault zone; CBF, Cabot fault; CCHF, Caledonia – Clover Hill fault zone; HF, Hollow fault; MFZ, Minas fault zone. (c) Geological map of southern New Brunswick, Canada. The black box shows the location of Figure 2.3. Faults are shown in red. Modified from Waldron et al. (2015). Abbreviation: F = Fault.

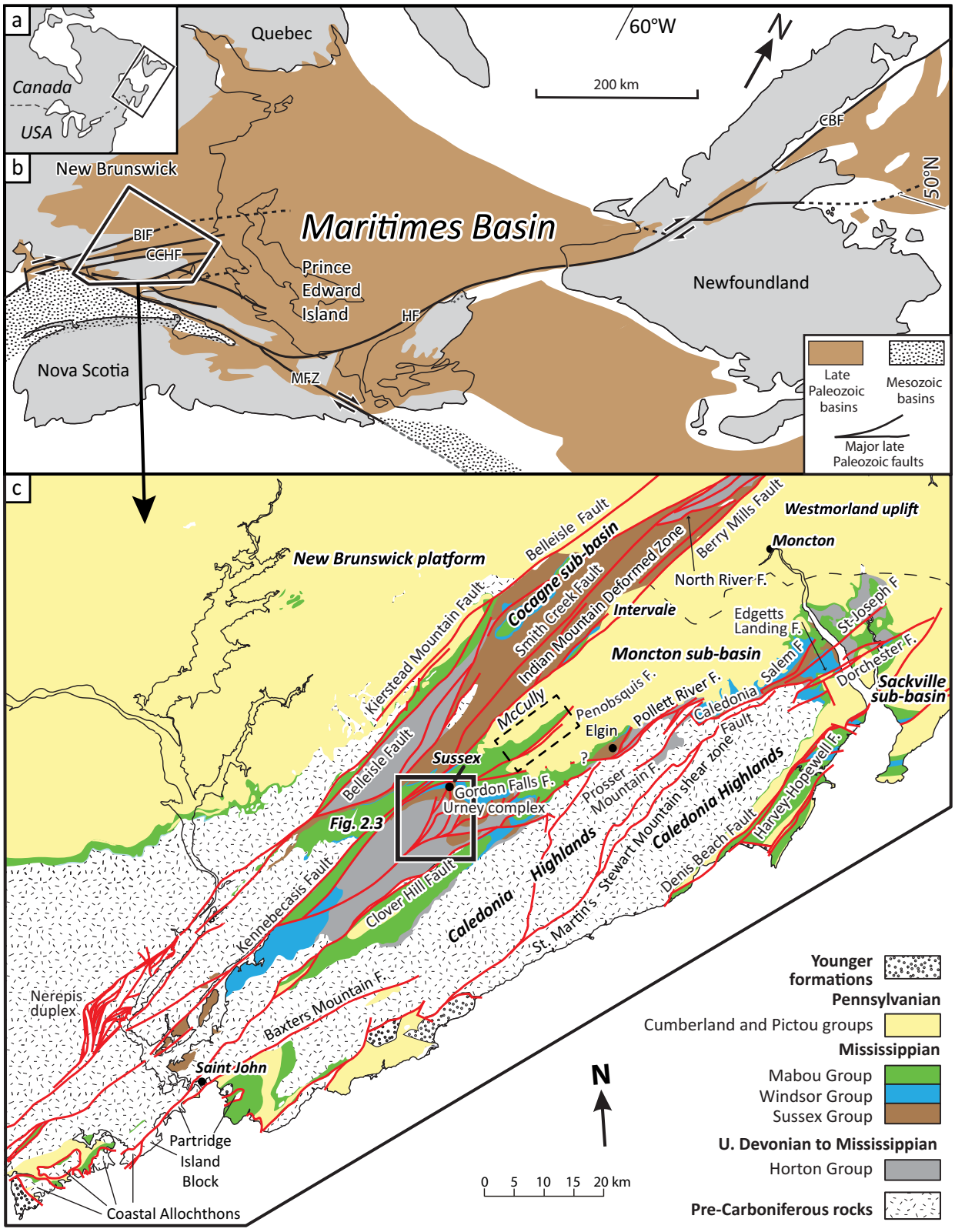
a
Canada
USA
Quebec
60°W
N
200 km
b
New Brunswick
Maritimes Basin
BIF
CCHF
Prince
Edward
Island
HF
CBF
50°N
Newfoundland
Nova Scotia
MFZ
Late
Paleozoic
basins
Mesozoic
basins
Major late
Paleozoic faults
c
New Brunswick platform
Belleisle Fault
Cocagne sub-basin
Smith Creek Fault
Indian Mountain Deformed Zone
Berry Mills Fault
Westmorland uplift
Moncton
North River F.
Intervale
Edgetts
Landing F.
St-Joseph F.
Moncton sub-basin
Salem F.
Dorchester F.
Sackville
sub-basin
Kierstead Mountain Fault
McCully
Penobsquis F.
Pollett River F.
Caledonia
Fault
Elgin
?
Sussex
Gordon Falls F.
Urney complex
Fig. 2.3
Belleisle Fault
Prosser
Mountain F.
Caledonia Highlands
Harvey-Hopewell F.
Stewart Mountain shear zone
Denis Beach Fault
Highlands
Caledonia
Clover Hill Fault
Kennebecasis Fault
St. Martin's
Nerepis
duplex
Baxters Mountain F.
Saint John
Partridge
Island
Block
Coastal Allochthons
N
0 5 10 15 20 km
Younger
formations
Pennsylvanian
Cumberland and Pictou groups
Mississippian
Mabou Group
Windsor Group
Sussex Group
U. Devonian to Mississippian
Horton Group
Pre-Carboniferous rocks

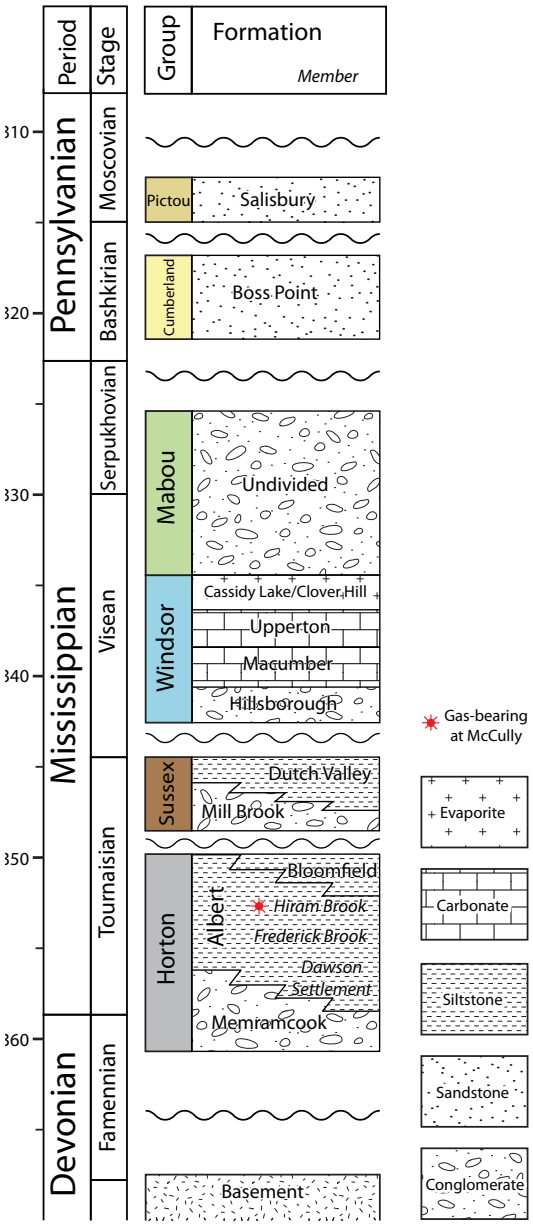

Figure 2.3. Geologic map of the Sussex area.

The location of the roadcuts in Figure 2.13 are shown. Modified from Hinds (2008a, 2008b). Abbreviations: cg = coarse-grained; mg = medium-grained; fg = fine-grained.

strike-slip faults (Figure 2.2c). The Caledonia Highlands mark the southern boundary of the sub-basin (Figure 2.2c; St. Peter, 1993; Barr and White, 1999); they are mainly intrusive and extrusive igneous rocks part of the Avalonia tectonostratigraphic assemblage of the early Paleozoic Appalachian orogen. The Caledonia – Clover Hill fault system separates the Caledonia Highlands from the Moncton Sub-basin (Figure 2.2c), which is probably underlain by the Appalachian domain Ganderia (Fyffe et al., 2011). Park et al. (2007) show that in the southwest, the Clover Hill fault zone is near vertical and displays up to 30 km of dextral strike-slip movement, documented by correlating facies in the earliest sub-basin sedimentary rocks. Towards the northeast, the Caledonia fault zone dips gently northwest where it displays strike-slip, normal, and reverse movements (Park and St. Peter, 2005; Park et al., 2007). The Kennebecasis – Indian Mountain fault zone separates the Moncton Sub-basin from the Kingston Uplift and the Indian Mountain Deformed zone (Figure 2.2c), acting as the northern boundary of the sub-basin (St. Peter, 1993). Park and St. Peter (2009) have interpreted this fault zone to dip gently southeast and, via correlating facies, to have had nearly 60 km of post-Devonian dextral strike-slip movement with a minor dip-slip component. Splays of the Kennebecasis – Indian Mountain fault zone, such as the Penobsquis and Gordon Falls faults (Figure 2.2c; 2.3), crosscut the sub-basin and ultimately link up with the Caledonia – Clover Hill fault zone (Wilson and White, 2006; Waldron et al., 2015).

Waldron et al. (2015) describe abundant NE – SW striking faults throughout the Maritimes Basin as having “Appalachian trend” (Figure 2.2) and suggested that movement along these faults was the primary control on sedimentation in the Moncton Sub-basin. Associated structures such as normal and reverse faults, folds, and secondary strike-slip faults formed throughout the sub-basin as a result of the major strike-slip deformation. Inversion of faults is commonly documented throughout the Moncton Sub-basin (e.g. Wilson, 2005; Wilson et al., 2006; Hinds and Park, 2009; Park et al., 2010), and may have occurred during later dextral transpression associated with approximately E-W striking faults of the “Minas Trend” (Figure 2.2; Waldron et al., 2015).

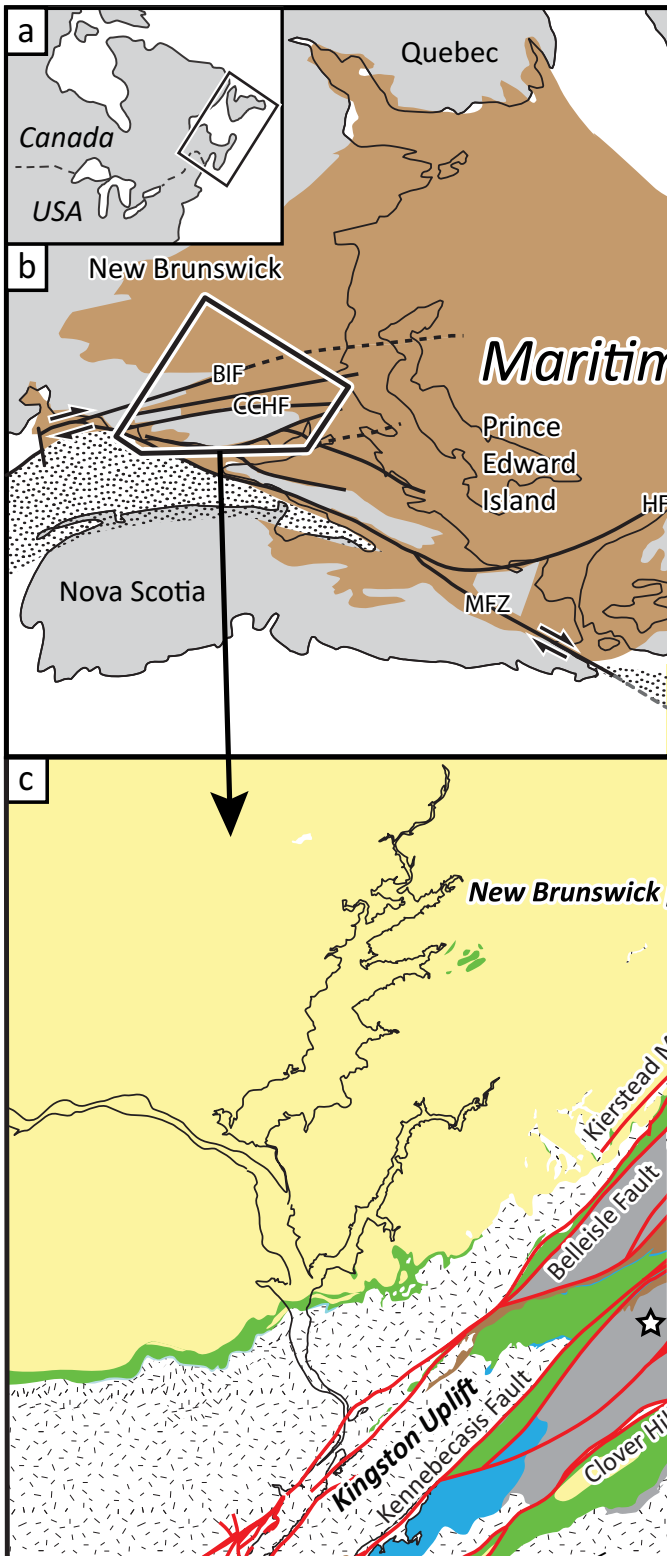

Figure 2.4. Stratigraphic chart of the western Moncton Sub-basin.

After Wilson and White (2006) and St. Peter and Johnson (2009). Dominant lithologies are shown. Ages and stages are from Davydov et al. (2012).

2.1.1.2. Western Moncton Sub-basin fill

The sedimentary fill of the western Moncton Sub-basin is up to 6 km thick and comprises terrestrial clastic sedimentary rocks with lesser marine carbonate and evaporite rocks (St. Peter and Johnson, 2009). The stratigraphy has been separated into 6 successions (Figure 2.4), which are, from the basement up, assigned to the Horton, Sussex, Windsor, Mabou, Cumberland, and Pictou groups (Wilson and White, 2006; St. Peter and Johnson, 2009). The Late Devonian to Early Mississippian (Tournaisian) Horton Group comprises terrestrial fine- to coarse-grained, red to grey clastic units. The later Tournaisian Sussex Group unconformably overlies the Horton Group and also comprises red to grey clastic units. The Visean Windsor Group is the only marine-influenced unit in the basin and contains coarse-grained clastic, limestone, and evaporite (gypsum, salt, anhydrite) rocks. The overlying Mabou, Cumberland, and Pictou groups primarily comprise terrestrial redbeds, mature mudstone beds, and quartzose sandstone beds with minor amounts of coal, spanning the upper Visean to lower Moscovian (Middle Pennsylvanian) stages.

In the western Moncton Sub-basin the Horton Group has been divided into the Memramcook, Albert, and Bloomfield formations, based on sedimentological variations between fine- to coarse-grained and red to grey units (Figure 2.4; Keighley, 2008; St. Peter and Johnson, 2009). Furthermore, because of the importance of its internal petroleum system, the Albert Formation (up to >1.5 km thick) has been separated into three members (Figure 2.4): the Dawson Settlement Member comprising dominantly grey sandstone and siltstone with minor dolomite; the Frederick Brook Member which contains dark colored kerogenous mudstone and siltstone with rare grey sandstone and conglomerate; and the Hiram Brook Member which comprises cycles of grey sandstone and organic-poor mudstone (Greiner, 1962; Keighley, 2008; St. Peter and Johnson, 2009). The members are probably partially laterally equivalent, reflecting lateral facies changes in the basin fill. The Albert Formation is interpreted to have been deposited in a fluvio-deltaic to lacustrine environment during the initiation of the western Moncton Sub-basin (Greiner, 1962; Keighley, 2008).

2.2. Methods

Detailed outcrop mapping was conducted at a set of four roadcuts, ranging length between 250 to 300 m, along Highway 1, SW of the City of Sussex. To make interpreted sections of each outcrop, photographs of the outcrops were taken and printed and interpretations were made directly on them in the field. The observed primary and secondary structural features included bedding, faults, slickenlines, folds, and cleavage planes. Strike and dip measurements were made on bedding planes at a minimum interval of 10 m along the length of each outcrop in order to identify outcrop-scale changes in the orientation of bedding. Fault planes were identified by recognizing offset bedding layers. Strike and dip measurements were made on all observed fault planes. Furthermore, the trend and plunge of slickenlines (lineations that indicate the movement direction of a fault) were measured where possible. The dip separation of each fault was measured – a measurement made parallel to each fault plane, down the dip of the fault between bedding plane cutoff lines (Figure 2.5). Fault heaves were calculated using a simple triangle construction of the dip separation and fault dip angle. Faults were then initially categorized based only on geometry; in some cases slickenlines provided additional information on kinematics. Thus faults were categorized as extensional if the hanging-wall cutoff was below the footwall cutoff and contractional if the hanging-wall cutoff above the footwall cutoff. For example, the fault in Figure 2.5 is considered an extensional fault because the dip separation is extensional, even though the strike slip (revealed by slickenlines) is large and the dip slip is actually reverse. In some cases, the apparent movement of the hanging wall relative to the footwall could not be distinguished. Although slickenlines represent the fault movement, they do not say which direction the fault moved along that line; chatter marks were used say which direction each side of the fault moved. In measuring folds, the trend and plunge of each fold axis was measured, and where possible, the strike and dip of the axial surfaces were also estimated or measured (Figure 2.6).

To aid in making interpreted outcrop sections and a geologic map for the set of roadcuts, 1115 photographs of the four roadcuts were taken. A digital interchangeable-lens camera with a

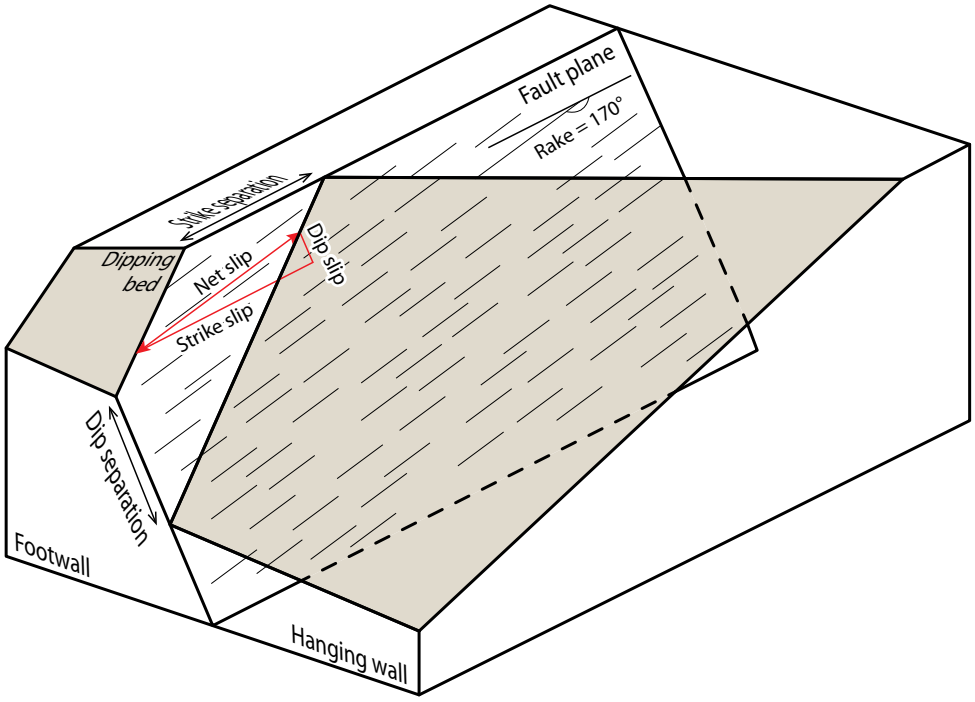

Figure 2.5. Block diagram of a dipping bed offset by a dextral strike-slip-dominated fault.

Faint lines on the fault plane represent slickenlines. The slickenlines have a rake of 170° in the fault plane. The definitions of dip-separation, strike-separation, net slip, strike slip, and dip slip are shown. The dip slip of this fault is reverse but the dip separation is normal.

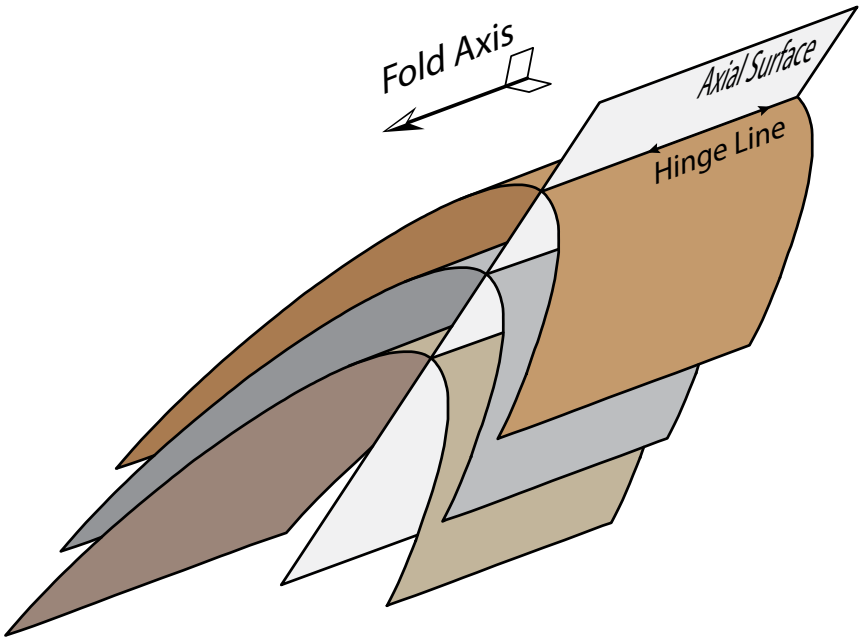

Figure 2.6. Schematic diagram of 3 folded beds.

The definitions of axial surface, fold axis, and hinge line are shown.

micro-four-thirds sensor was used, and each photograph had a resolution of 15.1 megapixels. Photographs were taken in fan arrays at an interval of 20 m along the length of the outcrop. Each roadcut had a set of close-up photographs, roughly 5 m away from the rock face, and a set of distant photographs, taken ~25 m away (Figure 2.7). This technique ensured that the photographs had the suggested (James and Robson, 2014) minimum of 60% overlap vertically and horizontally.

The photographs were then loaded into AgiSoft Photoscan software as *.jpeg* files. The photographs were taken during windy conditions which caused the vegetation to sway; trees and grass appear in slightly different positions in every photograph, which causes problems when AgiSoft Photoscan matches pixels between images. To account for this, the images were manually masked, removing pixels that were outside the rock face (Figure 2.8). Common marker points, such as traffic markers, placed cones, or distinct parts of the rock faces, were identified on each image to help AgiSoft correctly align the photographs in space (Figure 2.8). Each roadcut had a minimum of 7 marker points; more were added in complex places as needed. Each marker could be geospatially positioned by assigning GPS data. From there, the images were aligned in space by AgiSoft and common pixels were identified between the images (Figure 2.7). Typically, 1.5 to 2 million common pixels were initially found for each roadcut model. Following this, a dense point cloud (typically between 20 to 30 million points), a mesh (3D polygonal model of the outcrop), a texture (colored model of the outcrop), and a complete 3D model were made for each outcrop. Each model included ~2 million faces (Figure 2.9). High-quality orthomosaic photographs were made of each model (Figure 2.10). To do this, AgiSoft Photoscan orthorectified each model by taking out perspective and relief effects to create an image of the outcrop projected orthogonally onto a plane that has a constant scale throughout. Orthomosaic photographs were made in both vertical and horizontal planes. Vertical plane photographs were used for interpretations of each roadcut that approximated true cross-sections; horizontal plane photographs were used for making a geologic map (Figure 2.11). In these photographs, each pixel represents approximately 1 cm^2 of outcrop surface.

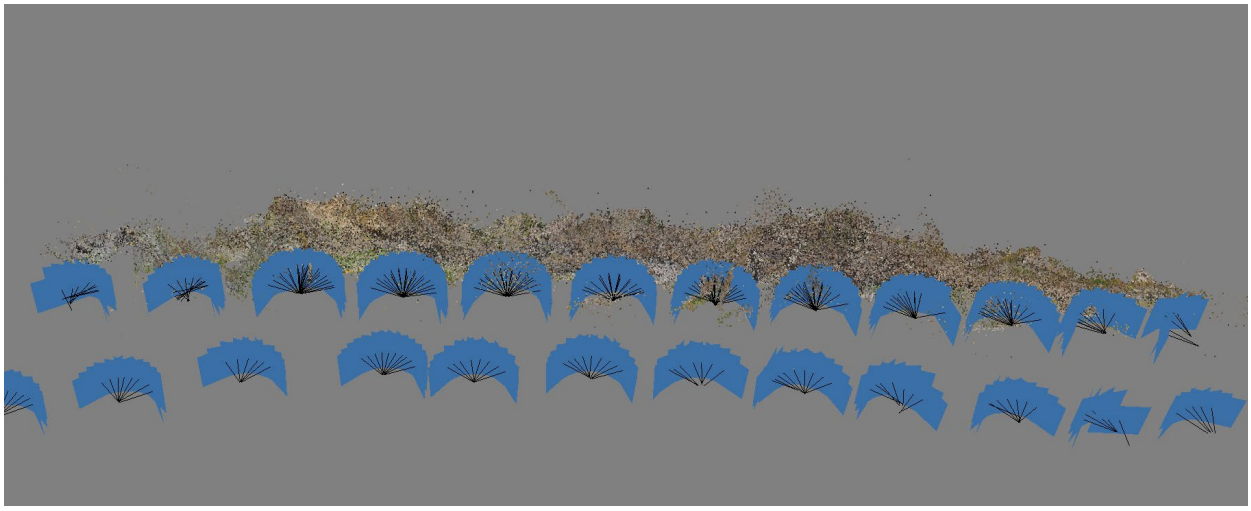

Figure 2.7. A screen capture from AgiSoft Photoscan Professional showing the aligned cameras.

The blue rectangles represent each photograph and the perpendicular black line shows where the image was taken from. See text for details on photography.

Figure 2.8. An example of a pre-processed photograph used in the 3D model created in AgiSoft Photoscan Professional.

Vegetation was masked (shaded areas) so that the changing position of trees and grass did not affect the alignment process of the images. A marker (yellow flag labelled 071) is placed at a recognizable fault; markers were used to better align the photographs.

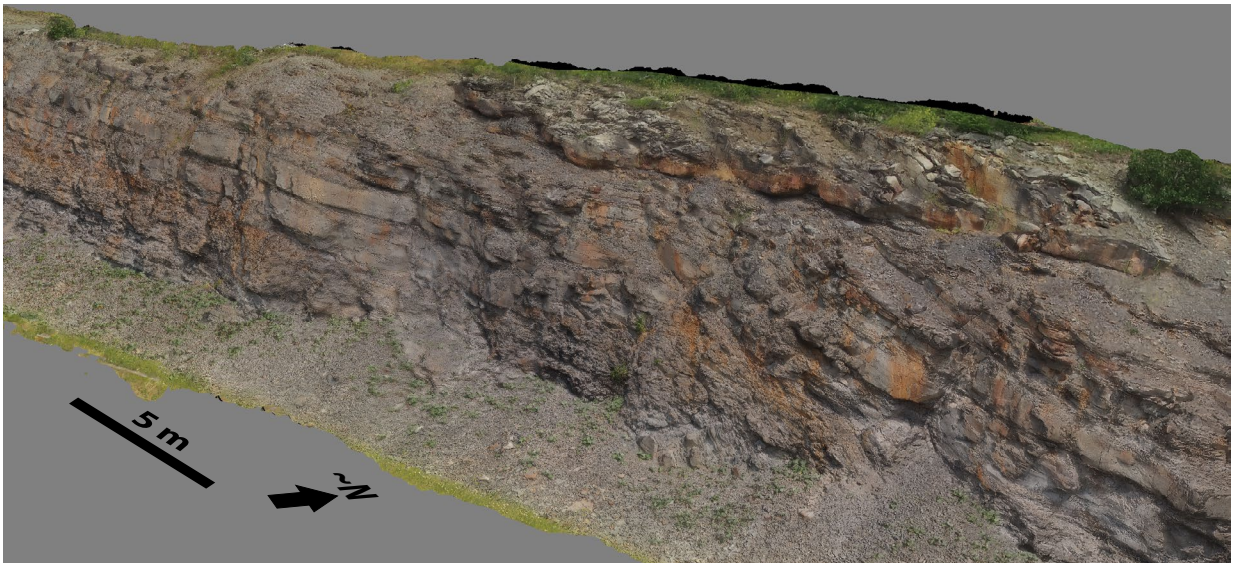

Figure 2.9. A screen capture of a 3D model of a small portion of the northern roadcut. The model is viewed at ~45° to the rock face to highlight the 3D nature of the model.

Figure 2.10. A small portion of a vertical orthomosaic photograph of the northern roadcut.

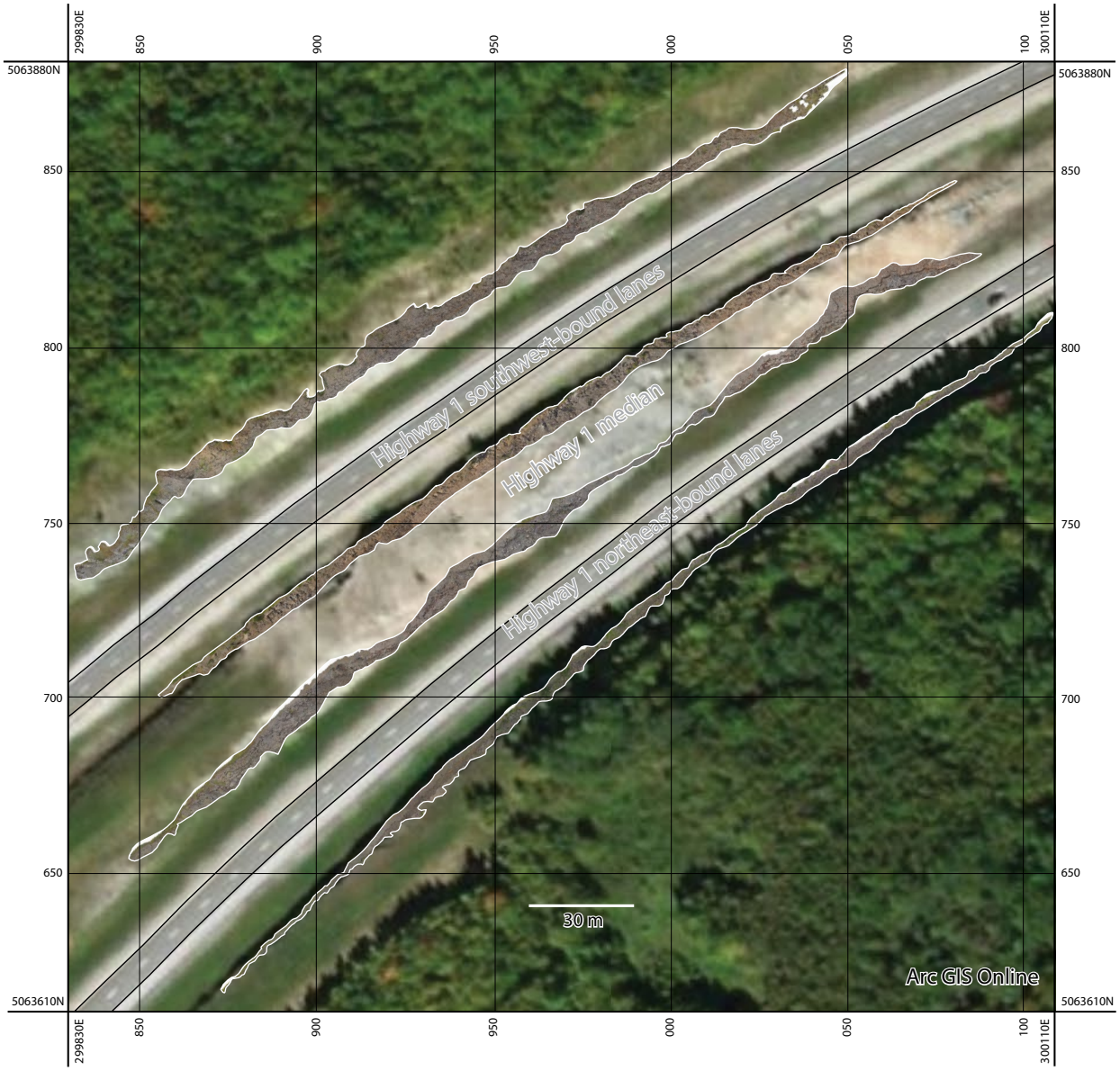

Figure 2.11. Top down orthomosaic photographs overlain on a satellite photograph.

Orthomosaic photographs of four outcrops (outlined in white) were made using AgiSoft Photoscan Professional. Stratigraphic boundaries and fault traces could be accurately traced on the top-down orthophotographs. Satellite photograph is provided by ArcGIS Online.

2.3. Stratigraphy

In general, the sedimentary rocks at the study area are dominated by interbedded sandstone, siltstone, and mudstone beds. These rocks are part of the Albert Formation (Figure 2.4) and likely belong to the Hiram Brook Member (S. Hinds, New Brunswick Department of Natural Resources and Energy, personal communication, 2017). The siltstone and sandstone beds are typically grey and the mudstone beds are typically dark grey to greenish. Less frequent lithologies include iron-rich siltstone, mudstone, and ooidal packstone beds that are reddish-orange. In total, more than 50 m of sedimentary section is present at the study area. The rocks are here separated into 5 units, individually measured by direct contact with a ruler perpendicular to bedding (Figure 2.12). The distribution of these units is shown in Figure 2.13. Some of the units have been further divided into sub-units (Figure 2.12) and the distribution of the sub-units is shown in Figure 2.14. The contacts between the sub-units are used as markers to allow correlation of stratigraphy across faults.

2.3.1. Unit 1 – Dark shale beds interbedded with thin sandstone beds

This unit dominantly comprises dark grey to black shale beds interbedded with thinly bedded, fine- to very fine-grained brown sandstone units. The shale is commonly planar laminated and recessive. Sandstone beds are typically <30 cm thick and are weakly laminated. In places, the sandstone beds are lenticular and pinch out along depositional strike. The fine-grained sandstone beds are commonly associated with rip-up clasts at the base of the beds and iron staining. The percent of shale is ~50% at the base of the unit and increases to >80% near the top of the unit. This unit has a thickness of ~6 m. However, the base is not observed at the roadcuts.

2.3.2. Unit 2 – Cross-bedded grey sandstone beds interbedded with dark shale beds

Unit 2 is dominated by grey fine- to medium-grained cross-bedded and wave-rippled sandstone beds. This unit has an erosional contact with unit 1. Sand beds are interbedded with dark shale beds and display an overall fining-upward sequence. The bed thickness also decreases upwards.

This unit is about 12 m thick.

Unit 2a. This sub-unit contains thick (>2 m) cross-bedded, medium-grained, grey sandstone units that fine upwards interbedded with dark grey to black shale interbeds that show planar laminae and create thick packages of >2 m. The sandstone beds commonly have sharp undulatory bases, contain rip-up clasts, and have plant material spread throughout. Sandstone accounts for about 60% of this sub-unit.

Unit 2b. The thickness of the beds and grain size of the sandstone units decrease upward from Unit 2a. Here, the sandstone beds are commonly <50 cm thick. Cross-bedding is rare but symmetrical ripples are common on the bases and tops of the sandstone units. Dark shale interbeds are poorly laminated and typically are <30 cm thick. The percentage of sandstone is >75%.

2.3.3. Unit 3 – Greenish grey paper shale

Unit 3 comprises greenish-grey planar laminated, extremely fissile shale, herein referred to as a paper shale. It is recessive except where coarser silty beds are present. Decimetre-scale silt beds commonly display chaotic and convolute laminae (Figure 2.15a). This unit gradationally overlies Unit 2 and has a total thickness of ~5 m.

2.3.4. Unit 4 – Blocky siltstone beds

This unit is dominated by blocky grey siltstone beds that are weakly laminated and interbedded with brownish-grey mudstone beds. The blocky siltstone beds are prominent in the outcrops as they are surrounded by recessive mudstone beds. The unit gradationally overlies Unit 3 and is about 10 m thick.

Unit 4a. At the base of this sub-unit grey siltstone beds are weakly laminated and ~20 cm thick, increasing to a maximum of 1.3 m. Decimetre-scale mudstone interbeds display planar laminae.

Unit 4b. This sub-unit comprises entirely a grey, weakly laminated blocky siltstone bed that is ~1 m thick. A thin (5 – 10 cm) shale bed separates sub-unit 4a and 4b.

Unit 4c. The thickness of the siltstone beds are typically <50 cm in this sub-unit. Sandy siltstone beds are commonly iron-rich, have rip-up clasts at the bases, and are bitumen stained. Siltstone and sandy siltstone are interbedded with weakly laminated mudstone. Sandstone dykes cutting up through siltstone layers are sporadic (Figure 2.15b; 2.15c).

2.3.5. Unit 5 – Interbedded grey sandstone and siltstone beds with minor mudstone and carbonate beds

This unit is dominated by grey cross-bedded sandstone and planar laminated siltstone, interbedded with minor amounts of dark grey mudstone. It is here divided into three sub-units. Sub-units a and c are lithologically similar, display an overall fining-upward sequence, and are separated by an iron-rich ooidal packstone bed of sub-unit b. Unit 5 has a sharp and undulatory contact with Unit 4. This unit is ~20 m thick in the outcrops with no observed top contact in the roadcuts.

Unit 5a. Grey, cross-bedded medium- to fine-grained sandstone beds with thicknesses ranging between 3 m to <30 cm are found at the base of Unit 5. The sands are interbedded with planar laminated mudstone. In some cases, the sandstone beds are channelized, pinching-out along strike, and show normal grading. It is common for the sandstone beds to contain rip-up clasts at their bases and sporadic plant material throughout. Symmetrical ripples are limited to the thinner sandstone beds. Sandstone accounts for ~70% of the rocks in this sub-unit.

Unit 5b. An orange, iron-rich ooidal packstone bed sharply overlies sub-unit 5a. This sub-unit ranges between 20 and 40 cm in thickness.

Unit 5c. This sub-unit comprises interbedded thin (typically <1 m thick) fine- to very fine-grained cross-bedded sandstone beds, planar laminated silty sandstone beds, and dark grey to black, planar laminated mudstone beds. The basal mudstone bed that sharply overlies the sub-unit 5b contains a large amount of fish-scale fossils. Sandstone comprises roughly 70% of the rocks at the base of this sub-unit and about 20% near the top. This sub-unit fines upwards to thicker bedded (up to 2.5 m), blocky siltstone beds near the top.

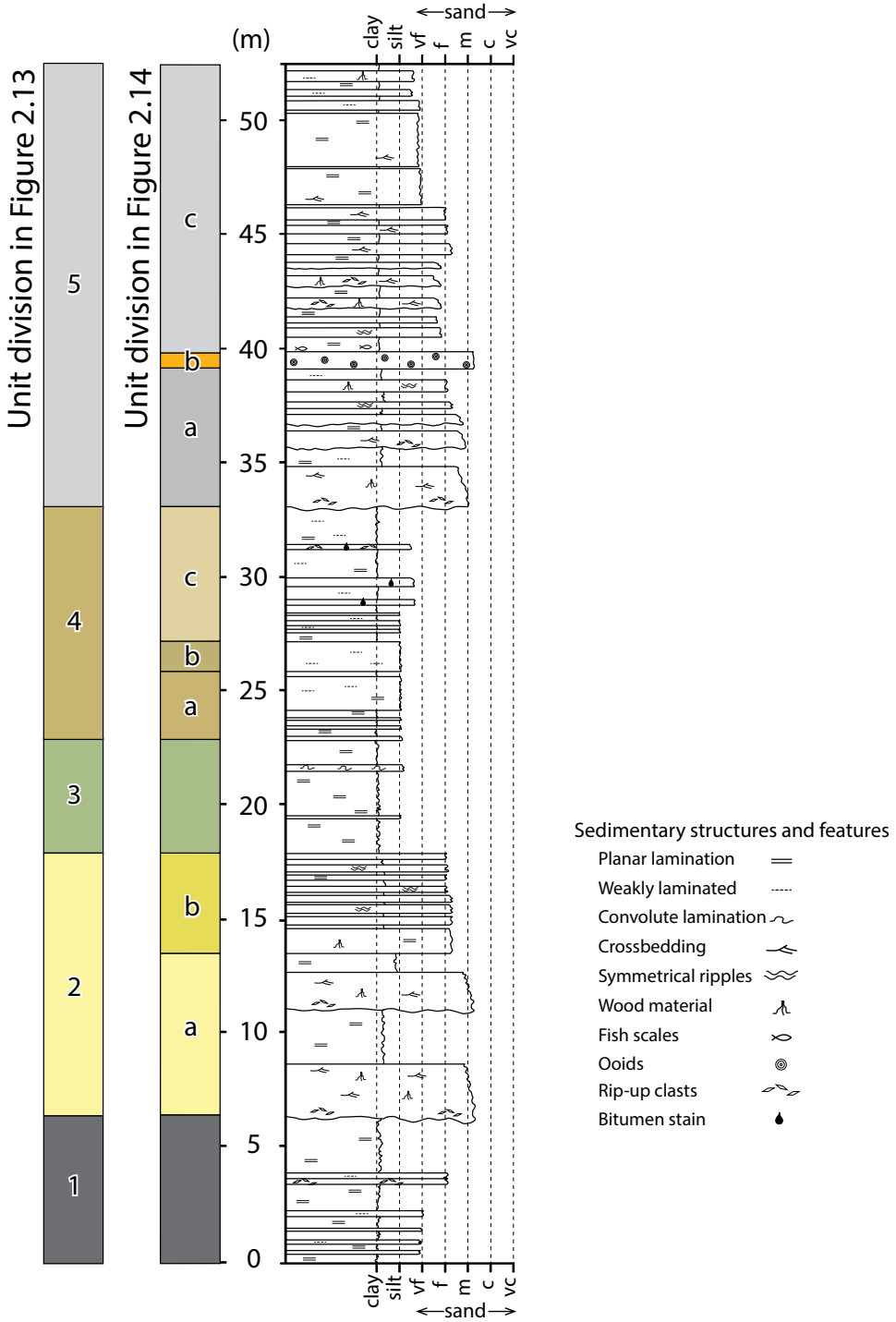

Figure 2.12. Generalized stratigraphic log of units 1-5 at the study area.

Figure 2.13. Geologic map of four roadcuts along Highway 1, roughly 3 km SW of the City of Sussex, New Brunswick.

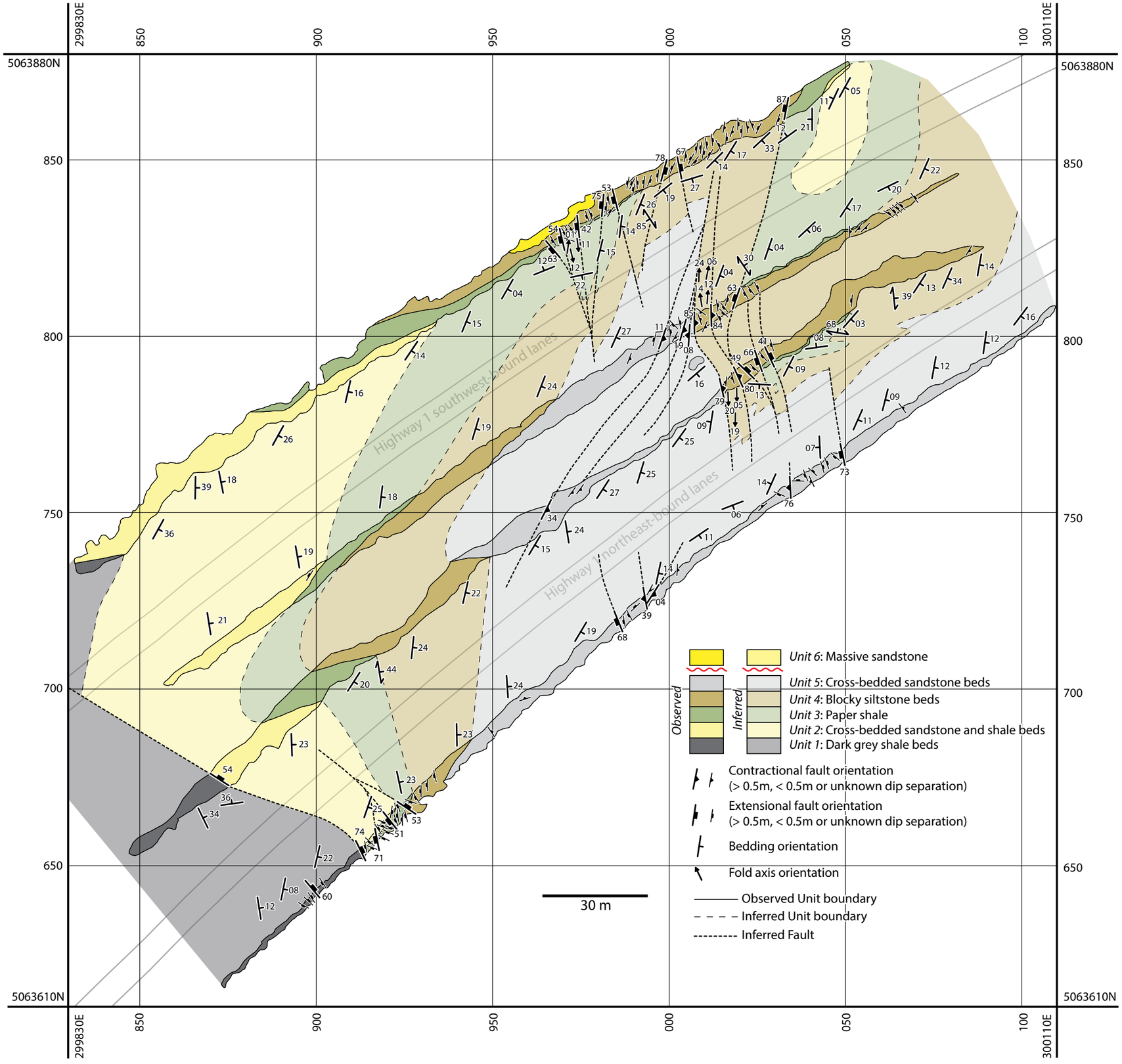

Figure 2.13. Geologic map of four roadcuts along Highway 1, roughly 3 km SW of the City of Sussex, New Brunswick.

Pocket

Figure 2.14. Interpreted vertical sections of the four roadcuts along Highway 1.

Orthomosaic photographs were made using AgiSoft Photoscan Professional. See Figure 2.12 for details on lithologies of each unit. (a) North face along SW-bound lanes. (b) North face of the median. (c) South face of the median. (d) South face of the NE-bound lanes.

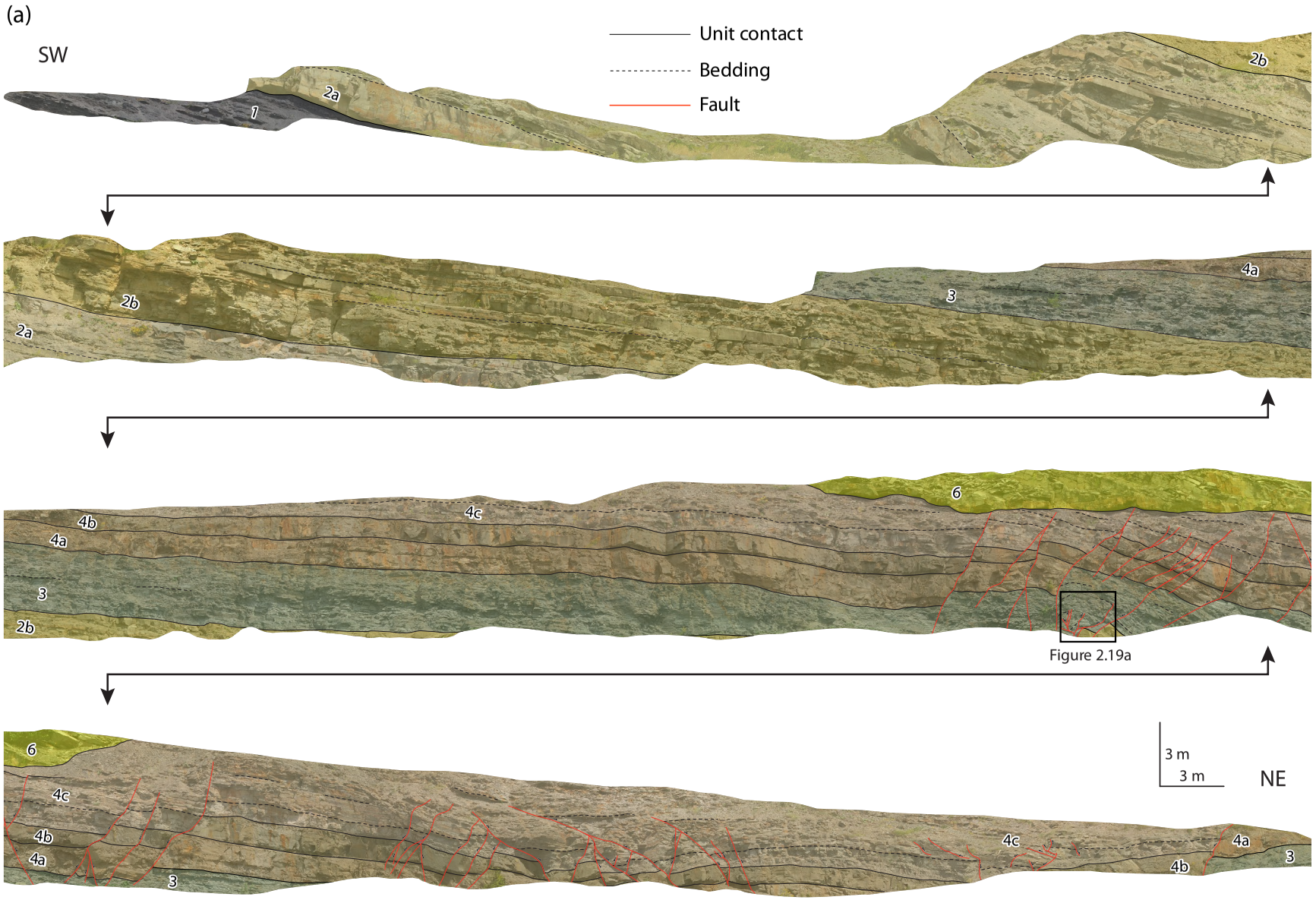
(a)
SW
Unit contact
Bedding
Fault
1
2a
2b
3
4a
4b
4c
6
Figure 2.19a
3 m
3 m
NE

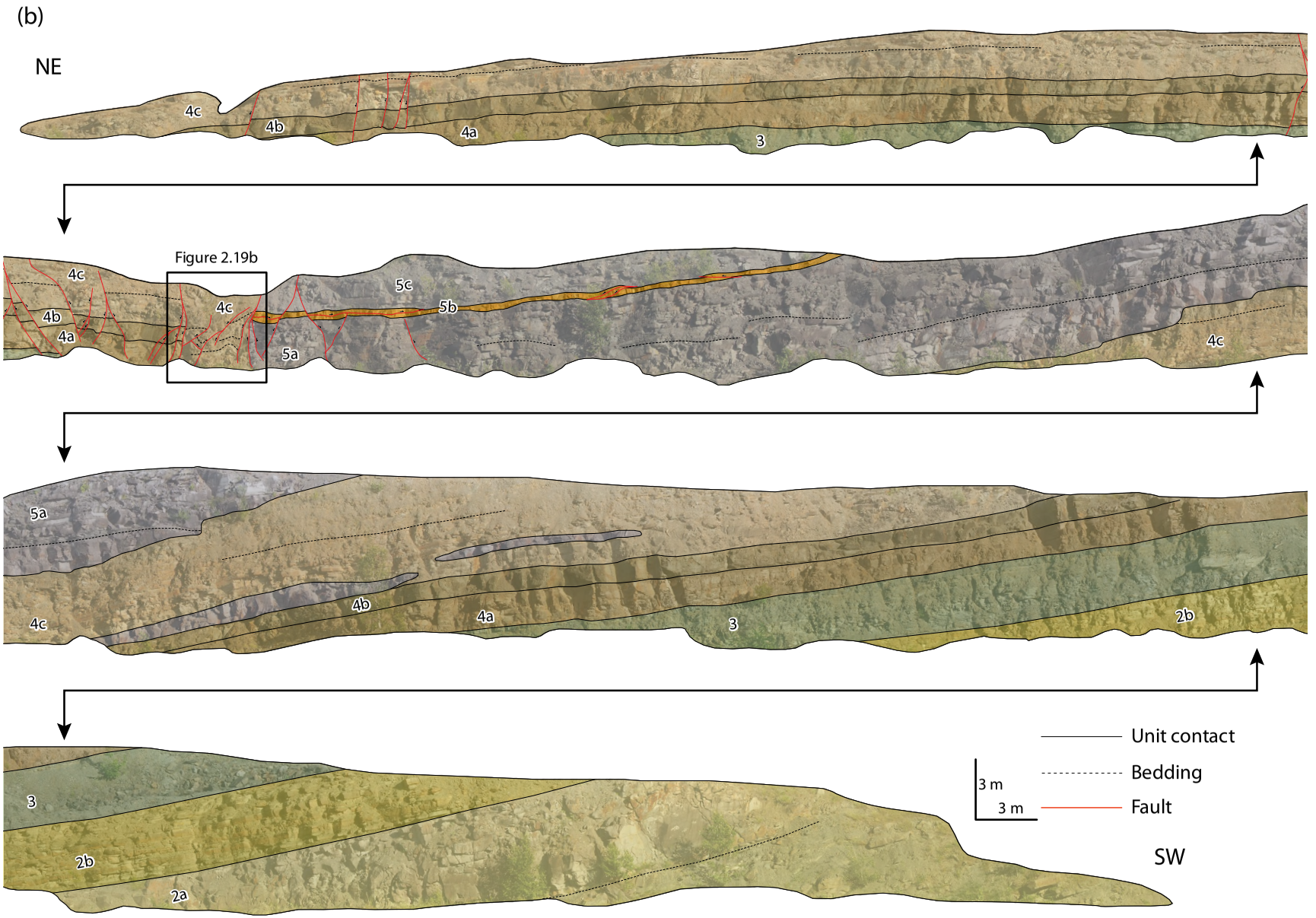
(b)
NE
4c
4b
4a
3
Figure 2.19b
4c
4b
4a
4c
5a
5c
5b
4c
5a
4b
4a
3
2b
4c
3
2b
2a
Unit contact
Bedding
Fault
3 m
3 m
SW

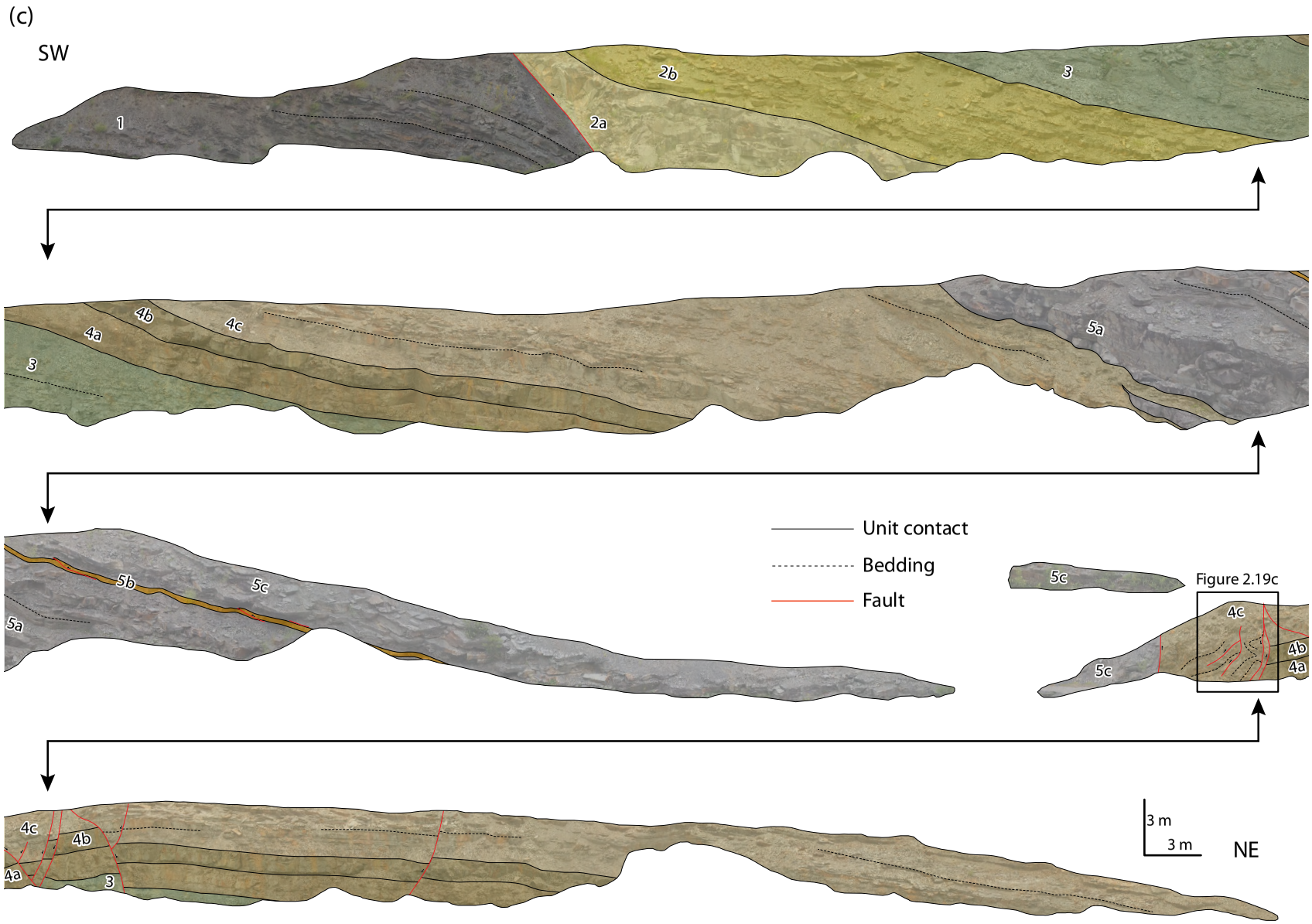
(c)
SW
1
2a
2b
3
3
4a
4b
4c
5a
5a
5b
5c
Unit contact
Bedding
Fault
5c
Figure 2.19c
4c
4b
4a
5c
4c
4b
4a
3
3 m
3 m
NE

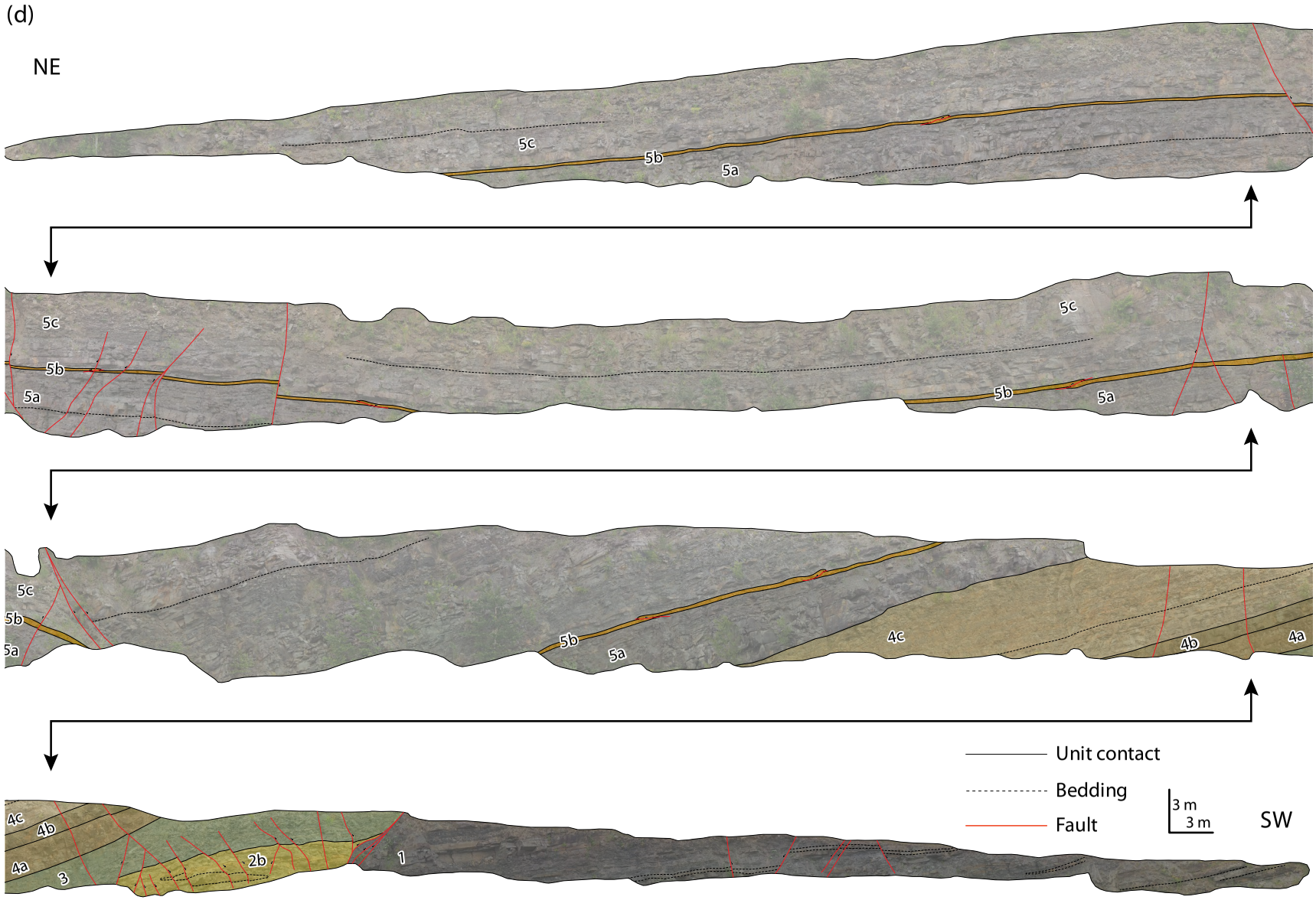
(d)
NE
5c
5b
5a
5c
5b
5a
5c
5b
5a
5c
5b
5a
4c
4b
4a
Unit contact
Bedding
Fault
3 m
3 m
SW
4c
4b
4a
3
2b
1

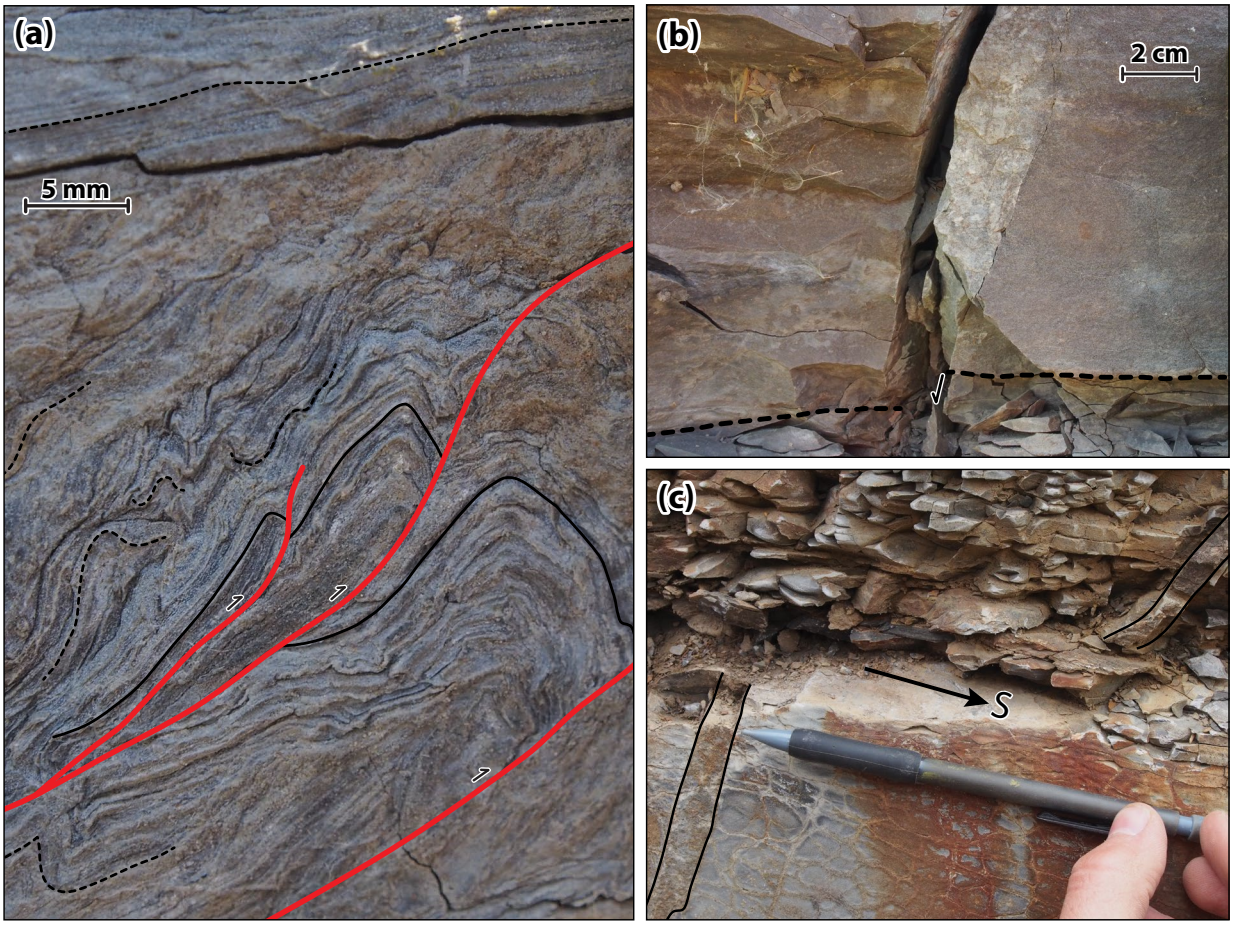

Figure 2.15. Structures observed in Units 3 and 4.

(a) Contractional faults and folds in laminae confined to a single bed in Unit 3. Note the parallel strata directly above the bed. Red lines indicate faults and black lines trace stratigraphy. (b) A sandstone dyke following an extensional fault plane in Unit 4. The black dashed line traces the offset bedding. (c) Sandstone dyke offset by an approximately bedding parallel fault in Unit 4. Abbreviation: S = slickenline orientation.

2.3.6. Unit 6 – Massive sandstone

This unit comprises a reddish brown, structureless, fine-grained sandstone that has a sharp and undulatory base.

2.4. Faults

Faults were the most abundant structure observed at the roadcuts. Extensional, contractional, and strike-slip faults were all observed to offset the strata. They ranged greatly in amount of dip separation, from a few centimetres up to a few metres. Dip separations could not be measured or accurately estimated on all faults. The core zone of the faults is typically <5 cm in width.

A total of 134 faults were measured; 93 showed some amount of extension; 23 showed some amount of shortening; and 18 showed no evidence of extension or shortening (Figure 2.16). 56 faults with calcite mineral lineations (slickenlines; Figure 2.17) were identified.

2.4.1. Extensional faults

Extensional faults were found in clusters throughout the roadcuts (Figure 2.13), often with a high density of faults near ones with large dip-separations. The highest density of faults was observed in the NE portion of the northern roadcut (Figure 2.13). The majority of faults extended vertically across the entire outcrop, except ones that were truncated by an erosional surface (Figure 2.14). The poles to the fault planes were plotted on an equal area projection, shown in Figure 2.16a. The plotted faults show that there is a system of conjugate extensional faults with mean orientations of 167/59 and 337/66. An angle of 56° separates the two average orientations. 26 extensional faults were observed to have calcite slickenlines, 17 of them having a rake ≤ 30° or ≥ 150°, indicating that a large portion of movement was strike-slip. Typically, extensional faults with large dip separation could be traced from one roadcut to another (Figure 2.13). However, many extensional faults with small dip separation could not be traced. When tracing the faults along strike, out of the rock faces, these faults commonly converge and likely join up

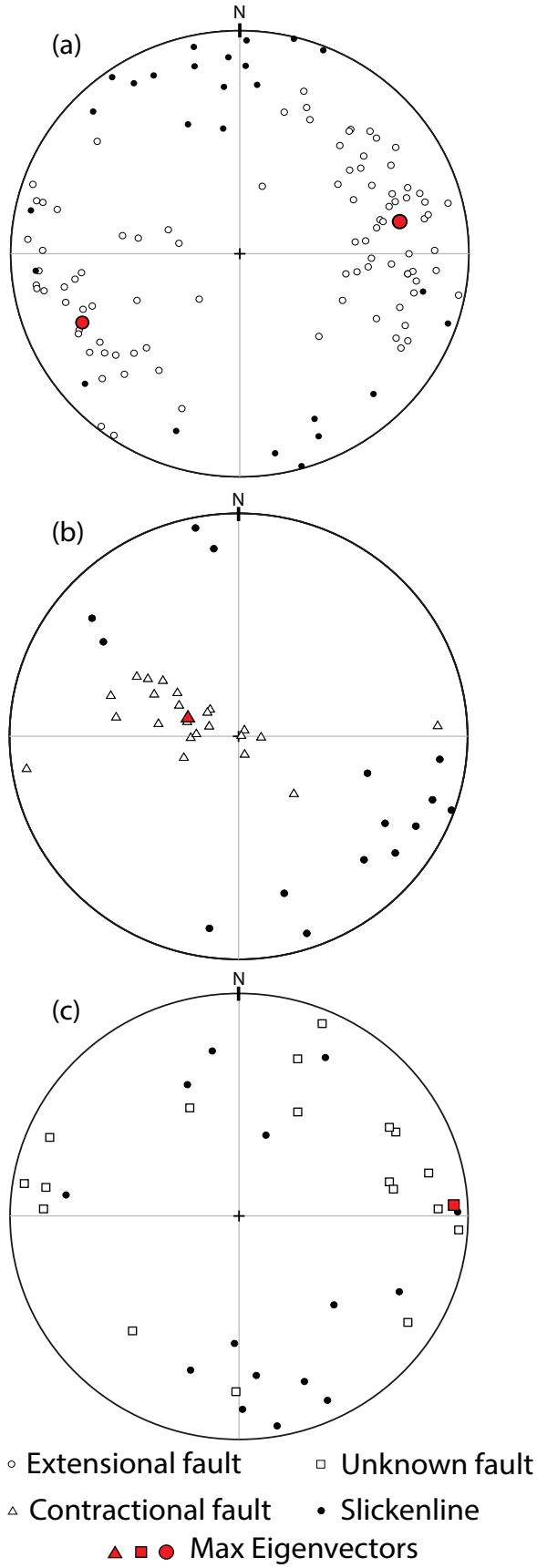

Figure 2.16. Equal-area projected stereoplots of poles to the fault planes at the four roadcuts along Highway 1.

(a) Poles to the extensional faults. Maximum eigenvectors are shown for each conjugate fault. (b) Poles to the contractional faults. (c) Poles to faults that did not show any evidence for extension or contraction. Note that no correction has been made for bias due to the preferred NE – SW orientation of the outcrops, which may have influenced these distributions.

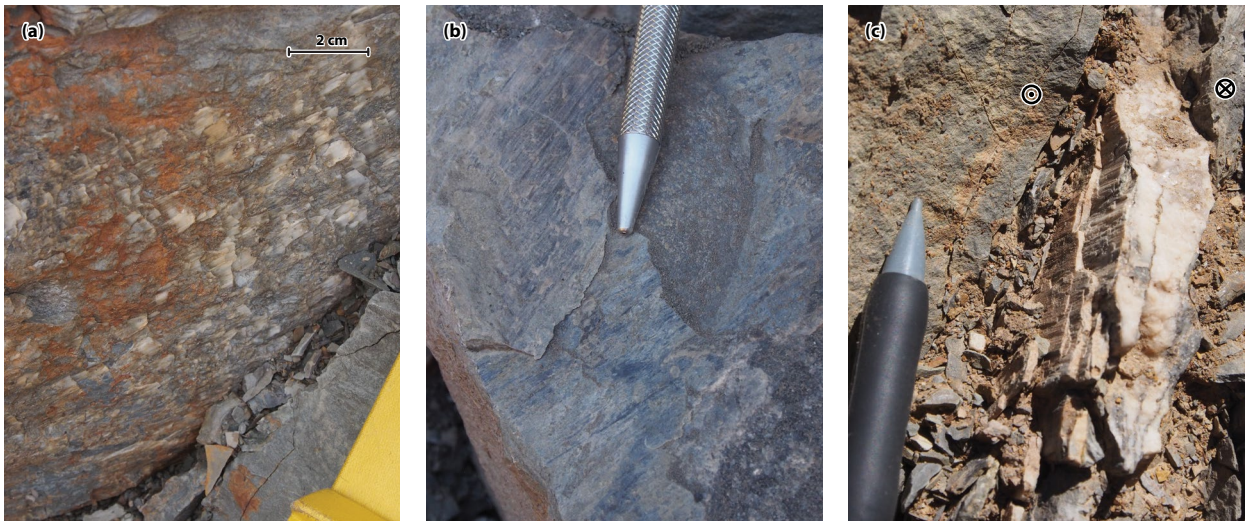

Figure 2.17. Calcite mineral lineations on fault surfaces.

(a) A steep fault plane with typical slickenline and chatter-mark structures. The chatter-marks indicate that the facing surface has moved to the left. (b) Overprinting slickenlines representing two generations of fault slip. (c) Typical calcite mineralization on fault planes containing slickenlines with a very shallow rake and chatter-marks. The footwall moved into the rock face and the hanging-wall moved out of the rock face (sinistral).

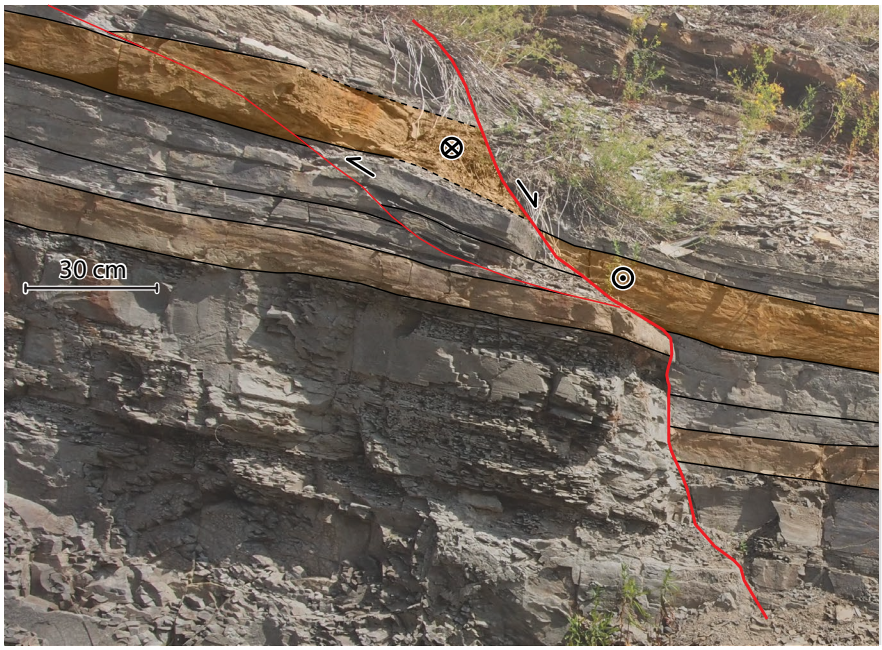

Figure 2.18. Interpreted outcrop photograph illustrating the complex relationship between extensional and contractional faults.

A curved extensional fault with dominantly strike slip movement has produced a contractional fault in the footwall of the extensional fault. The iron-rich siltstone (orange) creates a "knob" in the hanging wall at the curved portion of the extensional fault. The hanging wall of the extensional fault is interpreted to have moved towards the viewer, creating contractional deformation in the footwall.

(Figure 2.13). The dip of extensional faults varied along the height of the fault in places (Figure 2.18) typically showing gentler dips in finer-grained units. An extensional fault with a core zone width of ~50 cm and an interpreted large dip-separation is present at the SE end of the southern roadcuts (Figure 2.13). Due to the lack of exposure of Unit 1, reliable marker beds cannot be identified to stratigraphically position the siltstone beds in the footwall of this fault, so its exact separation is unknown.

2.4.2. Contractional faults

The contractional faults were mostly confined to the ooidal packstone beds (Unit 5b) and heavily deformed areas (Figure 2.19). These faults form a cluster on the equal-area stereoplot (Figure 2.16b) that has an average orientation of 020/21. Out of the 16 contractional faults containing calcite slickenlines, only 4 had a rake of $\leq 30°$ or $\geq 150°$, highlighting that the movement of these faults was primarily dip-slip and not strike-slip. Locally, contractional faults were also found next to extensional faults that had a changing dip (Figure 2.18).

2.4.3. Other faults

This category includes 18 faults where the dip-separation could not be estimated either due to the inability to match beds across the fault or because there was no apparent dip-separation. These faults have a similar conjugate relationship and orientations (Figure 2.16c) to the extensional faults (Figure 2.16a).

2.5. Folds

Folds are not as common as faults. At outcrop-scale, variations in the dip across the roadcuts define large open folds, such that when plotted on an equal-area stereoplot, poles to bedding measurements across all four roadcuts form a girdle about a calculated fold axis of 183-04 (Figure 2.20a). Locally, bedding is folded more tightly in the hanging walls and footwalls of faults with large dip separation (Figure 2.14). Smaller, tight folds are confined to heavily deformed areas of

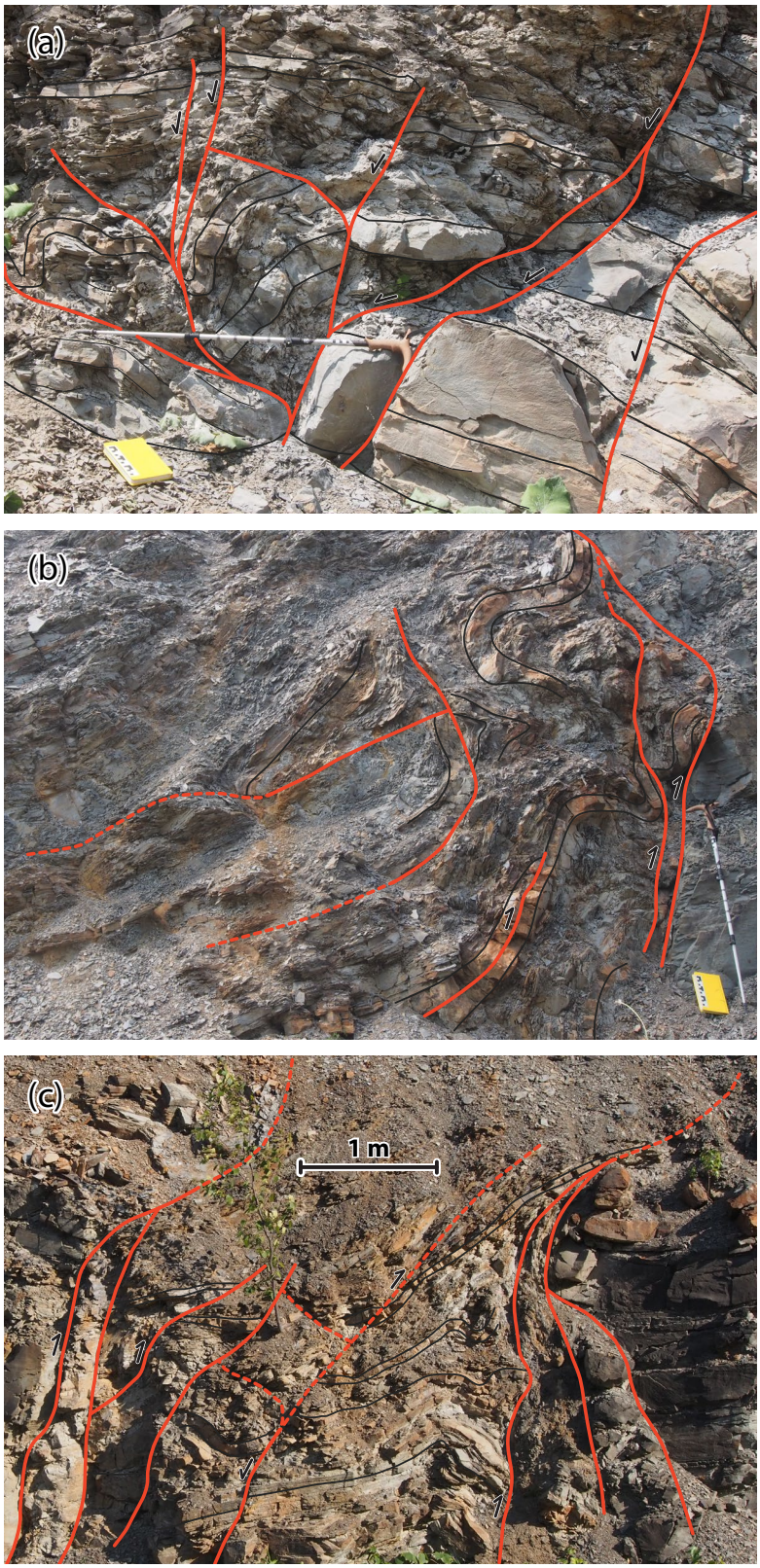

Figure 2.19. Close-up interpretations of heavily deformed areas.

Locations of (a), (b), and (c) are shown in Figure 2.14. The walking stick is 1 m long.

the northern roadcut and both roadcuts along the highway median (Figure 2.19). Amplitudes of the folds in these areas are decimetre-scale. The highly deformed area in the northern outcrop cannot be traced to other roadcuts and is likely truncated southward (Figure 2.13). However, a highly deformed area is present on either side of the highway median. This high-deformation zone trends roughly N – S, contains beds from Unit 4c, and is bounded by reverse faults on either side with less deformed rocks to the E and W (Figure 2.14b; 2.14c). This zone cannot be traced to the northern and southern roadcuts (Figure 2.13). In this high-deformation zone, fold axes generally gently plunge both N and S (Figure 2.20b) and axial surfaces have a range of orientations that form a rough E – W girdle on a stereoplot (Figure 2.20b). The variability in axial surface orientation could be a result of: (a) fault-related folds (e.g. listric faults, fault-bend folds, fault-propagation folds); or (b) a later deformation event that has folded earlier axial surfaces.

2.6. Unconformity

In the middle of the northern roadcut, faults that create clear offsets in Units 3 and 4 appear to be truncated by the base of Unit 6 at the top of the outcrop (Figure 2.14a). Additionally, beds within Unit 4 are truncated at the contact with the overlying Unit 6. The irregular character of the contact indicates that it is erosional and not tectonic in origin. This contact is herein interpreted to be an unconformity. The unconformity is only observed in the northern roadcut as it is interpreted to have extended above the highway median and the southern roadcut; it has been removed at these locations.

2.7. Discussion

2.7.1. Timing of deformation

Overall, observations made at the outcrops suggest that much of the deformation occurred soon after deposition. Small contractional faults and folds confined to decimetre-scale mudstone beds in Unit 3 (Figure 2.15a) are interpreted to have formed before the overlying, undeformed

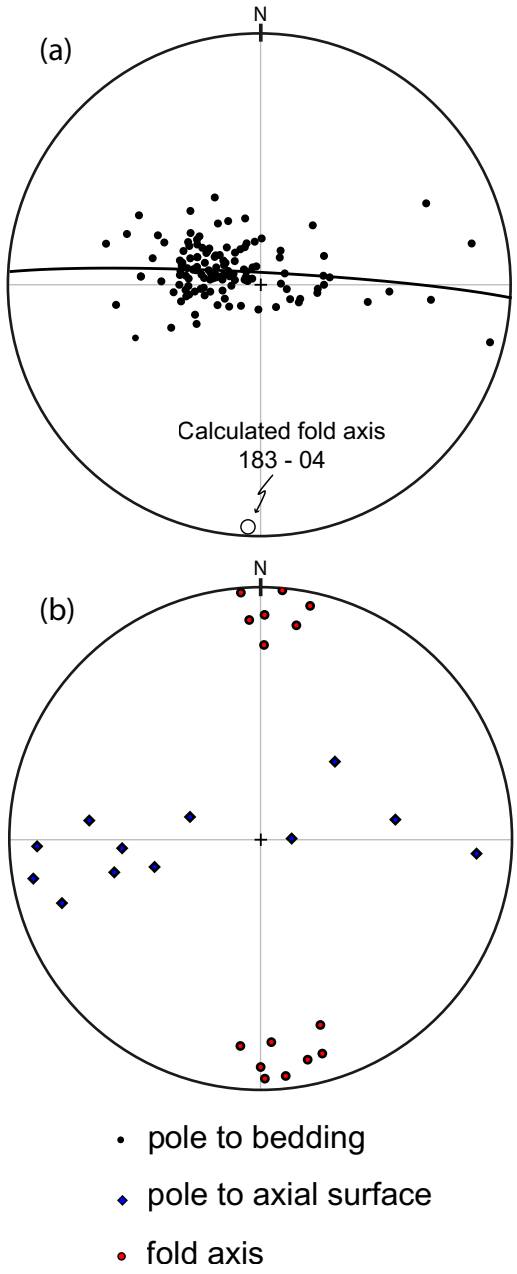

Figure 2.20. Equal-area projected stereoplots of poles to bedding, poles to axial surfaces, and fold axes at the four roadcuts along Highway 1.

(a) The poles to bedding form a girdle about a calculated fold axis of 183-04. (b) Majority of the axial surfaces and the fold axes measurements were made in the highly deformed areas in the three northern outcrops.

mudstone beds were deposited; there is no evidence of deformation along the contact. This highly convolute bedding may represent slumps resulting from periodic seismicity (Alsop and Marco, 2011). Additionally, the sandstone dykes that cut up through siltstone beds in Unit 4 are interpreted to have formed when fluidized sands were injected up into the overlying, unlithified siltstones (Jolly and Lonergan, 2002). Seismicity-induced liquefaction of recently deposited sand is common in tectonically active areas (Jolly and Lonergan, 2002). In cases where the sandstone dykes follow faults, it is interpreted that the sands were injected up pre-existing fault planes. Overall, these observations are interpreted to be results of soft-sediment deformation. Work by Wilson (2005) presents the idea that the soft-sediment deformation within the Horton Group in southern New Brunswick was likely triggered by earthquake activity. Furthermore, the interpreted unconformity at the top of the northern roadcut, where faults within the underlying Units 3 and 4 are truncated by Unit 6, suggests that the deformation that resulted in the development of the extensional faults ended before the sandstone was deposited. Together, these observations suggest that deformation of the Albert Formation at the study location occurred soon after deposition.

2.7.2. Tectonic environment

The structures observed at the four studied roadcuts along Highway 1 are consistent with the structures expected to form in a strike-slip tectonic setting (Harding, 1974). The critical observations include: (1) a set of conjugate extensional faults that have average orientations of 167/59 and 337/66 and corresponding slickenline orientations suggesting a large component of strike slip; (2) contractional faults that have an average orientation of 020/21 and corresponding slickenline orientations that suggest a large component of dip slip; and (3) gentle outcrop-scale folding of the bedding about a calculated mean fold axis of 183-04. The angle between the average strike of the contractional faults and of the dominant extensional faults (167/59) is 33° (Figure 2.21). The angle between the mean fold axis trend and the average strike of the dominant extensional fault is 16° (Figure 2.21).

In ideal strike-slip (simple shear), the extensional and contractional structures are expected to

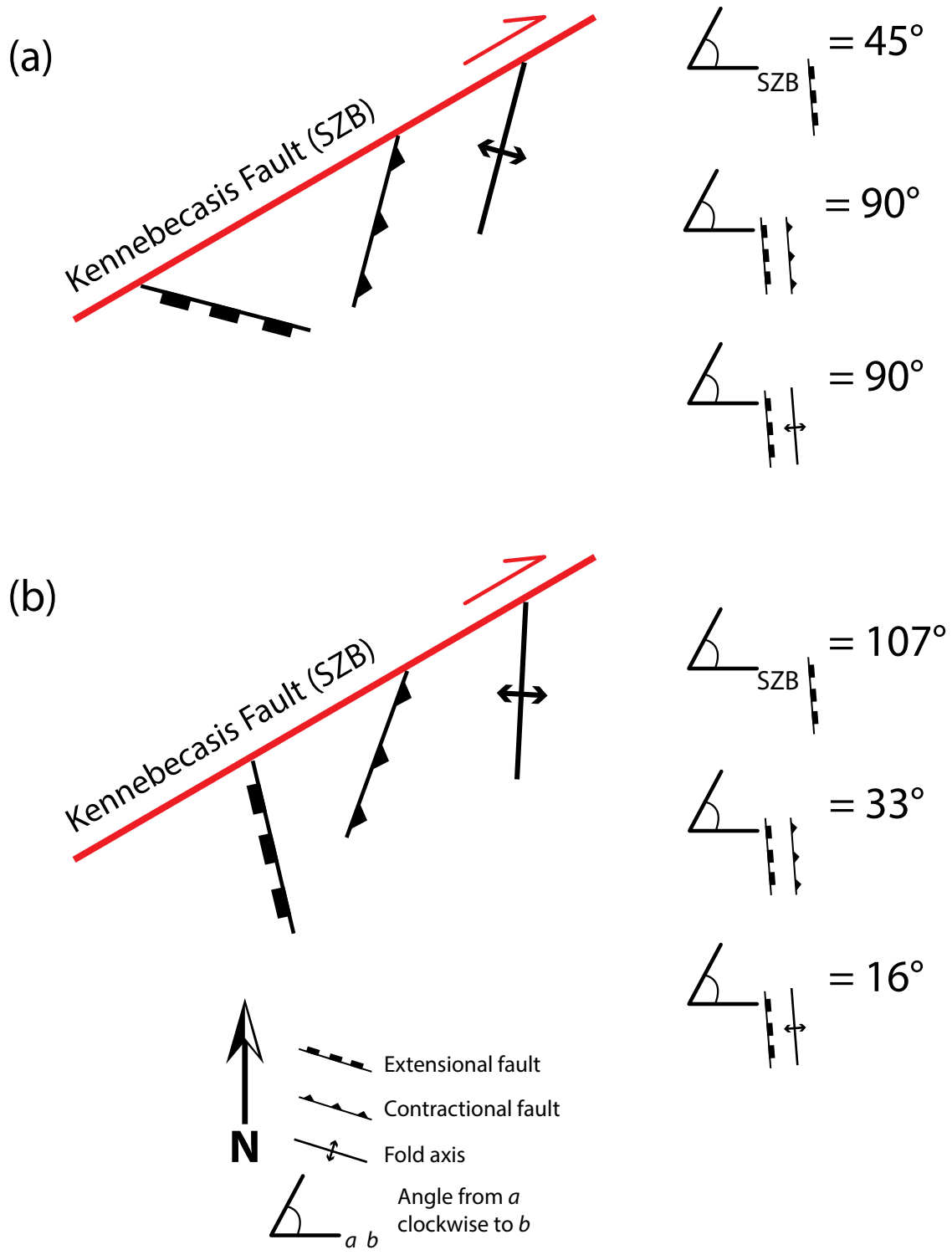

Figure 2.21. The expected initial and present-day observed orientations of structures relative to one another at the study location, in a simple-shear environment.

The Kennebecasis Fault is assumed to be the shear zone boundary (SZB) and has a strike orientation of 060° near the study location. (a) The expected structures and their initial orientations, as defined by (Harding, 1974). (b) The observed structures and their orientations at the study location.

form at 45° to the shear zone boundary (SZB) and perpendicular to each other (Figure 2.1a; 2.21a). The structures then rotate with progressive deformation (Figure 2.1b; 2.1c), changing both the angles between the structures and the slip direction along the faults. As a result of their initial orientations, extensional structures rotate at a faster rate than contractional structures (Waldron, 2005), resulting in a decrease in angle between them. Extensional faults that undergo a large amount of rotation gradually transition from being initially normal-sense dip-slip dominated, to strike-slip dominated, to reverse-sense dip-slip dominated (Figure 2.1). Likewise, contractional faults experience strike-slip movements as they rotate. Inversion of extensional faults starts once they rotate more than 45°, so that their orientation is past perpendicularity with the interpreted SZB (Figure 2.1c); however, at this point the faults are strike-slip dominated and the amount of contraction gradually increases as continued rotation occurs (Waldron, 2005).

Due to its proximity to the study area, the sub-basin-bounding Kennebecasis Fault is here assumed to be the orientation of the SZB, which has a strike of 060° in this area (Figure 2.22). The angle between the average strike of the dominant extensional fault and the SZB is 107°, where the extensional faults are clockwise from the SZB (Figure 2.21b). The extensional faults are 17° past perpendicularity to the assumed SZB orientation, implying a total rotation of 62° clockwise for these faults in a simple-shear setting.

Two end-member simple-shear models are considered here to explain the relative orientations of the structures observed at the study location (Figure 2.22): (a) extensional and contractional structures initiate at the same time and experience the same amount of deformation (but varying amounts of rotation); and (b) the extensional structures form early and the contractional structures form near the end of the deformation.

Scenario (a): Figure 2.22a shows the initial orientation of the structures based on the instantaneous strains at Time 1. Simple shear is applied to the structures, such that at Time 2 the extensional faults have rotated to the observed orientation at the study location (total of 62° of rotation). In this case, the contractional faults and fold axes rotate ~20°, resulting in angle between

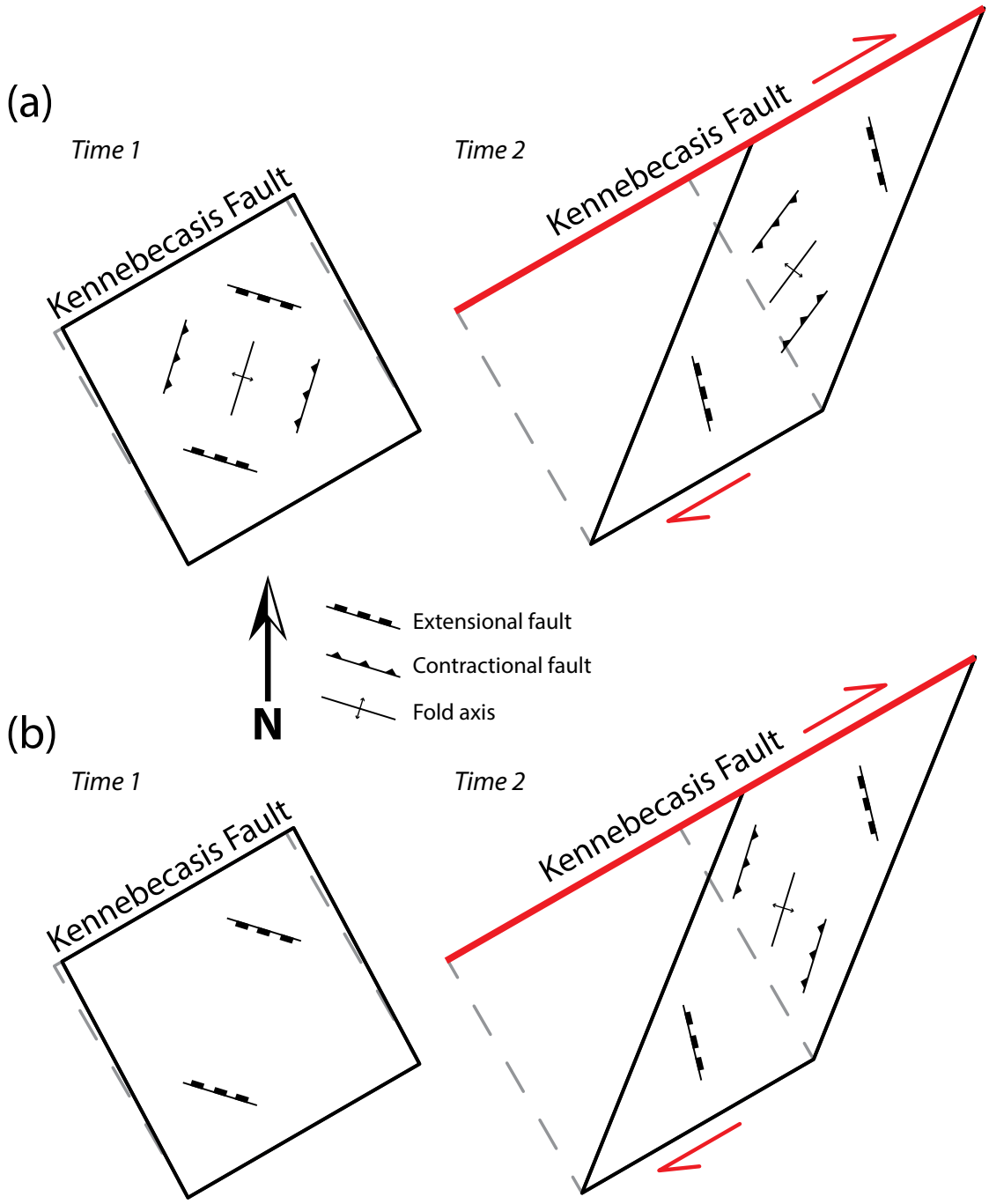

Figure 2.22. Simple-shear kinematic models illustrating the rotation of structures within a shear zone.

Time 1 represents the orientations of structures produced from the instantaneous strain and Time 2 displays the orientations of structures produced from the finite strain. (a) This scenario depicts synchronous initiation of extensional and contractional structures, resulting in a final angle between the different structures of ~50°. (b) This scenario initiates that extensional faults form first; then contractional structures form near the end of deformation. This results in an angle of ~30° between the extensional and contractional structures.

extensional and contraction structures of ~50°. The slip on both the extensional and contractional faults is expected to be dominated by strike-slip movements because they both have rotated out of their initial orientations. Initially extensional faults would have undergone partial inversion, but would still show overall extensional separation.

Scenario (b): Figure 2.22b shows the initial orientation of the extensional faults based on the instantaneous strain at Time 1. The same simple shear is applied, such that at Time 2 the extensional faults have rotated 62°. Toward the end of rotation, the contractional structures form, developing in response to the instantaneous strain. This results in an angle of ~30° between the extensional and contractional structures. The extensional faults are expected to have a large amount of strike-slip movement because they have undergone major rotation, whereas the contractional faults are not expected to show evidence for any strike-slip movement because they have not rotated. As in scenario (a), initially extensional faults would have undergone partial inversion, but would still show overall extensional separation.

Scenario 2 provides an outcome that is similar to the observed relative orientations of the structures at the study location. Additionally, the observed slickenline orientations (strike-slip dominated for extensional faults, dip-slip dominated for contractional faults) is achieved in the second scenario. Thus, it is likely that the extensional faults formed early and the contractional structures formed later, after the extensional faults had undergone significant amounts of rotation and strike-slip movement.

However, it is important to note that these scenarios are only modelled for simple shear; if deformation was transtensional, then an even greater amount of rotation is needed to explain the orientation of the extensional faults (because in this case initial extensional fault orientations are at angles less than 45° to the SZB) and a different model must be considered.

2.8. Conclusion

The roadcuts studied here provided an opportunity to observe the complex structure of deformed sedimentary rocks in a strike slip basin. Mapping combined outcrop logging and photogrammetric modelling to create an accurate map of the outcrops and interpreted vertical sections. Sedimentological observations including soft-sediment deformation structures and the identification of an unconformity that truncates faults suggests that the basin deformed close to the time of deposition. Based on the observed relative orientations of extensional and contractional faults to each other and to the sub-basin-bounding Kennebecasis Fault, the sedimentary rocks of the Hiram Brook Member at the study location likely experienced significant strike-slip deformation. If the rocks deformed in a tectonic setting close to ideal strike-slip (simple shear), then it is likely that the extensional faults have rotated upwards of 60° from their original orientation.

2.9. References

Alsop, G.I., and Marco, S., 2011, Soft-sediment deformation within seismogenic slumps of the Dead Sea Basin: Journal of Structural Geology, v. 33, p. 433–457.

Barr, S.M., and White, C.E., 1999, Field relations, petrology and structure of Neoproterozoic rocks in the Caledonia Highlands, southern New Brunswick: Geologic Survey of Canada, v. Natural Resources Canada.

Davydov, V.I., Korn, D., Schmitz, M.D., Gradstein, F.M., and Hammer, O., 2012, The Carboniferous Period, *in* Gradstein, F.M., Ogg, J.G., Schmidtz, M., and Ogg, G. eds., The Geologic Time Scale 2012, Elsevier, p. 603–651.

Fyffe, L.R., Johnson, S.C., and van Staal, C.R., 2011, A review of Proterozoic to Early Paleozoic lithotectonic terranes in the northeastern Appalachian orogen of New Brunswick, Canada, and their tectonic evolution during Penobscot, Taconic, Salinic, and Acadian orogenesis: Atlantic Geology, v. 47, p. 211–248.

Gibling, M.R., Culshaw, N., Rygel, M.C., and Pascucci, V., 2009, The Maritimes Basin of Atlantic Canada: Basin Creation and Destruction in the Collisional Zone of Pangea, *in* Miall, A. ed., Sedimentary Basins of the World 5, p. 211–244.

Greiner, H.R., 1962, Facies and sedimentary environments of Albert shale, New Brunswick: The American Association of Petroleum Geologists Bulletin, v. 46, p. 219–234.

Harding, T.P., 1974, Petroleum traps associated with wrench faults: American Association of

Petroleum Geologists Bulletin, v. 58, p. 1290–1304.

Hibbard, J., and Waldron, J.W.F., 2009, Truncation and translation of Appalachian promontories: Mid-Paleozoic strike-slip tectonics and basin initiation: Geology, v. 37, p. 497–490.

Hinds, S., 2008a, Geology of the Apohaqui area (NTS 21 H/12h), Kings County, New Brunswick: New Brunswick Department of Natural Resources: Minerals, Policy, and Planning Division.

Hinds, S., 2008b, Geology of the Sussex Corner area (NTS 21 H/11e), Kings County, New Brunswick: New Brunswick Department of Natural Resources: Minerals, Policy, and Planning Division.

Hinds, S.J., and Park, A.F., 2009, Structural and stratigraphic relationships between the Horton and Sussex groups (Tournaisian: Lower Carboniferous) around Elgin, southern New Brunswick 2009., *in* Merlini, S.A.A. ed., Exploration, Mining and Petroleum New Brunswick, Abstracts, p. 13–14.

Howie, R.D., and Barss, M.S., 1975, Upper Paleozoic rocks of the Atlantic provinces, Gulf of St. Lawrence, and adjacent continental shelf, *in* Van Der Linden, W.J.M. and Wade, J.A. eds., Offshore geology of eastern Canada, Volume 2 - Regional Geology, Geological Survey of Canada, Paper, v. 74–30, p. 35–50.

James, M.R., and Robson, S., 2014, Straightforward reconstruction of 3D surfaces and topography with a camera: accuracy and geoscience application: Journal of Geophysical Research, Earth Surface, v. 117, p. 1–17.

Jolly, R.J.H., and Lonergan, L., 2002, Mechanisms and controls on the formation of sand intrusions: Journal of the Geological Society, London, v. 159, p. 605–617.

Keighley, D., 2008, A lacustrine shoreface succession in the Albert Formation, Moncton Basin, New Brunswick: Bulletin of Canadian Petroleum Geology, v. 56, p. 235–258.

Park, A.F., and St. Peter, C.J., 2005, Deformation of Lower Carboniferous rocks in the Rosevale to Saint-Joseph area, Albert and Westmorland counties, southeastern New Brunswick, *in* Martin, G.L. ed., Geological Investigations in New Brunswick for 2004, New Brunswick Department of Natural Resources; Minerals, Policy and Planning Division, Mineral Resources Report 2005–1, p. 45–98.

Park, A.F., and St. Peter, C.J., 2009, Stratigraphy and structure of the Indian Mountain Deformed Zone, Maritimes Basin, Westmorland County, Southeastern New Brunswick: New Brunswick Department of Natural Resources; Minerals, Policy and Planning Division, Mineral Resources Report, v. 2009–1, 114 p.

Park, A.F., St. Peter, C.J., and Keighley, D.G., 2007, Structural styles in Late Devonian – early Carboniferous rocks along the southern margin of the Moncton Subbasin: Caledonia Mountain to Elgin, southeastern New Brunswick, *in* Martin, G.L. ed., Geological

Investigations in New Brunswick for 2006, New Brunswick Department of Natural Resources, Mineral Resources Report 2007–1, p. 87–125.

Park, A.F., St. Peter, C.J., Keighley, D., and Wilson, P., 2010, Overstep and imbrication along a sidewall ramp and its relationship to a hydrocarbon play in Tournaisian rocks of the Moncton Basin: the Peck Creek section, Albert Mines area, southeastern New Brunswick: Bulletin of Canadian Petroleum Geology, v. 58, p. 268–282.

Roliff, W.A., 1962, The Maritimes Carboniferous Basin of Eastern Canada: Geological Association of Canadian Proceedings, v. 14, p. 21–44.

St. Peter, C.J., 1993, Maritimes Basin evolution: key geologic and seismic evidence from the Moncton Subbasin of New Brunswick: Atlantic Geology, v. 29, p. 233–270.

St. Peter, C.J., and Johnson, S.C., 2009, Stratigraphy and structural history of the late Paleozoic Maritimes Basin in southeastern New Brunswick, Canada: New Brunswick Department of Natural Resources, Memoir, v. 3, 348 p.

Waldron, J.W.F., 2005, Extensional fault arrays in strike-slip and transtension: Journal of Structural Geology, v. 27, p. 23–34.

Waldron, J.W.F., Barr, S.M., Park, A.F., White, C.E., and Hibbard, J.P., 2015, Late Paleozoic strike-slip faults in Maritime Canada and their role in the reconfiguration of the northern Appalachian orogen: Tectonics, v. 34, p. 1661–1684, doi: 10.1002/2015TC003882.

Waldron, J.W.F., Rygel, M.C., Gibling, M.R., and Calder, J.H., 2013, Evaporite tectonics and the late Paleozoic stratigraphic development of the Cumberland basin, Appalachians of Atlantic Canada: Geological Society of America Bulletin, v. 125, p. 945–960.

Williams, E.P., 1974, Geology and petroleum possibilities in and around Gulf of St. Lawrence: AAPG Bulletin, v. 58, p. 1137–1155.

Wilson, P., 2005, Stratigraphy, structural geology, and tectonic history of the McCully area, Moncton Subbasin, southeastern New Brunswick: New Brunswick Department of Natural Resources; Minerals, Policy and Planning Division, v. Mineral Resource Report 2005-5, p. 104.

Wilson, P., and White, J.C., 2006, Tectonic evolution of the Moncton Basin, New Brunswick, Eastern Canada; new evidence from field and sub-surface data: Bulletin of Canadian Petroleum Geology, v. 54, p. 319–336, doi: 10.2113/gscpgbull.54.4.319.

Wilson, P., White, J.C., and Roulston, B.V., 2006, Structural geology of the Penobsquis salt structure: late Bashkirian inversion tectonics in the Moncton Basin, New Brunswick, eastern Canada: Canadian Journal of Earth Sciences, v. 43, p. 405–419, doi: 10.1139/e05-116.

Chapter 3: Fault development and the role of strike-slip deformation at the McCully gas field, New Brunswick, Canada

Sedimentary basins in strike-slip settings contain complex structures due to concurrent extensional, contractional, and rotational deformation, making it challenging to understand early basin configurations and depositional patterns. The kinematic history of such basins can be unraveled by measuring the heaves and orientation of fault arrays to quantify deformation. In the Moncton Sub-basin in southern New Brunswick, Canada, data from the McCully gas field reveal a complex structural geometry within the unconformity-bounded, Late Devonian to Early Mississippian Horton Group. The basin is elongated NE – SW between major bounding faults with interpreted dextral slip. The structural interpretation of a 3D seismic volume revealed a conjugate set of curved extensional faults is identified with typical ESE – WNW strike, along with contractional faults of various orientations. Gentle folds trend NE and SW. Analogous faults are found in highway outcrops, approximately 13 km SW of the subsurface data, along the strike of the general structure pattern. At McCully, subsurface measurements of the bulk strain show that the Frederick Brook shale horizon has an average apparent stretch (S^*) of 1.14, an average apparent shortening (S') of 0.986, and an average fault orientation relative to the shear zone boundary (θ') of 40°; these bulk strain values show that the early Moncton Sub-basin was deformed in a transtensional setting with a large angle of divergence (α = 59°). However, variations in S^* and θ' across the shear zone indicate that deformation was heterogeneous in space; away from the shear zone boundary, towards the SE, S^* gradually decreases and θ' gradually increases. Additionally, discrepancies in estimates of α between a method using finite strain and a method using instantaneous strain suggests that deformation was also heterogeneous in time; the initial deformation at McCully likely occurred in an environment with a large strike-slip component that later transitioned to an environment with a large extensional component. The SW-directed concave curvature of the extensional faults likely resulted from a combination of rotation and asynchronous fault

propagation, variable strain magnitude and direction across the shear zone, and inconstant deformation through time. Based on these estimations, the early Moncton Sub-basin likely deformed in an oblique-rift like environment with a N – S extension direction.

3.1. Introduction

Sedimentary basins which developed in strike-slip settings contain complex structures due to the concurrent extensional and contractional deformation (Figure 3.1a). Additionally, the rotation of the structures with continued strike-slip deformation (Figure 3.1; 3.2) creates ambiguity for understanding early basin configuration and depositional patterns, making resource exploration in these environments difficult. The McCully area (Figure 3.3; 3.4) in the transtensional Moncton Sub-basin in New Brunswick, Canada, is an excellent location to investigate strike-slip sedimentary basin kinematics because of the available wellbore, 2-dimensional (2D) and 3-dimensional (3D) seismic reflection data, and the presence of nearby outcrops of the same strata. Here, the unconventional onshore McCully natural gas field has sparked increased research into the sub-basin (e.g. Wilson, 2005; Wilson and White, 2006; Keighley, 2008); however, the amounts of subsidence attributed to strike-slip, transtensional, and extensional deformation during the formation of the Moncton Sub-basin are not fully understood. Furthermore, the amount of rotation that the basin's structures have undergone is unclear. In addition, the relationship between deformation interpreted in seismic data and that observed in outcrop, at sub-seismic scale, is poorly understood. To correctly understand the basin kinematics through time, both infinitesimal (Figure 3.1a) and progressive strains (Figure 3.1b; 3.1c) must be recognized and differentiated.

This paper aims to delineate the relative amounts of deformation attributable to strike-slip and extension during the Late Devonian – Early Mississippian in the Moncton Sub-basin using the structural interpretation of seismic reflection data. In addition, we quantify the deformation in an outcrop section, to gain perspective on the importance of structures at scales below the resolution of seismic data. This will improve the understanding of how strike-slip tectonism influenced the

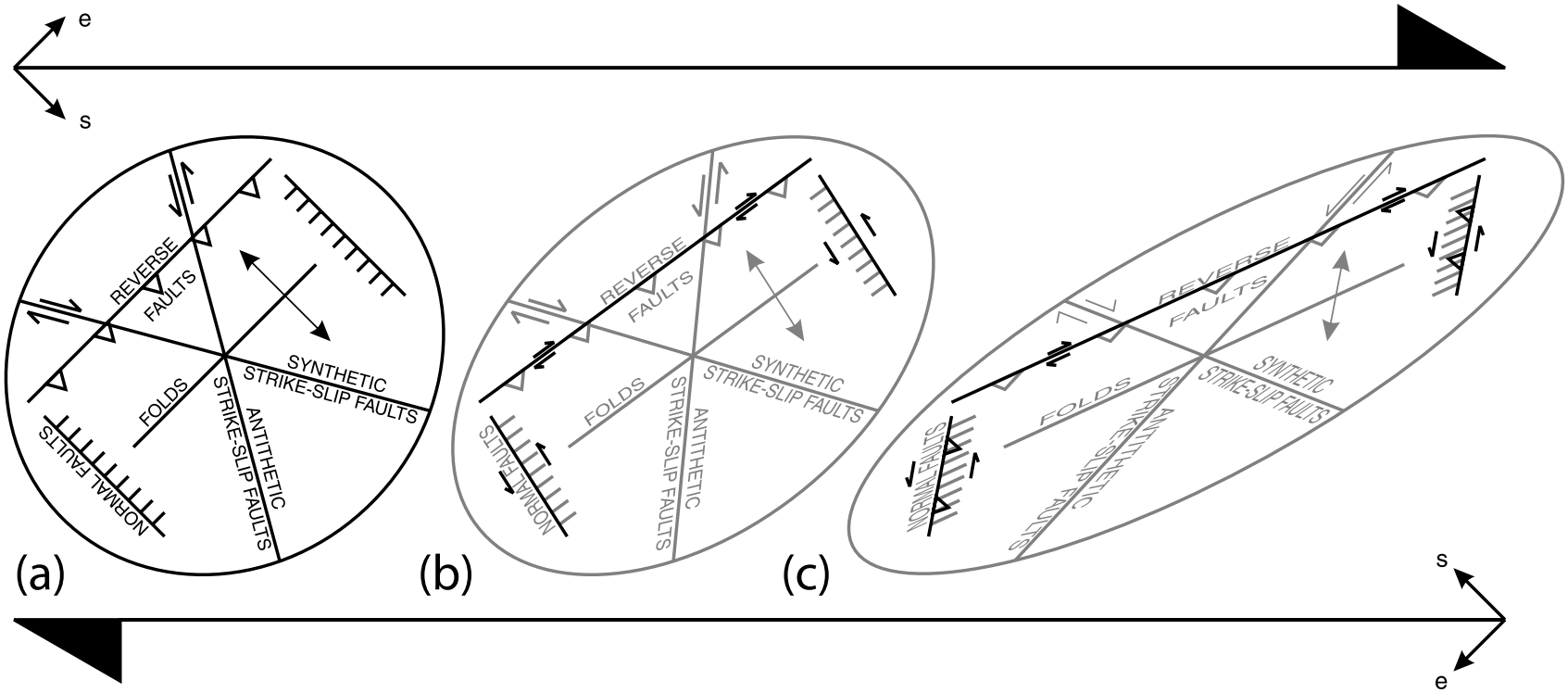

Figure 3.1. Typical structures found in simple-shear dextral strike-slip settings.

Symbols: *s* represents the instantaneous shortening direction; *e* represents the instantaneous extension direction. (a) Geometry of the structures found in strike-slip settings where there has been little strike-slip movement along the shear zone boundary, after Harding (1974). (b) and (c) Modification of (a) showing how structures rotate and change with continued movement along the shear zone boundary (Waldron, 2005).

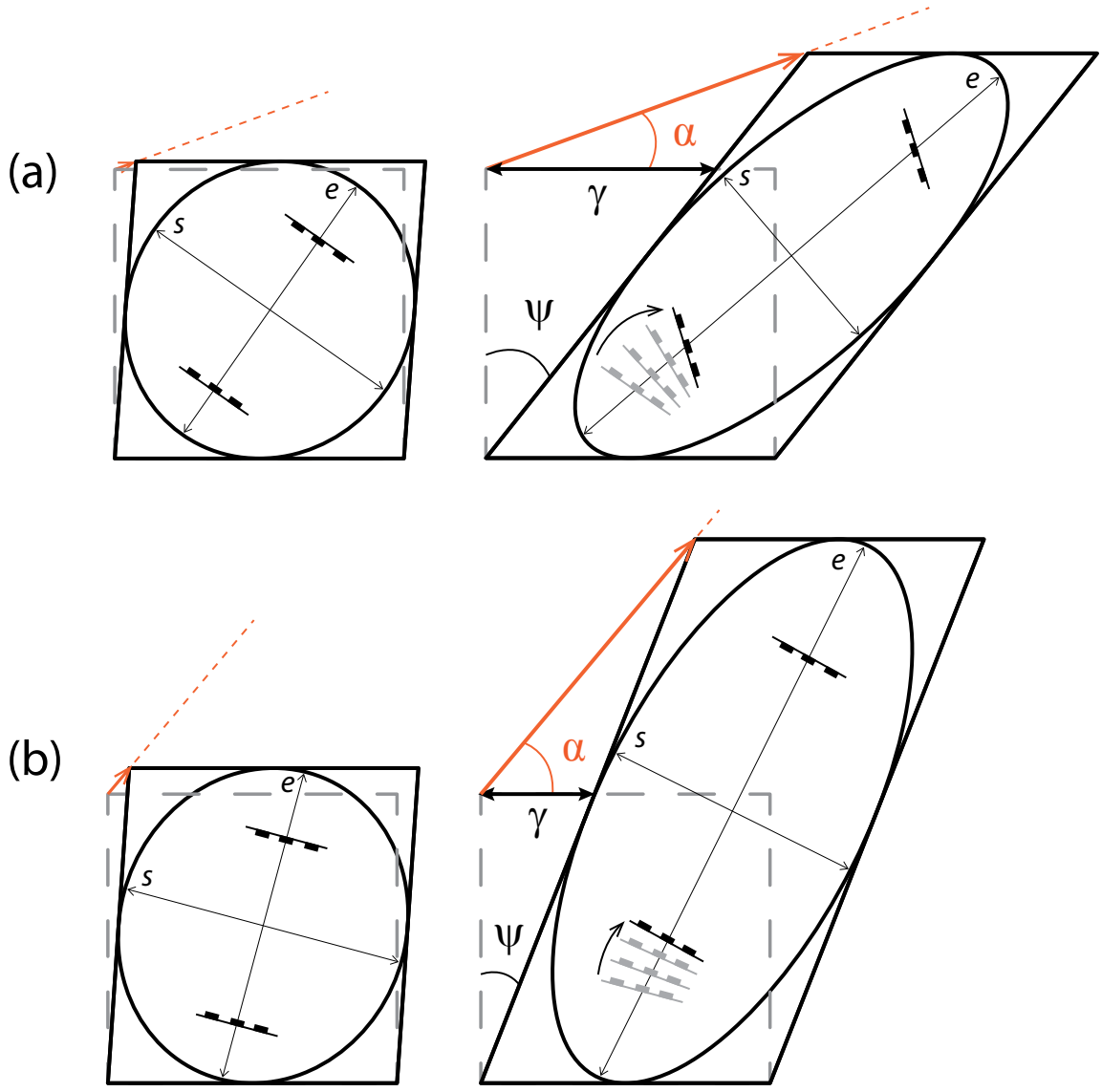

Figure 3.2. Definition of the transtensional *α*-angle.

The red arrows represent the displacement vector of particles in the shear zone. Symbols: ψ represents the angle of shear; γ represents the shear strain; α represents the divergence from simple shear. The instantaneous extension (*e*) and shortening (*s*) are shown for each strain ellipse. The infinitesimal and finite strains are shown for two tectonic environments. The finite strain illustrations have the same displacement vector length. (a) Illustration of a tectonic environment with a transtensional *α*-angle equal to 20°. The angle of the extensional faults relative to the shear zone boundary increases with increasing shear strain. (b) Illustration of a tectonic environment with a transtensional angle equal to 50°. Extensional faults form at smaller angles relative to the shear zone boundary than in (a).

Figure 3.3. Regional maps of the Maritimes Basin and the Moncton Sub-basin.

(a) Map of North America. The black box shows the location of (b). (b) Regional map of the Eastern Canada showing the extent of the late Paleozoic Maritimes Basin and major faults. Modified from Waldron et al. (2013). Abbreviations: BIF, Belleisle fault zone; CBF, Cabot fault; CCHF, Caledonia – Clover Hill fault zone; HF, Hollow fault; MFZ, Minas fault zone. (c) Geological map of southern New Brunswick, Canada. The black box shows the location of Figure 3.4 and the white star shows the location of the observed roadcuts along Highway 1. Faults are shown in red. Modified from Waldron et al. (2015). Abbreviation: F = Fault.

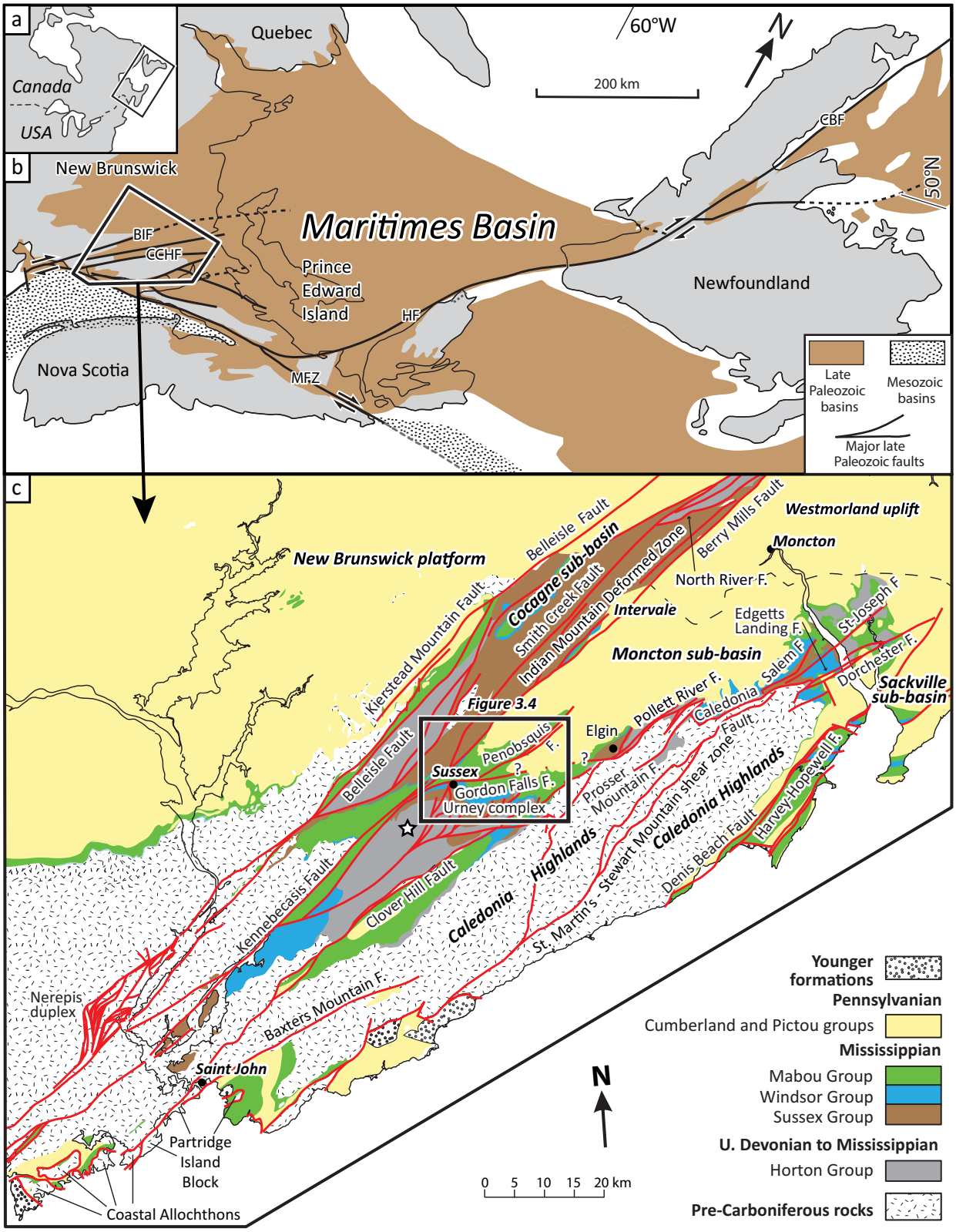
a
Canada
USA
Quebec
60°W
200 km
N
CBF
50°N
b
New Brunswick
Maritimes Basin
BIF
CCHF
Prince
Edward
Island
HF
Newfoundland
Nova Scotia
MFZ
Late
Paleozoic
basins
Mesozoic
basins
Major late
Paleozoic faults
c
New Brunswick platform
Belleisle Fault
Cocagne sub-basin
Smith Creek Fault
Indian Mountain Deformed Zone
Berry Mills Fault
Westmorland uplift
Moncton
North River F.
Intervale
Edgetts
Landing F.
St-Joseph F.
Moncton sub-basin
Salem F.
Dorchester F.
Sackville
sub-basin
Kierstead Mountain Fault
Figure 3.4
Caledonia
Pollett River F.
Elgin
Penobsquis
F.
Sussex
Gordon Falls F.
Urney complex
Belleisle Fault
Prosser
Mountain F.
Caledonia Highlands
Harvey-Hopewell F.
Denis Beach Fault
St. Martin's - Stewart Mountain shear zone
Fault
Highlands
Clover Hill Fault
Kennebecasis Fault
Caledonia
Nerepis
duplex
Baxters Mountain F.
Saint John
Partridge
Island
Block
Coastal Allochthons
N
0 5 10 15 20 km
Younger
formations
Pennsylvanian
Cumberland and Pictou groups
Mississippian
Mabou Group
Windsor Group
Sussex Group
U. Devonian to Mississippian
Horton Group
Pre-Carboniferous rocks

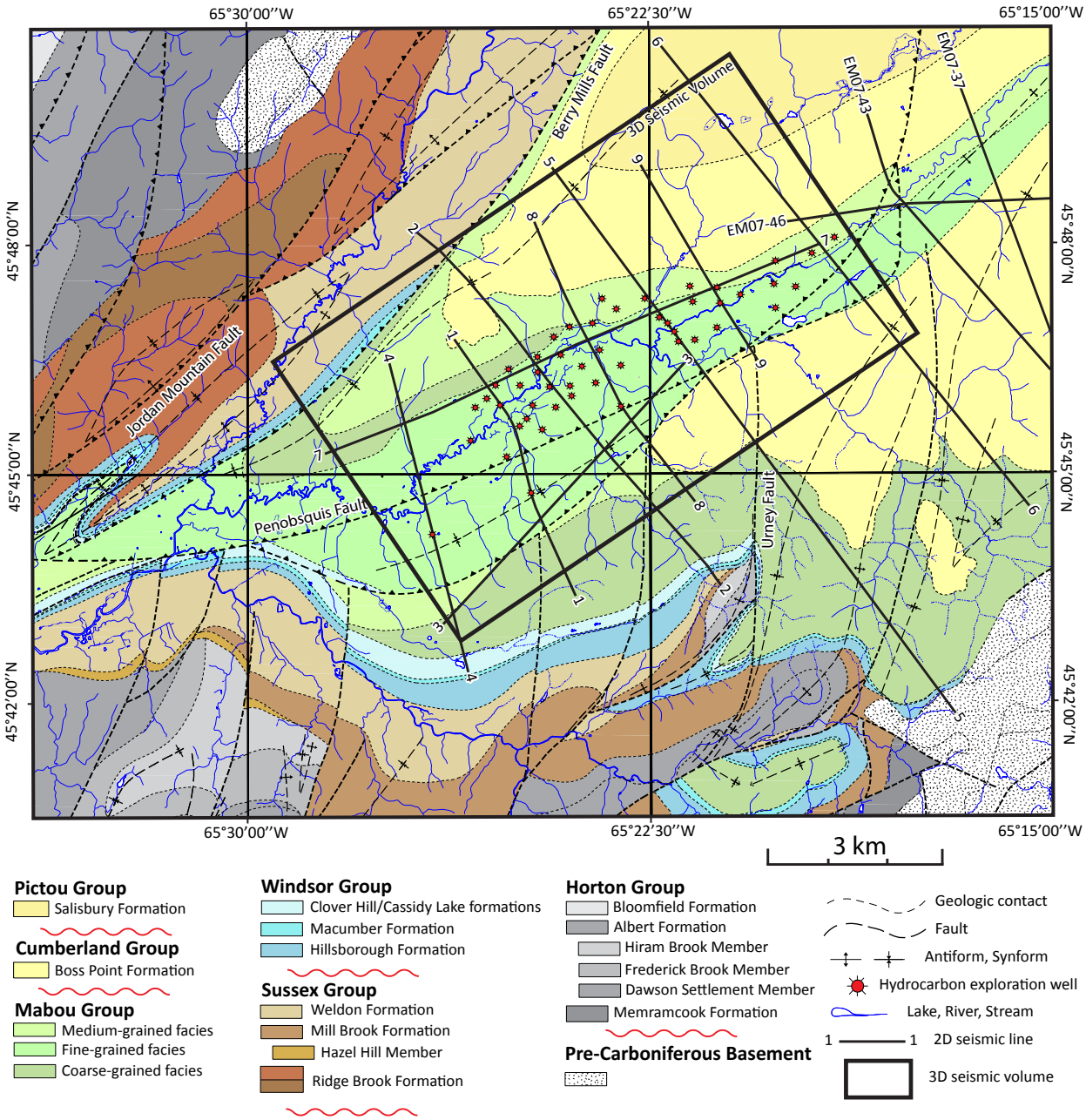

Figure 3.4. Geologic map of the McCully area.

The subsurface data locations are shown. The black box shows the extent of the 3D seismic reflection data volume and the bold black lines are the 2D seismic reflection data lines. The bottom-hole locations of 49 wells used in subsurface interpretation are displayed. Modified from Hinds (2008a, 2008b, 2008c, 2008d, 2008e) and Hinds and St. Peter (2008).

formation of the Moncton Sub-basin and greater Maritimes Basin and improve exploration of resources in similar basins elsewhere.

3.1.1. Kinematics of strike-slip sedimentary basins

Strike-slip shear zones are split into three categories based on the overall deformation styles experienced by the rocks in the shear zone: (1) simple-shear ideal strike-slip, in which the total area of the shear zone is conserved, meaning that the amount of shortening is exactly equal to the amount of extension; (2) transtension (strike-slip plus vertical shortening and surface area increase; Figure 3.2); and (3) transpression (strike-slip plus vertical extension accompanied by surface-area decrease; Wilcox et al., 1973; Sylvester, 1988; Dewey et al., 1998). Pronounced vertical shortening in the transtensional case leads to the typical development of deep sedimentary basins, in contrast to settings characterized by transpression or ideal strike-slip.

Transtensional tectonic settings have a horizontal extensional component that is perpendicular to the shear zone boundary (SZB), resulting in greater amount of extension than shortening (Figure 3.2). The additional extension component is measured by the angle α, which is the transtensional angle or the angle of divergence of particle paths from the SZB (Figure 3.2; Tikoff and Fossen, 1993). Basins which form in simple-shear or small-α angle tectonic settings are dominated by strike-slip faults and rotational strains, resulting in shallow basins with thin sedimentary fills (Allen et al., 1998). In contrast, basins which form in large-α angle tectonic settings are dominated by horizontal extensional strains, creating large amounts of subsidence and a thick sedimentary fill (Allen et al., 1998).

Typical structures found in simple-shear ideal strike-slip deformation zones include normal faults, reverse faults, strike-slip faults, and folds (Figure 3.1a). The extensional and compressional structures form at 45° to the SZB and perpendicular to each other; extensional structures developing perpendicular to the instantaneous extension axis and shortening structures developing perpendicular to the instantaneous shortening axis (Wilcox et al., 1973; Sylvester, 1988; Fossen and Tikoff, 1998). In transtensional settings, original orientations of structures are

different from those in ideal strike-slip settings since the instantaneous extension and shortening axes are at different orientations as they are a function of the α–angle. *En echelon* normal faults are typically the primary structure which accommodates the horizontal extensional component of deformation in basins formed in strike-slip and transtensional settings (Allen et al., 1998; Waldron, 2005).

The orientations of structures in shear zones can change with time; as progressive deformation occurs, these structures are rotated (Figure 3.1b; 3.1c) either clockwise (dextral strike-slip) or counter-clockwise (sinistral strike-slip; Garfunkel and Ron, 1985). The amount of shear strain experienced by such a basin can have a great influence on the geometrical relationship of structures found in the basin such that, with continued incremental rotations during progressive strain, inversion of structures may occur. If enough progressive deformation has occurred, extensional faults may pass perpendicularity to the SZB and into a field of shortening (Waldron, 2005). Thrust faults can never be rotated into a field of extension because they can never rotate such that they cross the SZB; they become increasing closer to the SZB but never become parallel.

Since strike-slip and transtensional basins are dominated by faults, the depositional patterns of the basins are controlled by the orientation and movement along the faults. The kinematics of basin formation in an ancient basin can be investigated through observations of its present-day geometry. Such observations typically show the bulk or total strain, which the rocks have undergone throughout their history. Working back to understand the instantaneous strain acting at a given time may be critical to making interpretations about the fault kinematics. As shown by Waldron (2005), fault orientations and heaves (the horizontal component of dip separation) can be used to quantify the distortion that a basin underwent during its formation and to determine the relative importance of strike-slip and extension in generating subsidence. Unravelling the kinematic history of the faults in such basins can lead to a better understanding of the depositional systems and structural relationships that are key for exploration for resources.

3.1.2. Regional geologic setting of the McCully Gas Field

3.1.2.1. Maritimes Basin

The late Paleozoic Maritimes Basin (Figure 3.3; Roliff, 1962; Gibling et al., 2009) is a large and deep (>12 km thick) basin in Atlantic Canada that formed in response to major transtension following the Acadian Orogeny (Williams, 1974; Hibbard and Waldron, 2009; Waldron et al., 2015). Smaller sub-structures, referred to as sub-basins, are separated by basement uplifts and major dextral strike-slip faults that dissect the basin (Howie and Barss, 1975; St. Peter, 1993; Gibling et al., 2009) as described in Chapter 1. The Moncton Sub-basin located in southern New Brunswick (Figure 3.3) is the focus of this paper. This sub-basin has a complex deformation history that includes subsidence, faulting, folding, inversion, and salt tectonism (Wilson and White, 2006; St. Peter and Johnson, 2009; Waldron et al., 2015).

3.1.2.2. Western Moncton Sub-basin

The western Moncton Sub-basin (St. Peter, 1993) extends ~100 km northeast to southwest (Figure 3.3). In the northeast the sub-basin is ~35 km wide but it thins to ~10 km in the southwest where the sub-basin-bounding Caledonia – Clover Hill and Kennebecasis – Indian Mountain fault zones converge (Figure 3.3).

The stratigraphy of the Moncton Sub-basin is summarized in Figure 3.5. The basin fill is dominated by terrestrial clastic rocks but includes marine carbonate and evaporite rocks in the Visean (see Chapter 2; Wilson and White, 2006; St. Peter and Johnson, 2009). The focus of this Chapter will be on the Albert Formation, which is a part of the initial basin fill assigned to the Late Devonian to Early Mississippian (Tournaisian) Horton Group. The Albert Formation has been separated into the lowermost Dawson Settlement Member (grey sandstone and siltstone with minor dolostone), the middle Frederick Brook Member (dark kerogenous mudstone and siltstone), and the uppermost Hiram Brook Member (interbedded grey sandstone and siltstone; Greiner,

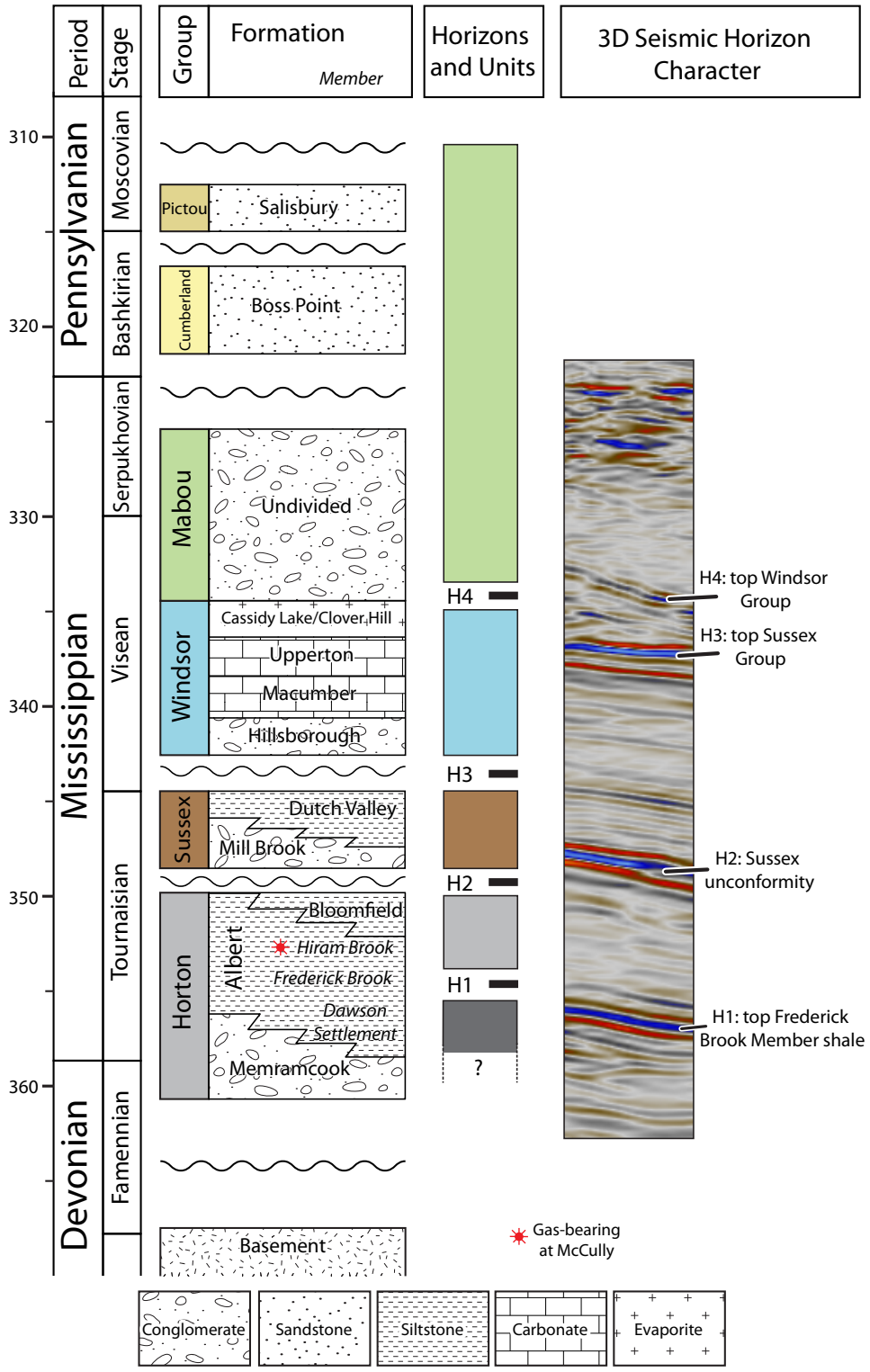

Figure 3.5. Stratigraphic chart of the western Moncton Sub-basin.

After Wilson and White (2006) and St. Peter and Johnson (2009). Dominant lithologies are shown. Ages and stages are from Davydov et al. (2012).

1962; Keighley, 2008; St. Peter and Johnson, 2009). The later Tournaisian Sussex Group unconformably overlies the Horton Group and comprises red to grey clastic units. The kerogenous mudstone units of the Fredrick Brook Member are likely the sources for the hydrocarbons found in the Hiram Brook sandstone units at the McCully gas field (Figure 3.4; Durling and Martel, 2003).

3.2. Subsurface data

3.2.1. Data sources and methods

Seismic reflection and wellbore data, supplied by Corridor Resources Inc., cover the McCully gas field, roughly 10 km NE of Sussex, New Brunswick (Figure 3.4). The seismic data include a 3D seismic survey with a surface area of 13.5 km by 8 km. The seismic data image up to 3 s of TWT (two-way traveltime), however, reflections below ~1.75 s are faint and difficult to interpret. The polarity of the seismic data are positive. The inline and crossline spacing of the data is 30 m, with the inlines oriented NW – SE and the crosslines oriented NE – SW. Additionally, twelve 2D lines with a combined length of 113 km were used in the subsurface interpretation. All but two 2D lines overlap the 3D volume. The vertical resolution of the data is roughly 40 m. The wellbore data, including varying amounts of wireline data, are derived from of 59 wells, 54 of which are within the 3D volume. Well tops (i.e. stratigraphic boundaries) picked by Corridor were used in this study. Furthermore, Corridor tied 49 of the wells to the seismic data using both sonic and density logs. Schlumberger's Petrel software was used to interpret the subsurface data. Interpretations of stratigraphic units throughout the data set provided by Corridor were used as a starting point and guide.

3.2.2. Stratigraphy

Reflectors within the Horton, Sussex, and Windsor groups are identified and interpreted in the data; the Mabou, Cumberland, and Pictou groups were not differentiated in this project (Figure 3.6). Reflectors are first identified by using well tops from 45 wells and then manually interpreted

Figure 3.6. Interpreted seismic sections from the 3D volume showing the major stratigraphic units and faults, displayed in two-way travel time.

Line of sections are shown in Figure 3.11. Sections (a), (b), and (c) are approximately perpendicular to extensional faults within the Horton Group. Sections (d) and (e) are approximately parallel to extensional faults within the Horton Group. The vertical exaggeration is approximately 2.

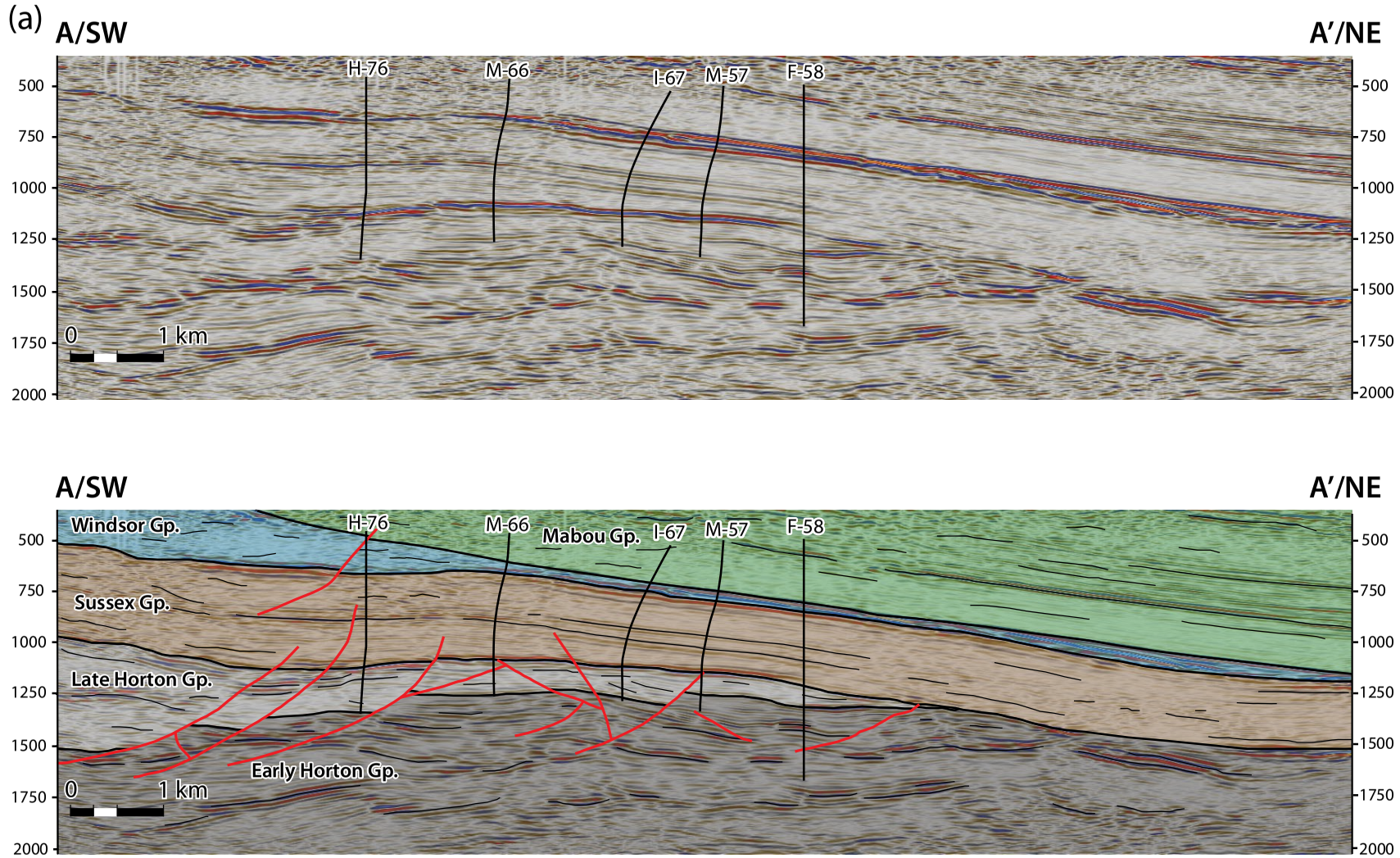
(a)
A/SW
A'/NE
H-76
M-66
I-67
M-57
F-58
500
750
1000
1250
1500
1750
2000
0
1 km
A/SW
A'/NE
Windsor Gp.
Mabou Gp.
Sussex Gp.
Late Horton Gp.
Early Horton Gp.

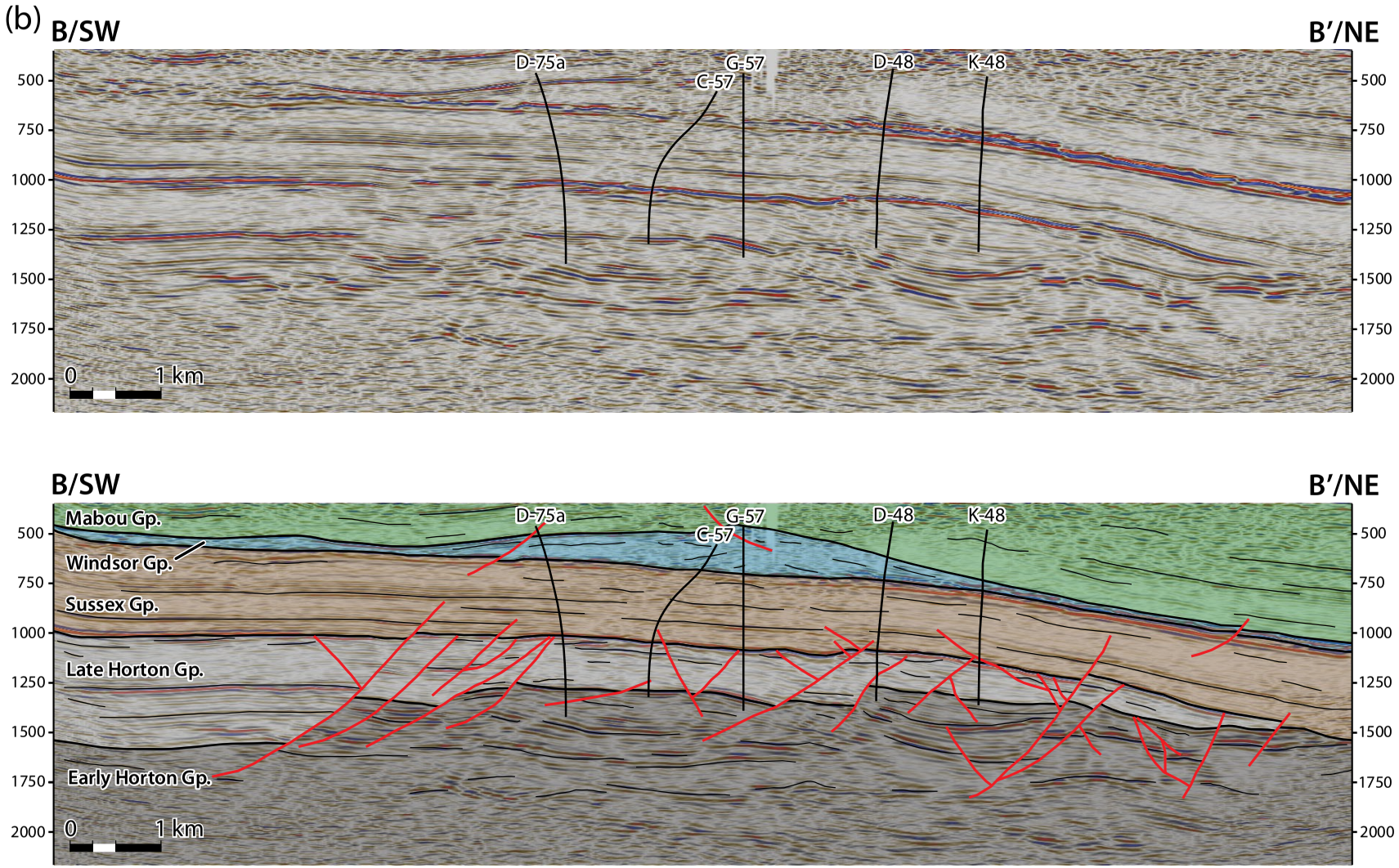
(b)
B/SW
B′/NE
D-75a
C-57
G-57
D-48
K-48
500
750
1000
1250
1500
1750
2000
0
1 km
B/SW
B′/NE
Mabou Gp.
Windsor Gp.
Sussex Gp.
Late Horton Gp.
Early Horton Gp.
D-75a
C-57
G-57
D-48
K-48
0
1 km

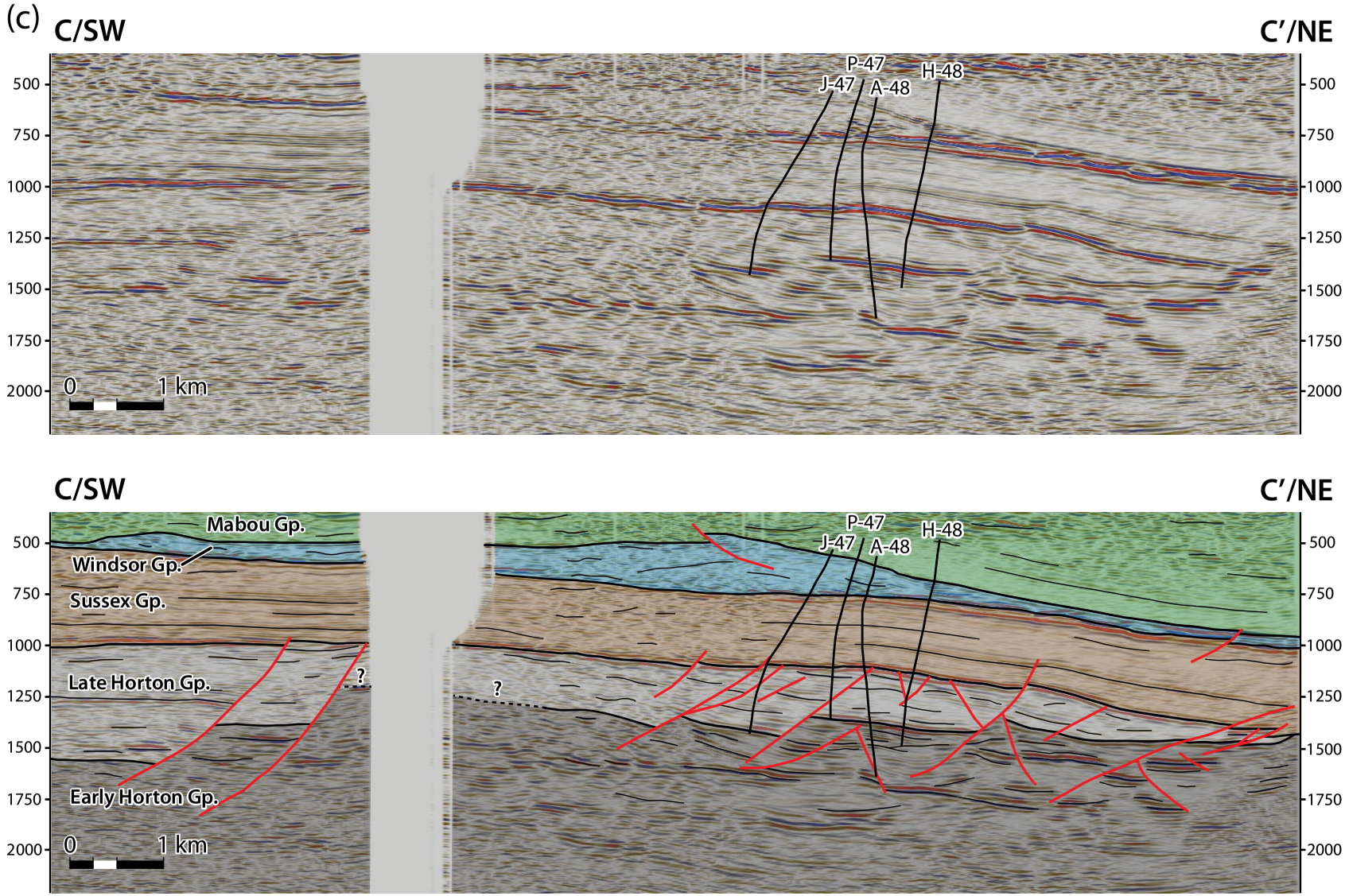
(c)
C/SW
C′/NE
P-47
J-47
A-48
H-48
500
750
1000
1250
1500
1750
2000
0
1 km
C/SW
C′/NE
Mabou Gp.
Windsor Gp.
Sussex Gp.
Late Horton Gp.
Early Horton Gp.
?
?
P-47
J-47
A-48
H-48
0
1 km

(d)

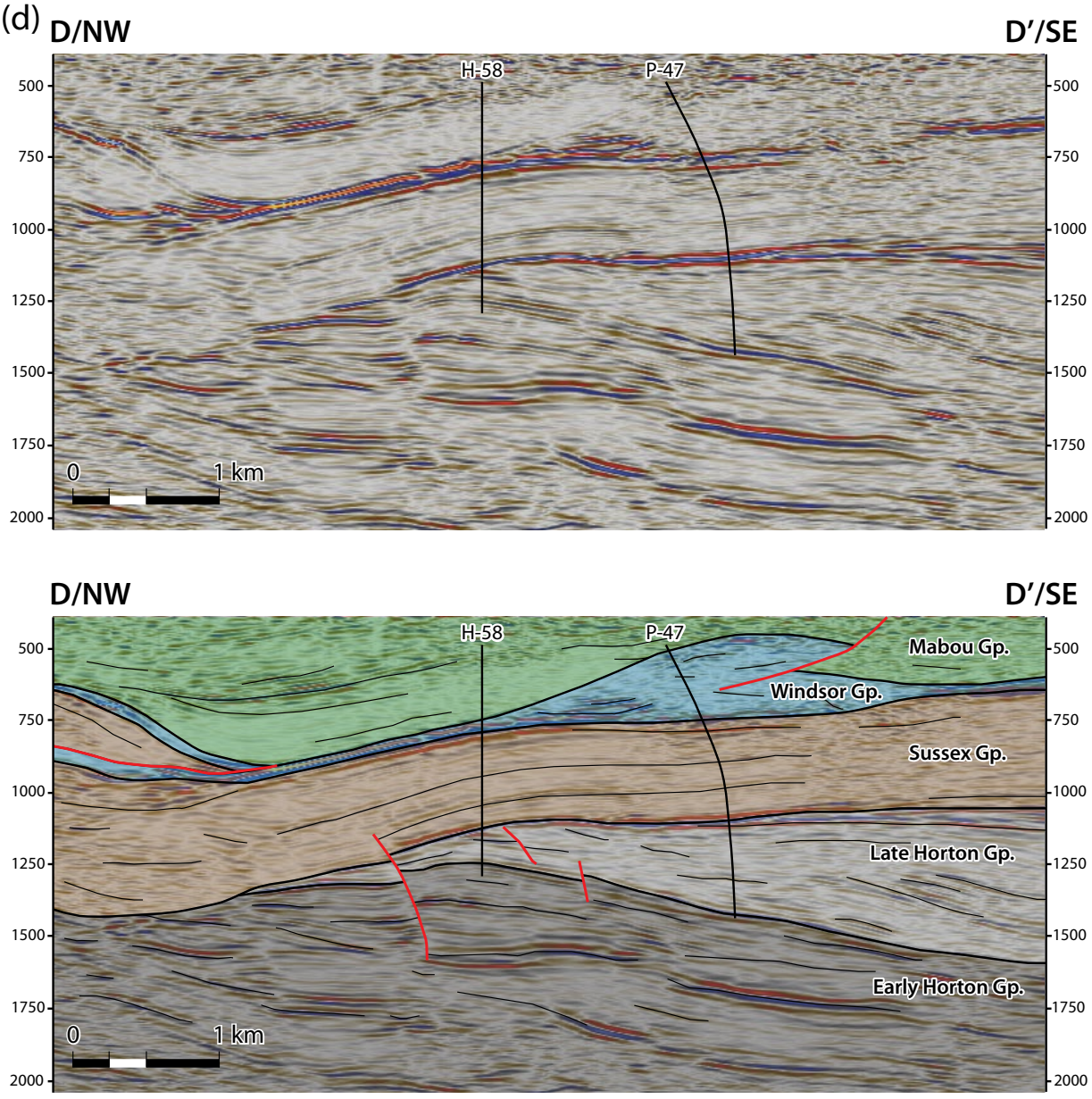
D/NW
D'/SE
H-58
P-47
500
750
1000
1250
1500
1750
2000
0
1 km
D/NW
D'/SE
H-58
P-47
Mabou Gp.
Windsor Gp.
Sussex Gp.
Late Horton Gp.
Early Horton Gp.
500
750
1000
1250
1500
1750
2000
0
1 km

(e)

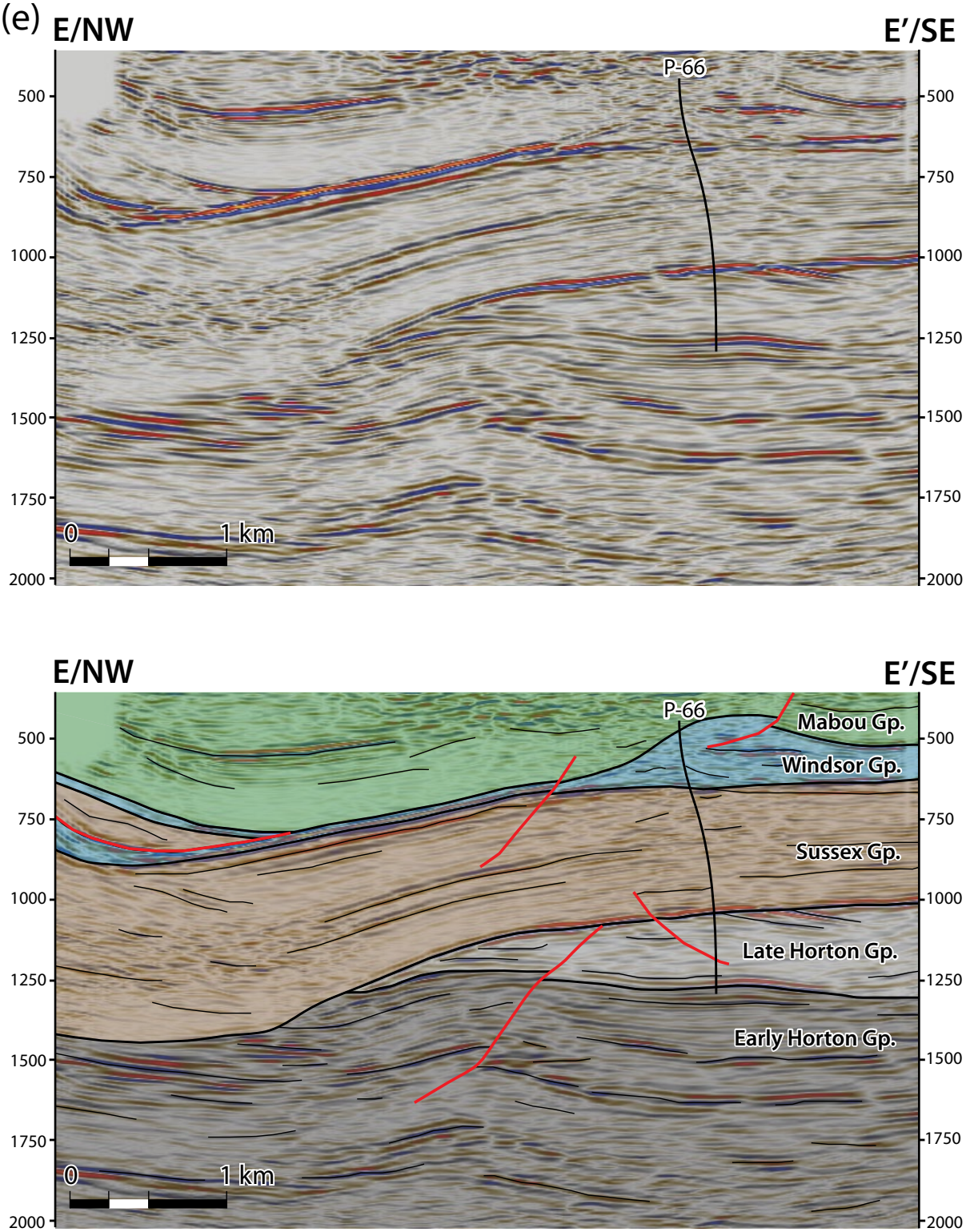
E/NW
E'/SE
P-66
500
750
1000
1250
1500
1750
2000
0
1 km
E/NW
E'/SE
P-66
Mabou Gp.
Windsor Gp.
Sussex Gp.
Late Horton Gp.
Early Horton Gp.
500
750
1000
1250
1500
1750
2000
0
1 km

away from the wells using their respective seismic characteristics (discussed below).

In the Horton Group, reflections only within the Albert and Bloomfield formations are consistently of high enough amplitude to be traced across the seismic volume. Reflections below the Albert Formation are faint and inconsistent and the transition between the Dawson Settlement and Frederick Brook members (more than 3 km deep) is not clear. The contact between the Hiram Brook and Frederick Brook members of the Albert Formation is marked by a relatively high-amplitude negative reflection (trough), representing the change from high velocity siltstone and sandstone units of the Hiram Brook Member to low velocity organic-rich mudstone units of the Frederick Brook Member. This boundary has been picked on 37 seismic-tied wells, allowing the members to be readily differentiated in the data. Figure 3.7a displays the subsurface structure of the top of the Frederick Brook shale horizon. Sandstone, siltstone, and shale units within the Hiram Brook Member are difficult to confidently interpret across the entire 3D volume due to lack of consistent high amplitude reflectivity; this is likely a consequence of both similar seismic velocities and rapid facies changes within the units. Folds and numerous extensional and contractional faults have been interpreted to deform the Albert Formation.

A strong negative reflection (tough) is identified at the angular unconformity between the Sussex and Horton groups (Figure 3.6), representing the downward change from high acoustic impedance of the conglomeratic units to low acoustic impedance, gas-filled siltstone and sandstone units. The unconformity has a general northward dip and is folded into a NW-trending synform in the NW part of the survey (Figure 3.7b). Reflections within the Sussex Group are dominantly parallel to the underlying angular unconformity. At this unconformity, reflections from the underlying Horton Group are truncated. The unconformity is observed to cut into the Bloomfield and Albert formations. Some of the faults which cut the Horton Group extend upward and also displace the Sussex unconformity (Figure 3.6).

The base of the Windsor Group is marked by a strong, high amplitude negative reflection between the overlying limestones of the Upperton and Macumber formations and the Sussex Group

clastics (Figure 3.5; 3.6), representing a downward reduction in seismic velocity and rock density. In places this reflection becomes faint, likely where the Hillsborough Formation conglomerate separates the Sussex Group and the Upperton Formation. The top of the Windsor Group is picked on a relatively faint negative reflection. A positive reflection is expected at the transition from Windsor Group salt to Mabou Group clastic rocks above, however the strongest reflector is a faint trough, possibly a result of major deformation of the Windsor evaporite units. The Windsor Group salt appears to have undergone significant halokinesis (Wilson, 2005; Wilson et al., 2006) and formed a large salt wall (Figure 3.6; 3.7c) near the middle of the 3D survey. At the top of the salt wall and along the steep flanks the amplitude of this reflector diminishes making interpretation difficult. Salt welds are also interpreted in the data where it appears that the salt has been largely expelled and Mabou clastic sedimentary rocks lie close to the top of the limestone rocks of the Upperton and Macumber formations (Figure 3.6d; 3.6e). Here, the top Windsor Group remains a high-amplitude reflection. Stratigraphic horizons in the Mabou Group onlap the Windsor salt and thin over the salt wall (Figure 3.6d; 3.6e). Locally, a thrust fault is interpreted to have displaced part of the Windsor Group (Figure 3.6; 3.7c).

3.2.3. Horton Group structures

3.2.3.1. Fault interpretation

Faults and fault cutoffs were identified in the Horton Group and lowermost Sussex Group, following the initial horizon interpretation. Although fault development is interpreted to have begun soon after deposition (Chapter 2), the presence of faults cutting the Sussex Unconformity shows that deformation continued at least into the latest Tournaisian. Our analysis of fault kinematics therefore relates to the total strain accumulated over this interval.

Fault interpretations provided by Corridor Resources were used as a starting point in interpretation. Faults were identified based on loss of continuity of reflectors, usually correlated with significant variations in the depths of unit boundaries in wells. Typically, the loss of continuity

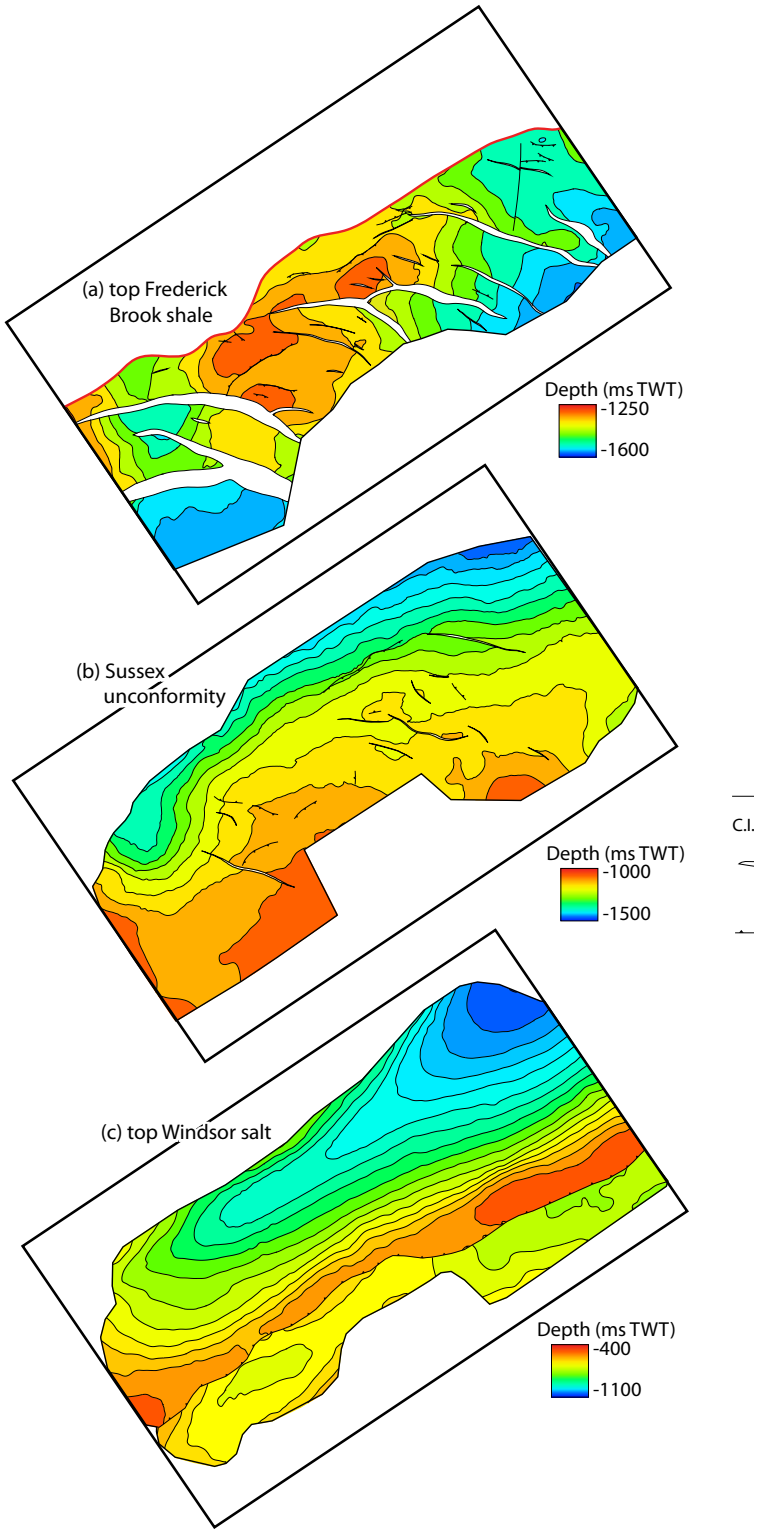

Figure 3.7. Subsurface time structure contour maps of the top Windsor salt, Sussex unconformity, and the top Frederick Brook shale horizons.

(a) Top of the Frederick Brook Shale. (b) Sussex unconformity. (c) Top of the Windsor salt. Structure contours are displayed in two-way travel time. Contour interval is 50ms of TWT.

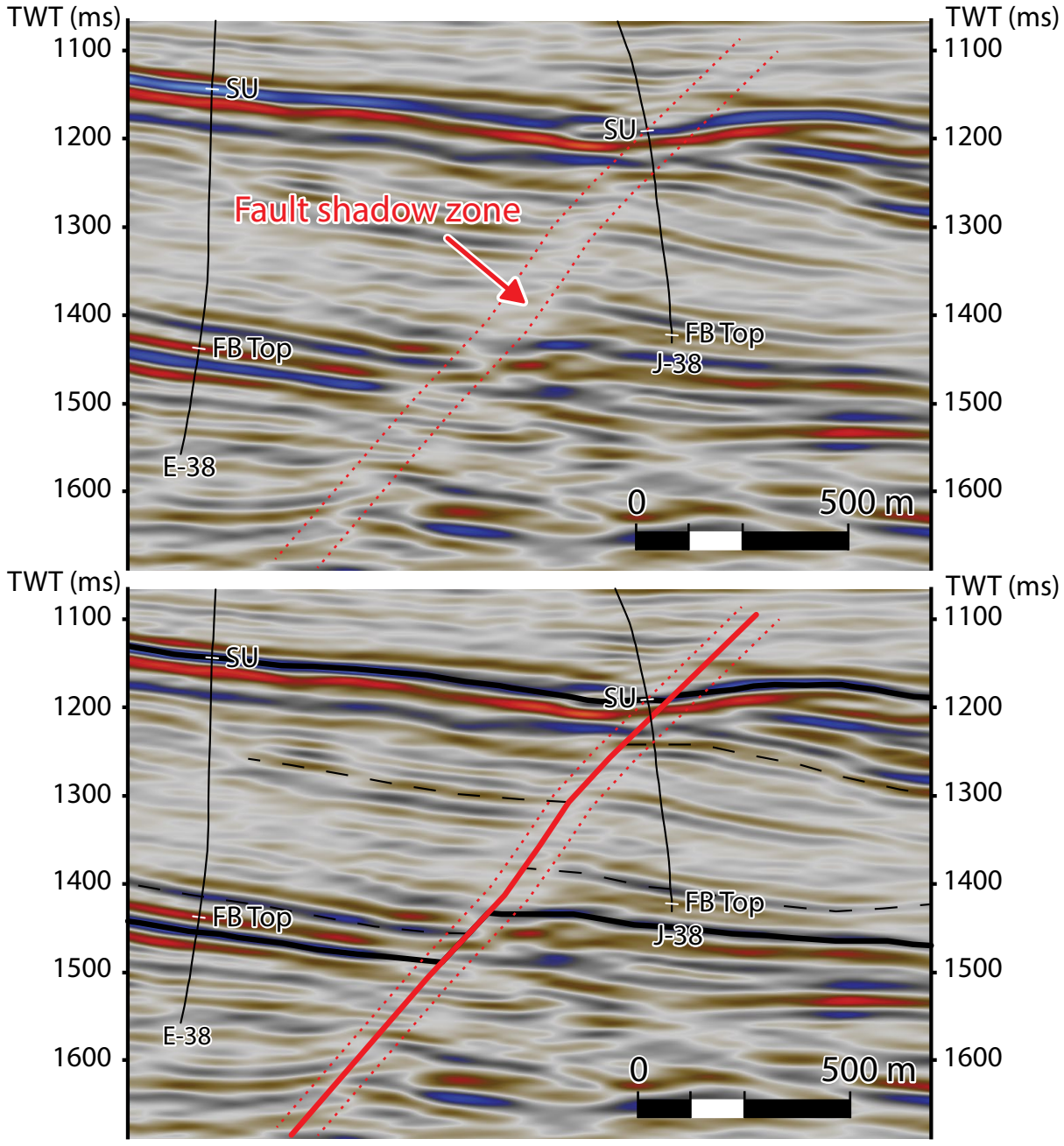

Figure 3.8. Illustration of a typical fault pick in the Horton Group within the 3D seismic data.

See text for details on fault shadow zones.

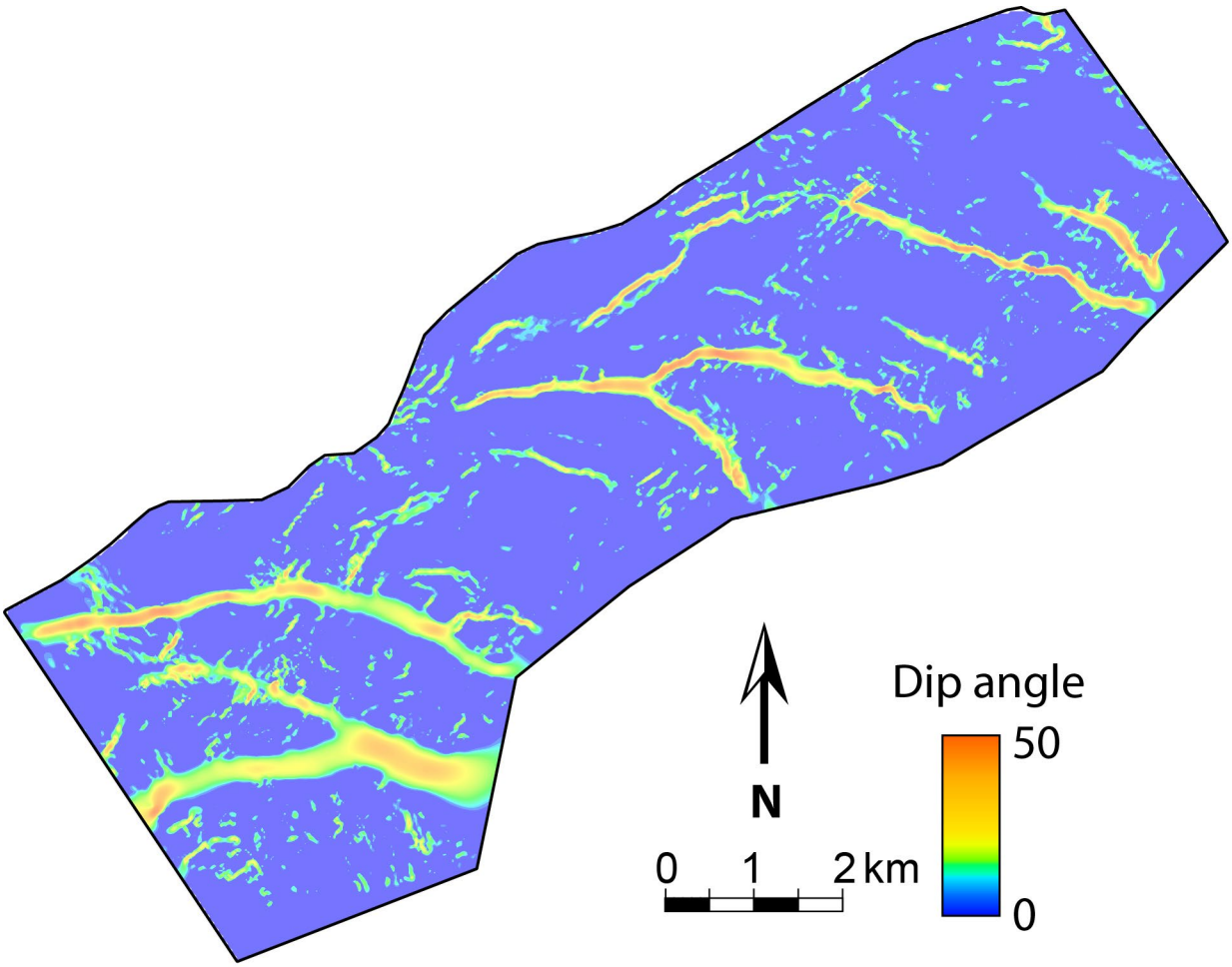

Figure 3.9. Structural dip map of the Frederick Brook shale at McCully.

The steep areas highlight where the Frederick Brook shale is offset by faults. See text for additional details.

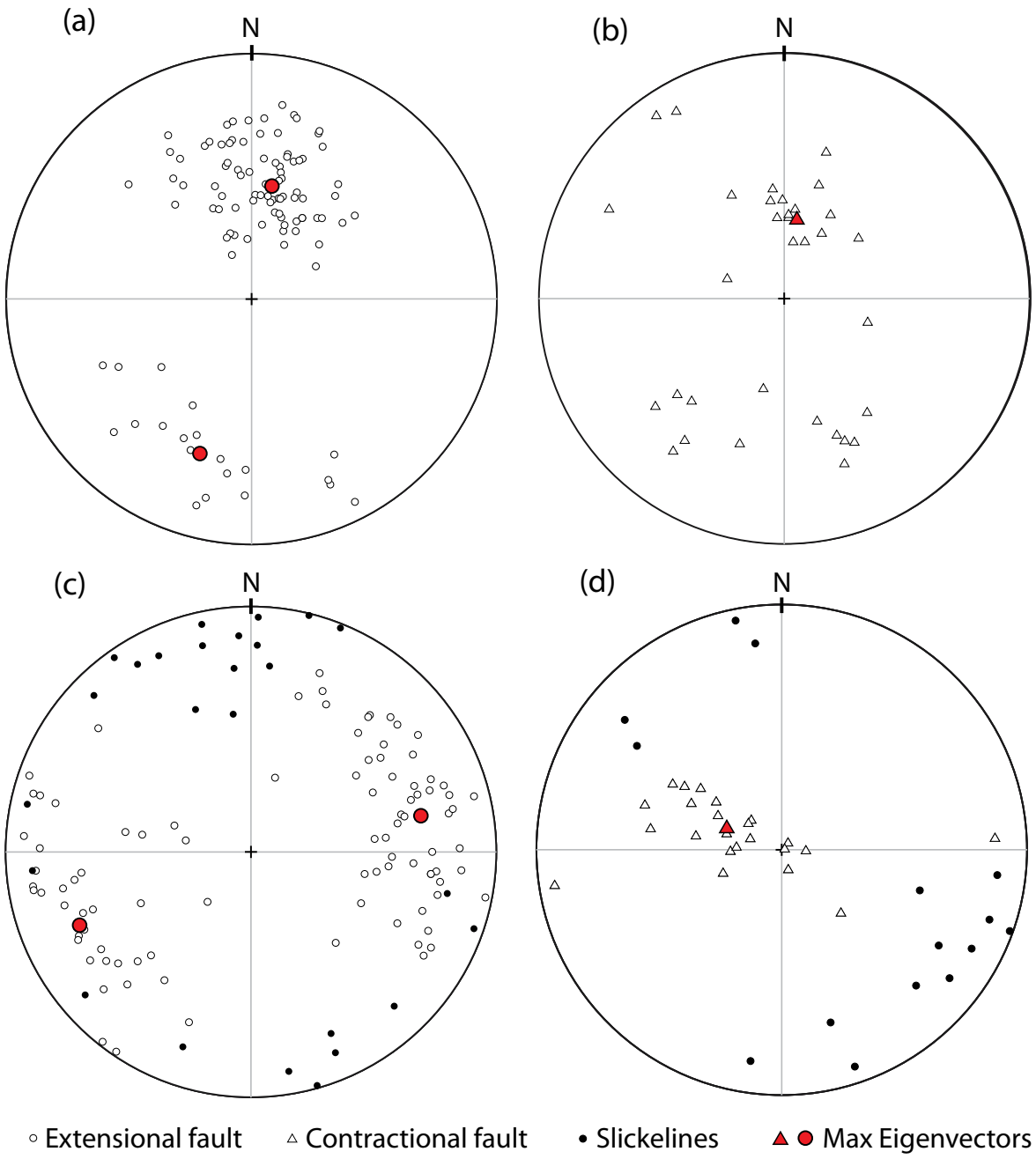

Figure 3.10. Equal-area stereoplots of fault data from the study area.

(a) Extensional faults observed in the seismic reflection data. Fault planes were measured at 500 m intervals along the strike of the fault, within the Frederick Brook shale-fault intersection lines. Fault dips were extracted from the structural model in Petrel, and converted to true angles in depth using an average velocity 4500 m/s, appropriate to the Albert Formation. Maximum eigenvectors are shown for each conjugate fault. (b) Contractional faults observed in the seismic reflection data. Sampling method same as (a). (c) Extensional faults observed in the outcrops along Highway 1. Maximum eigenvectors are shown for each conjugate fault set. (d) Contractional faults observed in the outcrops along Highway 1.

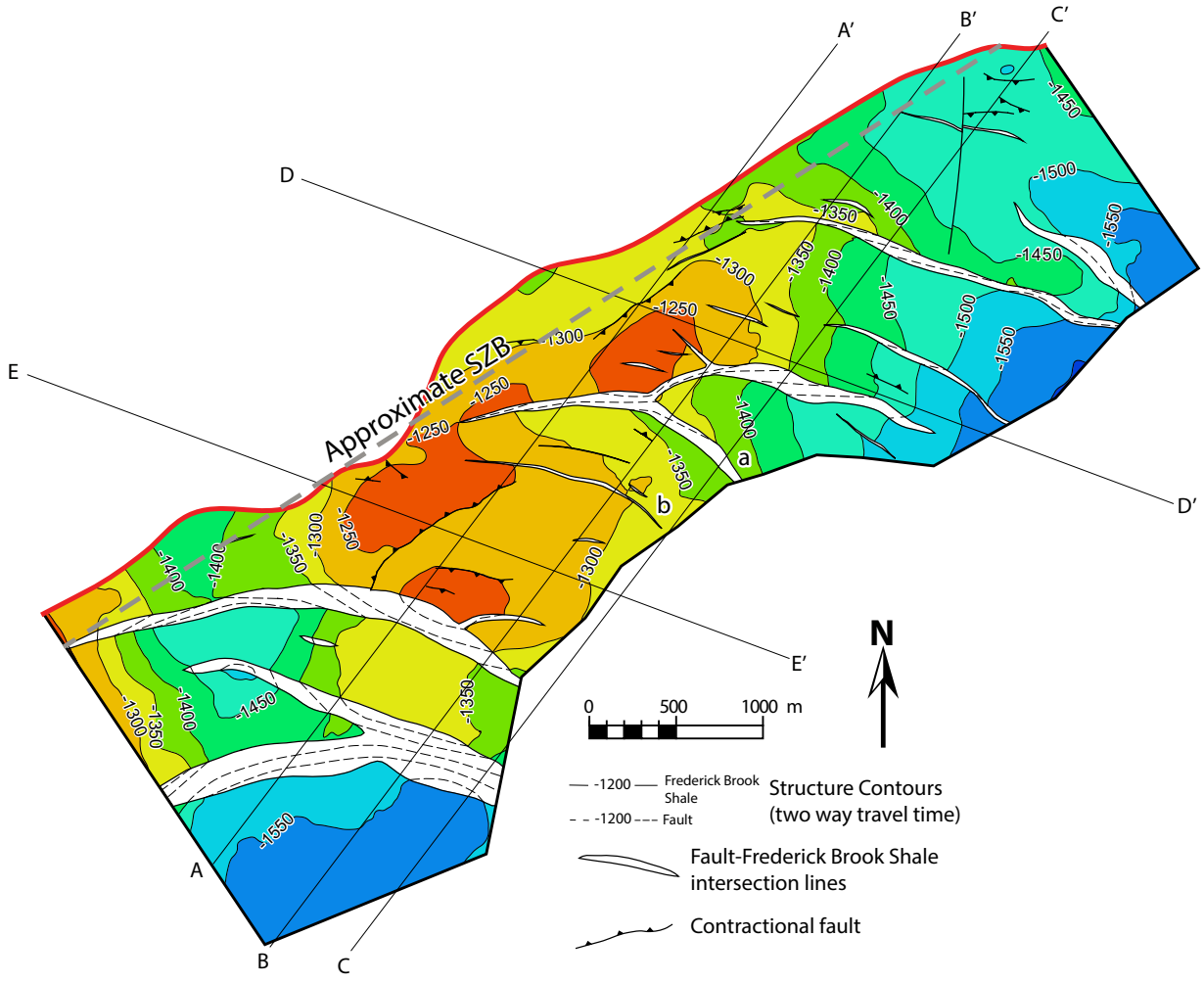

Figure 3.11. Subsurface time structure contour map of the top of the Fredrick Brook shale horizon.

Seismic section lines are shown for Figure 3.6. Structure contours are displayed in two-way travel time and have an interval of 50ms.

of reflectors due to faulting was not sharp, but rather showed as a region of faint reflectivity with a width of 50 – 250 m (Figure 3.8). This "shadow zone" on either side of the faults causes uncertainty when interpreting the fault plane orientation and the stratigraphic cutoff points. Faults were generally picked in the middle of the shadow zone. Reflectors with high amplitude (e.g. Sussex unconformity and the top of the Frederick Brook shale) display the discontinuities created by the faults clearly; thus these reflectors strongly influenced our fault interpretations. Furthermore, fault interpretation was aided by using structural dip maps of reflectors. In this method, smooth surfaces were created with the convergent interpolation method in Petrel, using the closely spaced horizon interpretations. After this, a structural dip map (Figure 3.9) was generated by calculating the dip of the surface over a tightly spaced (30 m) grid. Steeply dipping areas in the resulting surfaces mark where faults are present. Regions without faults have a relatively gentle dip. The dip maps show clearly where the corresponding horizon is likely to be offset by a fault (Figure 3.9).

Faults were initially picked on every second inline and crossline. After the general fault plane orientations were known, the faults were further picked along arbitrary planes in the 3D volume that were approximately perpendicular to the fault cutoff lines. These planes were chosen because they show the true dip and dip separation, allowing the fault plane and cutoff points to be more confidently interpreted. A typical fault pick is illustrated in Figure 3.8. Orientations of the fault planes were then measured at 500 m intervals along the strike of each fault due to the changing orientation of the faults. Figure 3.10 shows equal-area spherical projections of the resulting poles to fault planes. The angles of fault planes are used as relative reference values and should not be taken as absolute values since the seismic data are in time (s) and were not converted to depth (m).

3.2.3.2. Extensional faults

The most abundant structures observed in the seismic data are extensional faults that strike WNW – ESE (Figure 3.10a). Fifty-three faults displaying some amount of extension were interpreted in the late Horton. These faults range greatly in along-strike length (less than 200 m to more than 4000 m) and dip separation (less than 3 ms up to ~275 ms). Clear offsets in the Frederick Brook shale and Hiram Brook sandstones and mudstones are observed at these faults. The heave and throw of the faults generally increases towards the SW. The majority of these faults are confined to the Horton Group, although some major faults continue up through the Sussex unconformity (Figure 3.6). Observing these faults beneath the Frederick Brook shale becomes difficult as the resolution of the data decreases with depth. It is interpreted that the major faults become listric and probably flatten into a detachment horizon near the top contact with the underlying Dawson Settlement Member (Figure 3.6). Many of the lines where extensional faults intersect stratigraphic horizons are curved in map view (Figure 3.11). Although the heave and throw distances along these faults can be confidently identified, the amount of strike-slip movement, parallel to the fault surfaces, is unclear. As an example, the total heaves along a 12.7 km line perpendicular to fault strike (Figure 3.6b) amount to 1.58 km, creating an apparent stretch (S^* as defined by Waldron, 2005) along this line of:

$$S^* = (12.77 \text{ km} + 1.76 \text{ km}) / 12.77 \text{ km} = 1.14$$

Note that this stretch value does not account for out-of-plane movement.

3.2.3.3. Contractional faults

Contractional faults are much less abundant than extensional faults and are typically much smaller in strike length, throw, and heave. Like the extensional faults, the majority of the contractional faults do not extend above the Sussex unconformity. Many contractional faults are difficult to trace below the Frederick Brook shale horizon. Twenty-two faults displaying some amount of shortening were interpreted at the late Horton. These faults are typically linear. Most of the

contractional faults have strikes oriented roughly E – W (Figure 3.10b) and create minor amounts of stratigraphic repetition (up to ~40 ms of dip separation). Overall, these faults are responsible minimal shortening. For example, the total heaves along a 5.6 km line perpendicular to fault strike, shown in Figure 3.6d amount to 25 m, creating an apparent shortening along this line of:

$$S' = (5.6 \text{ km} - 25 \text{ m}) / 5.6 \text{ km} = 0.996$$

As in the case of the extensional faults, the amount of strike-slip movement along these faults is unclear.

3.2.3.4. Folds

Overall, the Horton Group is non-cylindrically folded into a NE – SW trending doubly-plunging anticline throughout the 3D data volume (Figure 3.11). Additionally, smaller folds occur where there are variable amounts of dip separation on large extensional faults (e.g. eastern part of Figure 3.11); synforms found in the hanging walls are focused near the middle of a fault where the separation is greatest. Fault-propagation folds are observed in the hanging walls of reverse faults (Figure 3.6d) where a large amount of dip separation is present (>30 ms). These folds are only imaged near large faults, probably because their scale is dependent on both the length and amount of separation of the associated faults. It is likely that similar smaller-scale folds are associated with most faults, but are not properly imaged by the seismic data as a result of the vertical and horizontal resolution limits. Overall, folding is responsible for most of the apparent shortening (*S'* as defined by Waldron, 2005). For example, along the cross-section line in Figure 3.6d, the line-length of the top of the Frederick Brook shale is 5.66 km whereas the length of the section is 5.6 km; the folding accounts for approximately 1.1% of apparent shortening, compared to the 0.4% attributed to fault-related shortening.

3.3. Outcrop objectives and methods

Because of the possibility of deformation at sub-seismic scale, we sought an outcrop analogue for the subsurface data. A series of 7 roadcuts containing strata from the Sussex and Horton groups are present along Highway 1 between Sussex and Norton (Figure 3.3). A roadcut, roughly 13 km SW from the location of the subsurface data, containing 4 outcrops, was chosen to be examined in this study based on the quality of exposure of the Horton Group and the proximity to the seismic data. The outcrops were analyzed to gain an understanding of the amount of deformation that has occurred in the Horton Group rocks on a sub-seismic scale.

In order to quantify the amount of extension within the Horton Group that is unresolved in the seismic reflection data, every fault was systematically measured; the strike, dip, and amount of dip separation of the faults was measured or estimated (Figure 3.12). A total of 134 faults were measured; 93 showed some amount of extension; 23 showed some amount of shortening; and 18 showed no evidence of extension or shortening. The trend and plunge of slickenlines were measured on 56 faults. Slickenlines were most common where calcite mineralization had occurred on the fault surface.

Extensional faults were the most common structure observed (Figure 3.13). The observable dip separation ranged from a few cm to 1.7 m. However, dip separations could not be measured or accurately estimated on all faults, so it is possible that some faults have more than 1.7 m of dip separation. Slickenlines were found on 26 extensional faults, 17 of them having a rake $\leq 30°$ or $\geq 150°$ (Figure 3.10c). As in the seismic data, two sets of normal faults were observed; a NW-striking set and a SE-striking set, as shown on the equal-area stereoplot of the normal faults (Figure 3.10c). An angle of 56° separates the average orientations of the two normal fault sets. The total heaves along a 243 m outcrop oriented roughly perpendicular to extensional fault strike (part of the outcrop shown in Figure 3.13) amount to 5.3 m, creating an apparent stretch along this line of:

$$S^* = (243\ \text{m} + 5.3\ \text{m}) / 243\ \text{m} = 1.022$$

Figure 3.12 (facing page). Map of the northernmost roadcut at the study location along Highway 1.

Location in Figure 3.3. Equal-area stereoplot of the poles to bedding and fold axes. Poles to bedding fall on a girdle.

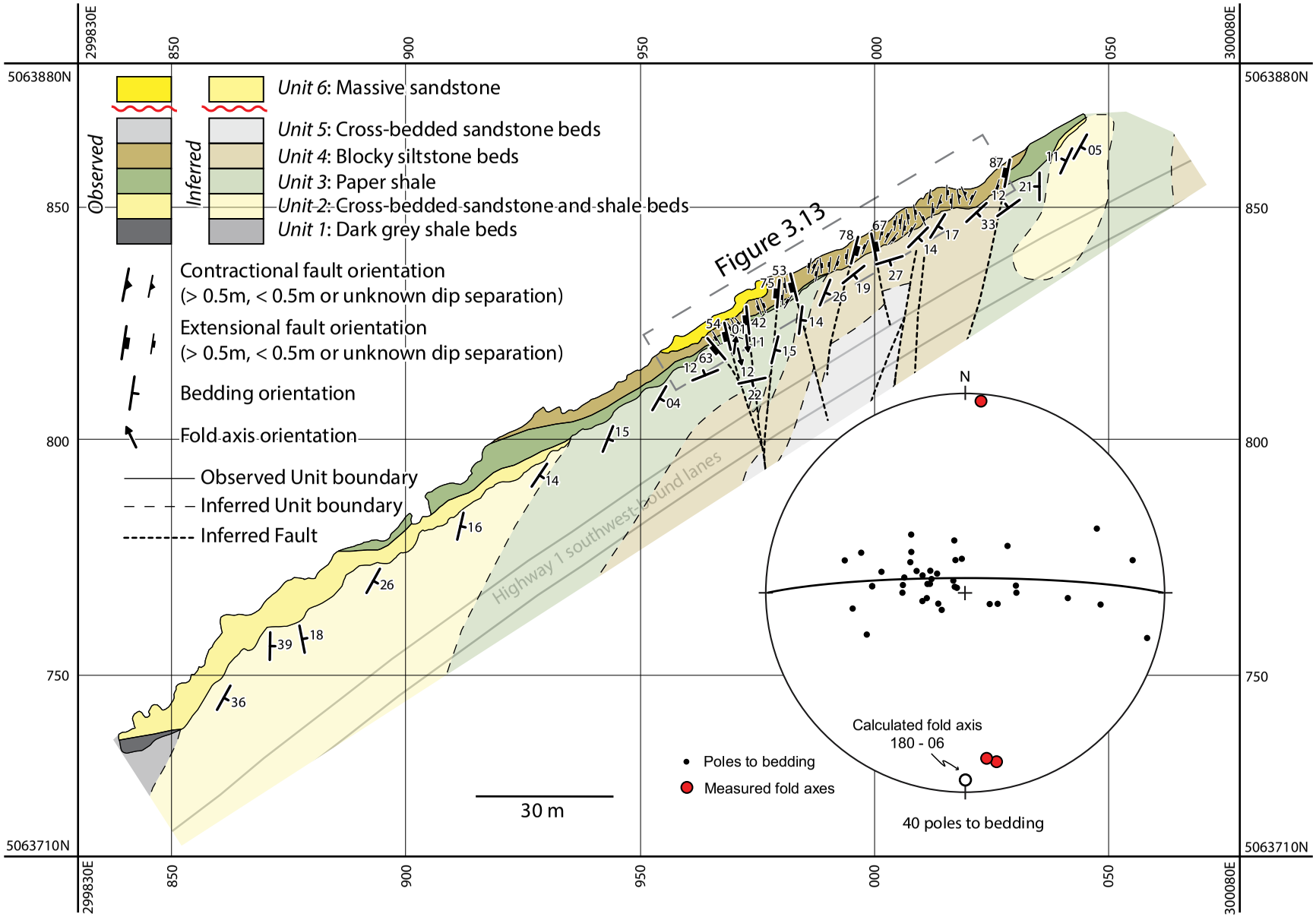
299830E
850
900
950
000
050
300080E
5063880N
850
800
750
5063710N
Observed
Inferred
Unit 6: Massive sandstone
Unit 5: Cross-bedded sandstone beds
Unit 4: Blocky siltstone beds
Unit 3: Paper shale
Unit 2: Cross-bedded sandstone and shale beds
Unit 1: Dark grey shale beds
Contractional fault orientation
(> 0.5m, < 0.5m or unknown dip separation)
Extensional fault orientation
(> 0.5m, < 0.5m or unknown dip separation)
Bedding orientation
Fold axis orientation
Observed Unit boundary
Inferred Unit boundary
Inferred Fault
Figure 3.13
Highway 1 southwest-bound lanes
30 m
N
Poles to bedding
Measured fold axes
Calculated fold axis
180 - 06
40 poles to bedding

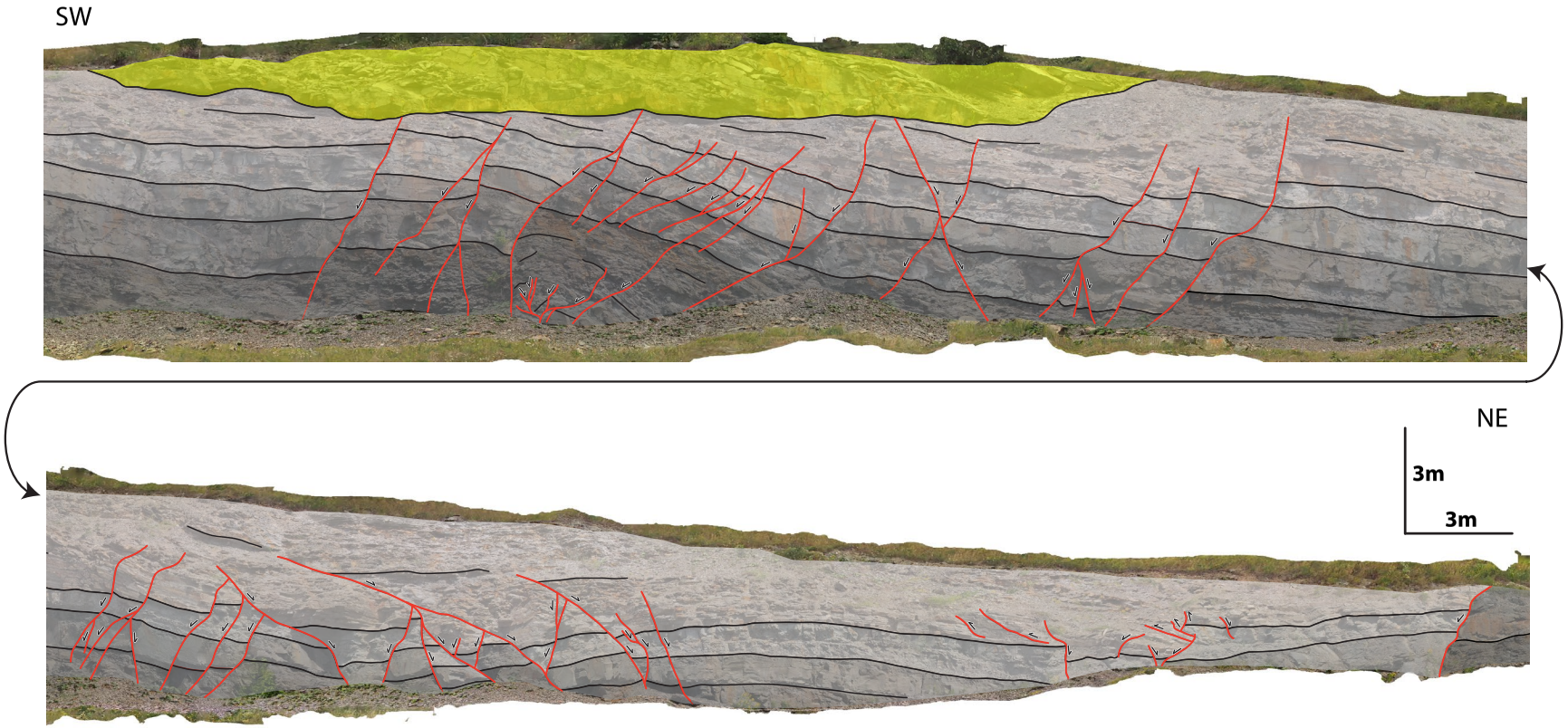

Figure 3.13. Interpreted orthomosaic photo of the Highway 1 roadcut.

Stratigraphy is traced with black lines and faults are traced with red lines with dip-separation arrows. Location of the road cut is shown on Figure 3.3 and the portion of roadcut in the orthomosaic photo is shown on Figure 3.12. The orthomosaic photo was made in Agi-Soft Photoscan Professional.

Note again that this stretch value does not account for out-of-plane movement.

Contractional faults were not as common as extensional and were mostly found within heavily deformed areas, and in the ooidal packstone bed. Dip separations are everywhere less than 1.5 m. An equal-area stereoplot of the reverse faults displays the general northward strike (Figure 3.10d). An apparent shortening calculation was not made because the NE – SW orientation of the roadcuts was roughly parallel to the contractional faults in the seismic data.

3.4. Discussion

3.4.1. Comparison of outcrop and subsurface datasets

The outcrops are located roughly 13 km southwest of the seismic data and are geographically closer to the bounding faults (Figure 3.3c), which are not parallel but converge to the southwest producing an overall funnel shape. The sedimentary rocks at the outcrops likely belong to the Hiram Brook Member (S. Hinds, New Brunswick Department of Natural Resources and Energy, personal communication, 2017). However, because the Hiram Brook can be up to 800 m thick in the Moncton Sub-basin (St. Peter and Johnson, 2009), the outcrops cannot be tied to an exact stratigraphic location in the seismic data, where the thickness ranges between 0 to 800 m.

3.4.1.1. Amount of deformation

The patterns of fault orientations are similar in both datasets; however, the absolute orientations are different (Figure 3.10). The conjugate extensional faults in the seismic data strike roughly WNW – ESE, whereas the outcrop conjugate extensional faults have strike orientations roughly NNW – SSE. The contractional faults interpreted in the seismic data show a weak conjugate relationship in contrast to the outcrop data where the orientations of the contractional faults are similar. The contractional faults in the seismic data strike roughly E – W, whereas in outcrop the contractional faults have strike orientations roughly NNE – SSW. Furthermore, shallowly-plunging slickenline on extensional faults orientations from the outcrops (Chapter 2; Figure 3.10c)

suggest that a large component of the slip along these faults was lateral, leading to the interpretation that the outcrops have undergone deformation which is closer to ideal strike slip.

The differences in structure between the outcrops and seismically imaged region may be related to the overall funnel-shape of the sub-basin. The width of the overall shear zone between the basin-bounding faults becomes narrower to the southwest, but the total amount of strike slip is probably near constant along strike. Thus rotational strain may be greater towards the southwest, resulting in greater deformation at the outcrops than at the McCully area. Because the strike-slip movement in the Moncton Sub-basin was likely dextral (Waldron et al., 2015), the structures within the shear zone have probably rotated in a clockwise direction; therefore, it is possible that the faults at the outcrop location may have rotated further clockwise than the faults in the seismic data based on the orientations in Figure 3.10. If this is the case, the estimate of the apparent stretch obtained from the outcrops (2.2%) is likely an overestimate of the deformation that occurred between the seismic-scale faults in the McCully area. This value should therefore be regarded as a maximum.

3.4.1.2. Timing of deformation

Variations in stratal thickness across large normal faults and cross-cutting relationships can be used to constrain the timing of deformation in the seismic data. Sand units within the Hiram Brook Member have been identified by Corridor Resources in 43 wells using core and well log data. Wells drilled in the hanging walls of major extensional faults commonly show equal thickness of these sands in the hanging walls and footwalls. Therefore, deposition of the lower to middle Hiram Brook Member was probably not significantly controlled by the extensional faults interpreted herein. The distribution of the upper Hiram Brook Member is much more limited because the Sussex unconformity has eroded these sands nearly across the entire survey. However, in the SSW region of the survey, where upper Hiram Brook Member sediments are present, individual sand units are thicker in the hanging walls of extensional faults (Figure 3.6a; 3.6b;

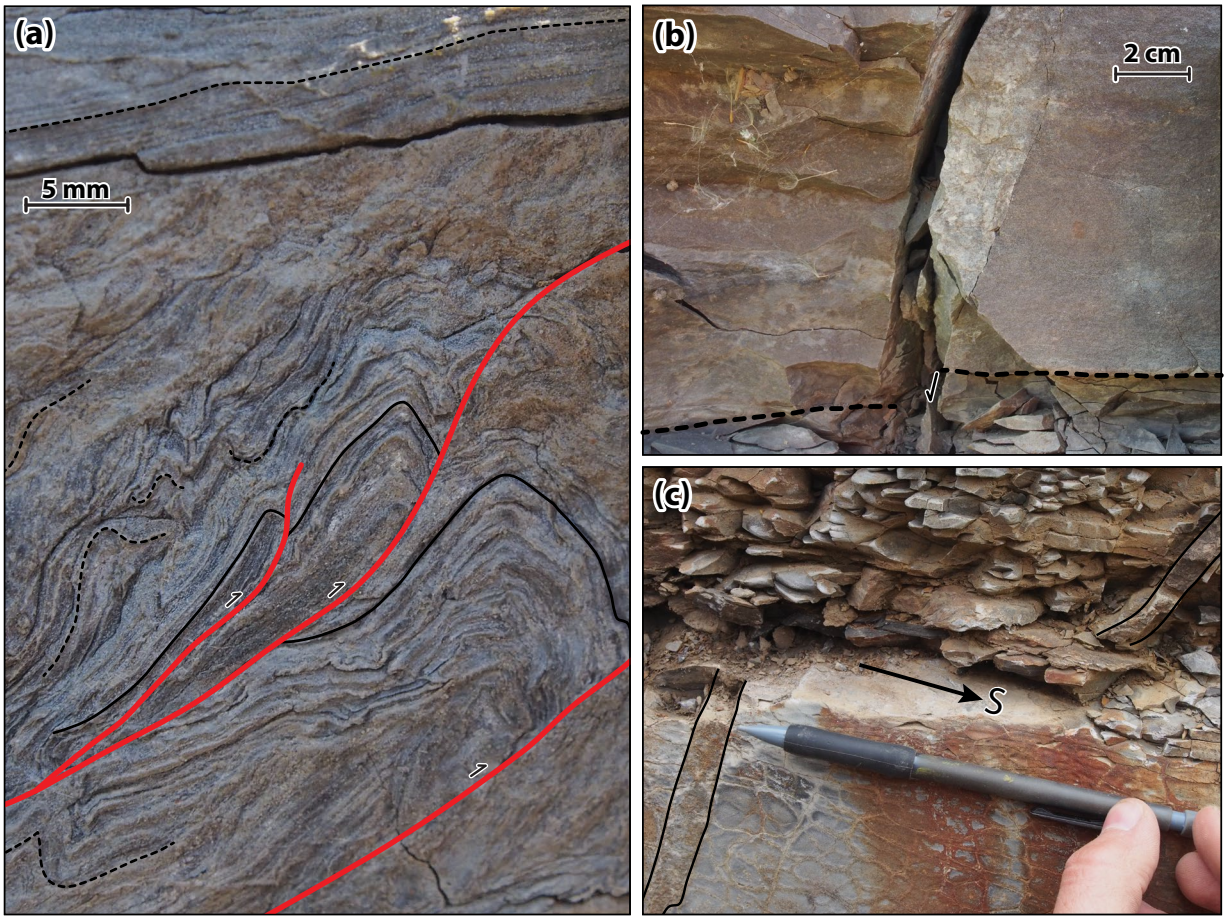

Figure 3.14. Field photographs of the Highway 1 roadcuts.

(a) Contractional faults and folds in laminae confined to a single bed. Note the parallel strata directly above the bed. Red lines indicate faults and black lines trace stratigraphy. (b) A sandstone dyke following a fault plane. The black dashed line traces the offset bedding. (c) Sandstone dyke offset by an approximately bedding parallel fault. Abbreviation: S = slickenline orientation.

3.6c), suggesting that deformation began during the deposition of these units. This deformation is interpreted to have concluded before Sussex Group deposition because the majority of the faults do not cut up through the unconformity.

Observations from the outcrops also suggest that the deformation in the Horton Group occurred early in the basin history. Structures seen in outcrop suggest soft-sediment deformation (Figure 3.14). For example, folds and contractional faults confined to single beds, with sharp contacts to parallel laminae above and below, suggest soft-sediment deformation (Figure 3.14a). Furthermore, sandstone dykes locally follow fault planes (Figure 3.14b). It is interpreted that sands were injected up existing fault planes after being fluidized. Wilson (2005) suggested that much of the soft sediment deformation found in the outcrops along Highway 1 may have been triggered by earthquake activity. In addition, the intra-formational unconformity shown in Figure 3.13, where faults within the grey siltstones cannot be traced up through the erosion surface at the top of the outcrop, further suggests early deformation of the basin while the Hiram Brook Member was being deposited.

The orientation of the contractional faults is similar to the extensional faults in the seismic data (Figure 3.10). This is not an expected observation in a strike-slip tectonic environment, where these faults are predicted to be roughly perpendicular to each other as occurs in the outcrop data (Figure 3.10). It is possible that the contractional faults were originally extensional and have become inverted during later contractional deformation of the sub-basin. Several authors (eg. St. Peter, 1993; Wilson and White, 2006; St. Peter and Johnson, 2009) have suggested that the Moncton Sub-basin has undergone inversion events throughout its geologic history, many of which are suspected to be a result of transpression along the E – W Minas Fault Zone (Figure 3.3b; Wilson and White, 2006). It is possible that the contractional faults formed during later transpressional phases, however, several of these faults are truncated by the Sussex Unconformity and must have formed before this inversion event. Any quantitative estimates for finite strain (below) derived from structures in the Moncton Sub-basin therefore includes both the

opening of the basin (probably transtensional) and its later Carboniferous transpression, meaning an overestimate of *S'* is possible.

3.4.2. Qualitative kinematic analysis

3.4.2.1. Introduction

The structures observed in both the seismic and outcrop data sets are consistent with dextral strike slip (Harding, 1974). The dominance of extensional faults over contractional features (faults and folds) in both the quantity of structural features and amount of deformation suggest that the basin was deforming in a transtensional environment early in its history, and that the location of the outcrop data was significantly more deformed than the subsurface volume.

Faults in the seismic data vary in curvature. The extensional faults show stratigraphy-fault intersection lines (cutoff lines) which curve in map view (Figure 3.11), with the concave side facing towards the SW; the contractional faults are typically linear. The dip-direction of a fault does not appear to influence the concavity direction. For instance, on Figure 3.11 the extensional fault polygons marked *a* and *b* have roughly opposite dip-directions (probably conjugate faults) but are curved in the same direction. There are several ways that stratigraphy-fault intersection lines may become have curved:

(1) the faults were folded after formation;

(2) early-formed faults may have rotated during deformation before propagating in response to a constant instantaneous extension direction (Sylvester, 1988);

(3) the magnitude of the total strain may have been heterogeneous across the shear zone;

(4) the direction of the instantaneous extension axis may have varied across the shear zone;

(5) the strain magnitude and/or orientation may have varied in time; or

(6) any combination of the previous possibilities.

These options are considered in turn in the following sections.

1) Faults folded after formation. The fault plane data in Figure 3.10a do not form any apparent girdle, which would suggest that the faults were not folded by a single later contractional event. Furthermore, to create curved faults which are concave in the same direction but have opposite dip-directions, the extensional component of folding would have to have been horizontal. This type of folding is not observed in the stratigraphy, where gentle antiforms and synforms are found throughout the 3D volume. Thus, it is unlikely that the present-day fault geometry has formed in this way; later folding may be ruled out as a cause of fault curvature.

2) Rotation and asynchronous fault propagation. On Figure 3.11, the parts of the faults which are near the SZB are at smaller clockwise angles (θ') from the SZB than the parts of the faults which are further from the SZB. In this transtensional setting the extensional faults would have initiated in response to the instantaneous strain. With progressive dextral deformation, these faults would begin to rotate clockwise. When the fault further propagated after rotation, the new part of the fault would form in response to the instantaneous strain. As this continued, a curved fault would have formed with the oldest portion being rotated more than the younger. For this to be the case at McCully, we would predict that the faults would have initiated in the SE and propagated north-westwards with time towards the SZB. If this hypothesis is correct, the NW ends of the faults display deformation that is closer to the instantaneous strain than the SE ends, which display the finite strain.

3) Heterogeneous magnitude of strain in space. Another possible explanation for the curved fault-stratigraphy intersections is that shear strain may have had a heterogeneous magnitude across the shear zone. In many shear zones, the shear strain varies throughout, the maximum magnitude being at the center of the shear zone and the minimum occurring at the SZB (Fossen,

2016). In the case considered here, portions of faults that formed near the SZB would be expected to show a smaller *θ'*-angle (Figure 3.2b) than portions of faults that formed away from the SZB. The curvatures of the faults at McCully are consistent with these expectations; the fault traces are at greater angles to the SZB away from the SZB in the SE.

4) Heterogeneous direction of strain in space. It is also possible that the curved extensional fault traces formed in response to a variable instantaneous extension direction across the shear zone. Tectonic environments with different *α*-angles will have different strain ellipses; as the α-angle increases, the instantaneous extension axis becomes closer to perpendicularity with the SZB (Figure 3.2a). This means that extensional faults which form in high-*α* transtensional environments are less oblique to the SZB; as the *α*-angle decreases, the extensional faults are expected to be at greater angles to the SZB. As stated earlier, the extensional faults are oriented at greater angles to the SZB away towards the SE. If this scenario is true for the McCully area, then it is expected that the α-angle decreases towards the SE.

5) Heterogeneous strain in time. Moreover, the fault curvature may be a result of changes to the instantaneous strain over time. As stated earlier, it is possible that the faults initiated in the SE of the data volume and propagated NW. The curvature of the faults observed at McCully could be accounted for if the initial faults developed in a strike-slip-dominated setting (low α, high *θ'*; Figure 3.2) and later portions of the faults developed in a more extension-dominated setting (high α, low *θ'*; Figure 3.2).

3.4.3. Quantitative kinematic analysis

Despite the uncertainties about the development of the curvature of the faults mentioned in the previous section, the bulk strain can still be examined for insights into the kinematics of the Moncton Sub-basin during the Late Devonian – Early Mississippian. A simple model developed by Waldron (2005) is here applied to these data to calculate the finite kinematic parameters of the basin (Figure 3.15). This model quantifies the amount of rotation that the structures have undergone and gives an estimate of the angle of divergence (*α*), assuming that the sub-basin formed

in a strike-slip to transtensional setting. The model's concept is as follows. As progressive deformation occurs along the SZB, the amount of shear strain increases. The instantaneous strains involve extension and shortening in perpendicular directions (Figure 3.1a). The ratio of the two carries implications for the amount of transtension (versus ideal strike-slip) that the sub-basin has undergone: in ideal strike-slip the ratio of extension to shortening is equal, whereas extension is greater than shortening in transtensional settings. When dealing with finite deformation, the same relationships between principal strains apply, but the rotation of structures has to be taken into account (Figure 3.1). As shear strain increases, the amount of rotation of fault blocks within the zone boundaries increases (Figure 3.15). The combined effect of increasing strain and rotation causes the heaves of the extensional faults to increase. The stretch accommodated by the fault heaves can be measured and used to obtain an estimate of the amount of shear strain and rotational deformation that a basin has undergone (Figure 3.15). However, the model is complicated in transtensional settings since extensional faults do not form at 45° to the SZB (Figure 3.2). To account for this, the orientation of the extensional faults is crucial for determining kinematic parameters in transtensional settings.

The required observable parameters (Figure 3.15) for this model include the orientation of the SZB, the orientation of the extensional faults today relative to the SZB (θ'), and the change in widths of the block segments to calculate the apparent stretch (S^*) and apparent shortening (S'). (The stretch and shortening values are "apparent" because the quantities do not take into account the amount of strike-slip movement that has occurred parallel to the faults during block rotation.) It is assumed that as strike-slip deformation progresses, fault-bounded blocks are rotated about a vertical axis to create fault heaves. The apparent stretch is calculated by summing the widths of the segments (w) and the heaves (h) and then expressing the sum as a proportion of the width of the segments (Figure 3.15), so that the apparent stretch is:

$$S^* = (h + w) / w \qquad (1)$$

In ideal strike-slip tectonic settings the apparent shortening is the reciprocal of S^* since area is

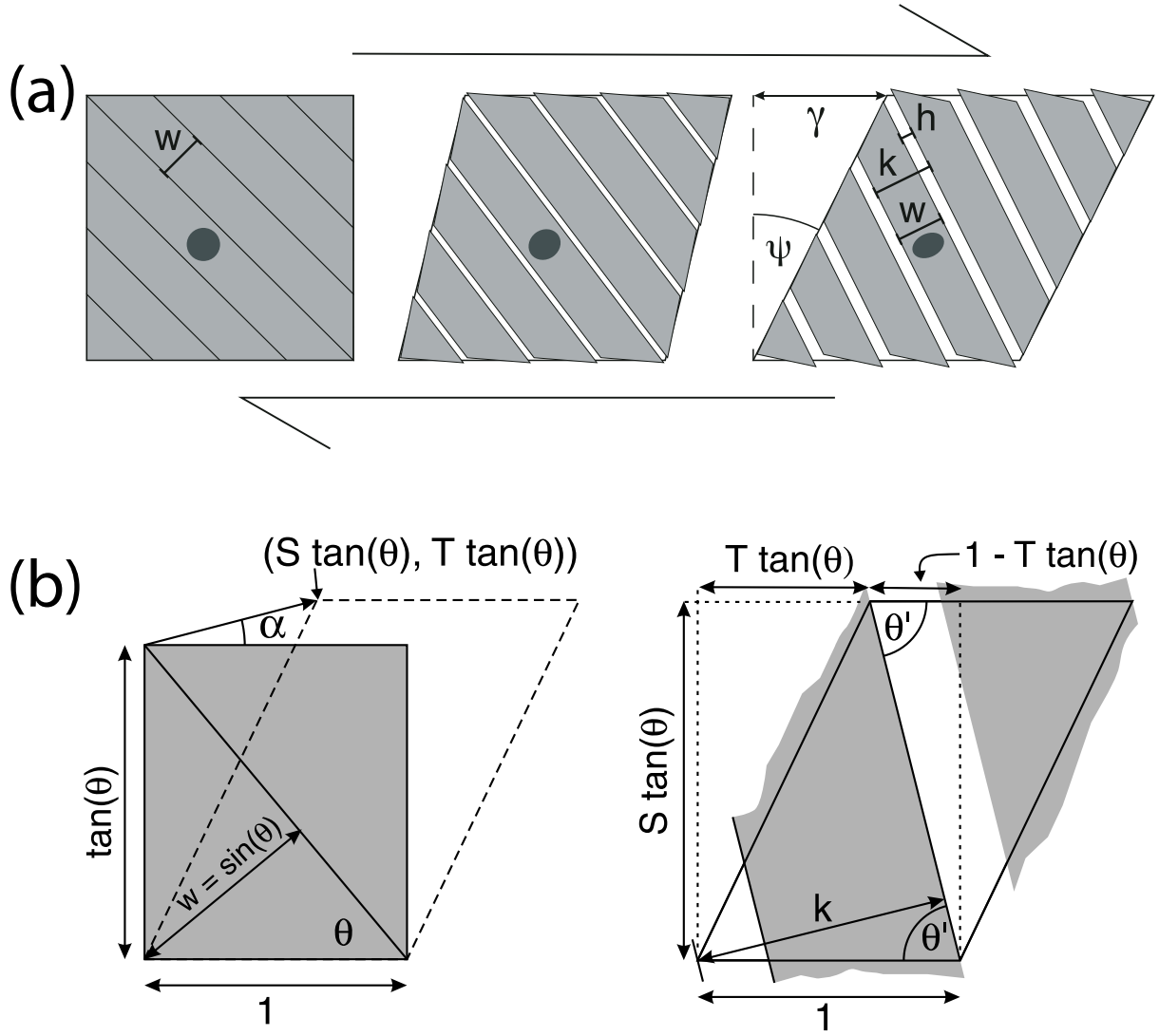

Figure 3.15. Diagrammatic representation of strike-slip block faulting.

Modified from Waldron (2005). (a) Simple shear ideal strike-slip case. As progressive strike-slip deformation occurs, the combined effect of increasing shear strain and rotation of fault blocks results in increased fault heaves (*h*). (b) Transtensional case. Quantities are defined in text.

conserved. Waldron (2005) shows that the relationship between S^* and γ is relatively simple in such settings, where:

$$S^* = 1 / \sqrt{(1 - \gamma + \gamma^2 / 2)} \quad (2)$$

However, it is not as simple in transtensional settings where S^* is greater than S'; the ratio between these two values increases with increasing α and shear strain. Waldron (2005) showed that the (finite) transtensional variables T (displacement gradient parallel to the SZB), S (displacement gradient perpendicular to the SZB), θ (initial fault orientation), γ (the amount of shear strain), and the angle of divergence (α) can be estimated using the measured values of S^*, S', θ' through the equations:

$$S = S^* S' \quad (3)$$

$$\sin\theta = \sin\theta' / S^* \quad (4)$$

$$T = \cot\theta - S\cot\theta' \quad (5)$$

$$\gamma = T / S \quad (6)$$

$$\tan\alpha = (S - 1) / T \quad (7)$$

Furthermore, it can be tested whether these transtensional variables changed through time by assuming that the faults initiated in an orientation perpendicular to the instantaneous extension axis. Waldron (2005) shows that θ is simply dependent on α, where:

$$2\theta = 90 - \alpha \quad (8)$$

The transtensional parameters are considered constant throughout the deformation of the basin if α determined via equation (7) is the same as that given by equation (8). If different α-values are attained, then it is likely that the deformation was heterogeneous through time.

Excluding outcrop S^* estimate

	S^*	θ'	θ	α (finite variables)	α (initial fault orientations)	γ
Bulk	1.14	40°	34°	57°	21°	0.111
A - A’	1.16	37°	31°	63°	27°	0.114
B - B’	1.14	47°	40°	48°	10°	0.131
C - C’	1.12	55°	47°	37°	~0°	0.144

Including outcrop S^* estimate

	S^*	θ'	θ	α (finite variables)	α (initial fault orientations)	γ
Bulk	1.162	40°	33°	59°	23°	0.123
A - A’	1.182	37°	30°	66°	29°	0.123
B - B’	1.162	47°	39°	50°	12°	0.145
C - C’	1.142	55°	46°	39°	~0°	0.162

Figure 3.16. Kinematic parameters of the Moncton Sub-basin at the Frederick Brook shale horizon.

Quantities are defined in text. Bulk strain was calculated using the average apparent stretch S* from lines A-A’, B-B’, and C-C’. For locations of lines see Figure 3.11. Average fault strike θ’ was determined from eigenvalues shown in Figure 3.10.

3.4.3.1. Bulk strain at McCully

At McCully, the SZB azimuth is estimated at 057°, by connecting the northernmost extensional fault tips (Figure 3.11). Obtaining an accurate estimation of the orientation (θ') of the faults in the data volume relative to the SZB is difficult because of the mentioned curvature of the faults. For simplicity, a θ'-value of 40° was determined from the mean of the fault orientations. (The curvature of the faults is examined in more detail in later sections.) The *S** values of the cross-sections in Figure 3.6a, 3.6b, and 3.6c are shown in Figure 3.16; an average *S** value of ~1.14 is used as a bulk apparent stretch. Likewise, cross-sections in Figure 3.6d and 3.6e have *S'* values of 0.987 and 0.985 respectively, resulting in an average bulk apparent shortening of ~0.986. As identified earlier, a basin formed in a purely simple-shear regime is predicted to show a reciprocal relationship between *S** and *S*', meaning that there is no overall vertical extension or contraction. Because the calculated values of *S** is much greater than 1/*S*' (Figure 3.16), the sub-basin has experienced a large horizontal extension component, consistent with a transtensional origin.

Estimates of strain derived from seismic data potentially under-estimate true strain because small-scale ("sub-seismic") faults are not resolved. Therefore, outcrops were examined to estimate the amount of deformation between the seismic-scale faults that is unresolved in the seismic data. A sub-seismic *S** of 2.2% was calculated for the northernmost outcrop. However, as stated earlier, it is likely that the outcrops show more deformation than the rocks imaged in the seismic data. This means that the *S** value calculated from the outcrops is an upper limit to what is expected at the seismic data location. Kinematic parameters were calculated for two cases: seismic parameters only and seismic parameters plus the sub-seismic *S** estimate (Figure 3.16). It is likely that the true sub-seismic *S** is somewhere between 0 and 2.2%, so these two cases are used as upper and lower limits.

The bulk kinematic parameters derived from these data were calculated using equations (3) through (7) and are summarized in Figure 3.16. Figure 3.17 shows the simplified schematic

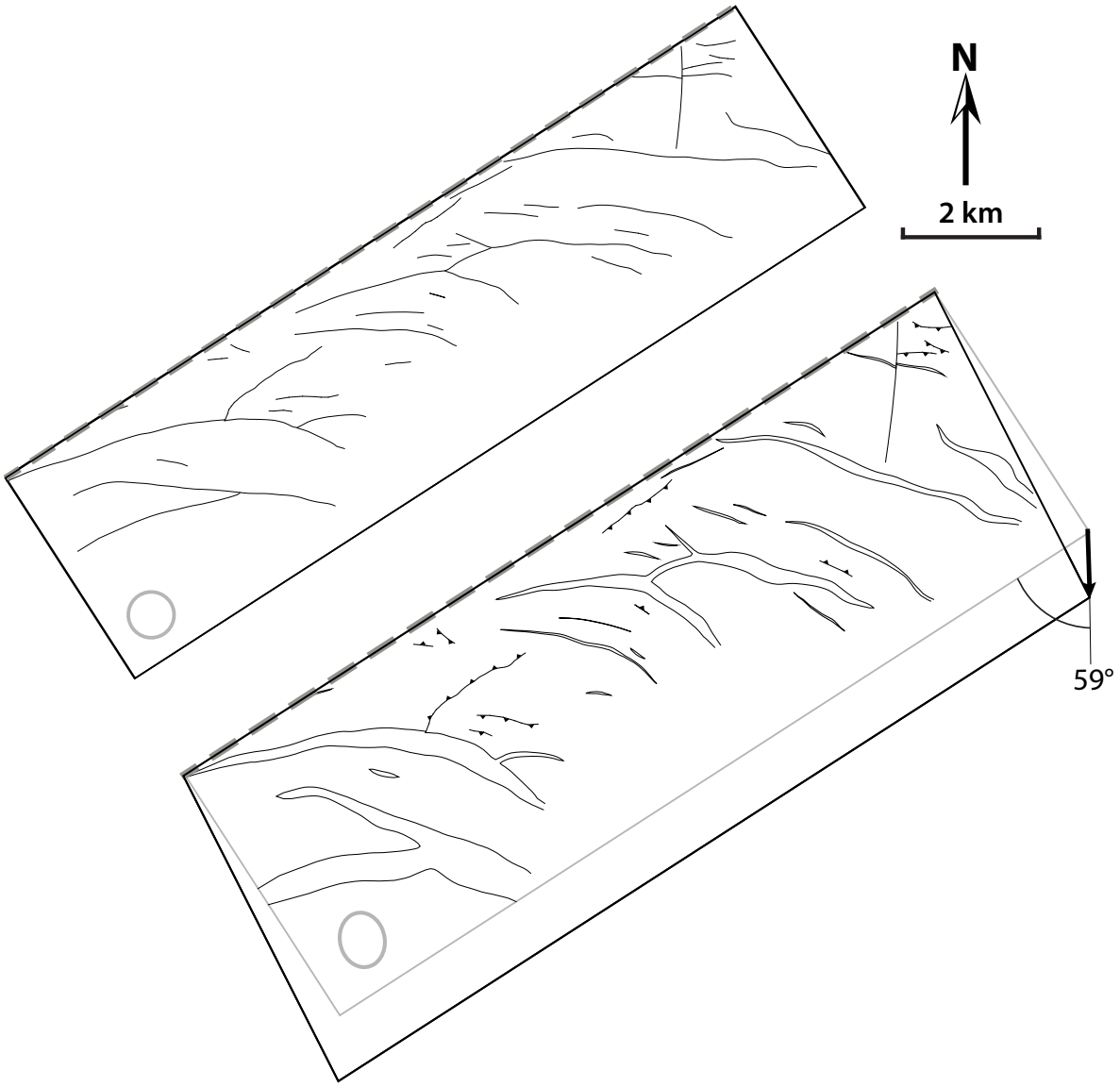

Figure 3.17. Reconstruction of the top of the Frederick Brook shale-fault intersection lines.

(a) Schematic retro-deformed map of the Frederick Brook shale. (b) Present-day Frederick Brook shale-fault intersection lines. The ellipse displays the required strain needed to produce the present-day geometry of the faults. The arrow indicates the divergence of 59° from the shear zone boundary (grey dashed line).

reconstruction of the Frederick Brook shale, showing the geometry before and after the bulk transtensional deformation.

3.4.3.2. Spatial variation

To determine the extent of spatial variation in the deformation at McCully, unique kinematic parameters were calculated along lines of sections across the data volume. Because the faults are curved, each cross-section perpendicular to the extensional faults required a unique estimation of the orientation of the faults (θ'). A weighted vector mean based on the amount of heave for each was used to get an accurate representation of θ' along each cross-section. Values of S^* and θ' were determined for each seismic-section in Figure 3.6a, 3.6b, and 3.6c. Because the variability in the S' across the data volume is marginal, the average value of 0.986 is used for each case. The SZB orientation is the same as in the bulk strain calculations above. The S^* and θ' values for each line of section is summarized in Figure 3.16.

The finite kinematic parameters were also calculated using equations (3) to (7) along each line of section and are summarized in Figure 3.16. Note that towards the SE (away from the SZB) the S^*, θ', and α values decrease, whereas the γ-value and fault rotation increase.

3.4.3.3. Temporal variation

The strain parameters obtained above were tested to determine whether the transtensional parameters changed through time by using the θ-values for each line of section and equation (8). The results are summarized in Figure 3.16. Since the α-values calculated based on instantaneous strains are much lower than the α-values calculated earlier (finite parameters), it is likely that the faults initiated in a tectonic environment that was strike-slip-dominated, which then became increasingly transtensional with time.

3.4.3.4. Curved fault kinematics

The strike orientation of the majority of the extensional faults that cut the Horton Group within the data volume varies between 15° and 25° along strike (Figure 3.11). This means that initial portions of the faults would have had to rotate between 15° and 25° clockwise before the latest portions of the faults propagated to account for the curvature. The results above show that the faults only have rotated a maximum of 9°; thus rotation (*possibility 2*) cannot account for the entire curvature of the faults. However, assuming that the faults initiated in the SE and propagated northwestwards, it is likely that rotation did play a role in curving the faults.

As shown above, the shear strain (γ) at the McCully increases from a minimum of 0.114 in the NW to a maximum of 0.162 in the SE. This implies that the magnitude of deformation was heterogeneous across the shear zone (*possibility 3*). The increasing γ to the SE supports the curvature of the faults because as γ increases, the angle between the faults and the SZB (θ') increases (Figure 3.2a).

Furthermore, the finite α-angle decreases from a maximum of 66° in the NW to a minimum of 37° in the SE. This implies that the instantaneous strains were heterogeneous in direction across the shear zone (*possibility 4*), transitioning from a highly extension-dominated environment in the NW to a higher proportion of strike-slip deformation in the SE. This is consistent with the concavity direction of the faults; it is expected that higher α-angles result in faults with lower θ'-values than lower α-angles (Figure 3.2).

Moreover, the discrepancy in the above estimations of the α-angle between the finite strain parameter method (equations 3 to 7; 37° to 66°) and the instantaneous strain method (equation 8; 0° to 29°) illustrate that the basin likely started in a strike-slip-dominated setting and transitioned to an extension-dominated setting with time (*possibility 5*). Again, the observed curvature of the faults could be explained by fault initiation in the SE and asynchronous propagation to the NW. The faults may have initiated in a strike-slip-dominated setting, resulting in high θ'-angles

(Figure 3.2) in the SE. The tectonic setting could have then transitioned to an extension-dominated setting such that younger NW-portions of the faults developed lower θ'-angles (Figure 3.2).

The arguments above suggest that the curvature of the extensional faults at McCully formed in response to several factors. These factors include a combination of fault propagation and rotation with progressive deformation (*possibility 2*), variable magnitudes of the shear strain across the shear zone (*possibility 3*), and heterogeneous instantaneous strain directions across the shear zone (*possibility 4*). Furthermore, it is likely the tectonic environment changed through time (*possibility 5*), originating in a strike-slip-dominated regime, and developing into a transtension-dominated regime, further adding to the curvature of the faults. It is not possible to quantify how much each factor contributed to the overall curvatures, but all factors probably played a role (*possibility 6*).

3.4.4. Implications to the greater Maritimes Basin

Based on the above estimate from the subsurface data of the bulk transtensional angle (α between 57° to 59°), the extension direction for the early Moncton Sub-basin is predicted to have been almost N – S, resulting oblique extension. This result is different from previous work (e.g. Waldron et al., 2015) that favors a higher proportion of strike-slip deformation and a NE – SW extension direction. This means that the Moncton Sub-basin deformed more like an oblique rift and less like a pull-apart basin during the early Tournaisian. The variability in the α-angle across the shear zone suggests that the Moncton Sub-basin deformed heterogeneously in space and time; this result should raise questions about how uniform deformation was between sub-basins within the greater Maritimes Basin, let alone within a single basin. Although similarities can be found between sub-basins, it is unlikely that each basin developed and deformed in an identical way.

3.5. Conclusions

The observations made here highlight the geometrical complexities of transtensional basins, as a result of rotation and concurrent extension and contraction. Although unraveling kinematic

histories is difficult in such settings, this has herein been achieved in the McCully area of the western Moncton Sub-basin. 3-dimensional seismic mapping of the Frederick Brook Member unveiled a set of curved conjugate extensional faults and lesser contractional faults. Using the model developed by Waldron (2005), apparent stretch (S^*) and shortening (S') measurements were combined with fault orientations relative to the shear zone boundary (θ') to make estimates of the angle of divergence (α) at the Frederick Brook Member level. The measurements herein of the S^* (average of 1.14) is an order of magnitude more than the S' (average of 0.986), illuminating the transtensional origin of the early Moncton Sub-basin. Furthermore, extension was manifested more on a seismic scale than a "sub-seismic" scale; an S^* measurement made on an outcrop of sedimentary rocks from the Hiram Brook Member is 1.022, compared to the average S^* of 1.14 measured on seismic data. Additional observations from the outcrop data suggest that deformation occurred soon after deposition. It is likely that majority of the faults within the late Horton developed before the inversion event resulting in the Sussex Unconformity; however, it is possible that some contractional faults may be related to this and later transpressional events. When considering the bulk strain, the Moncton Sub-basin likely deformed in a setting with a large α-angle (57° to 59°). However, away from the SZB, S^* gradually decreases and θ' gradually increases, together resulting in a decrease in α across the shear zone towards the SE. Additionally, comparing the estimates of α from a finite strain method (high α-values) to the estimates of α from an instantaneous strain method (low α-values) shows that the faults likely initiated in a strike-slip-dominated setting that transitioned to a more extension-dominated setting with time. The variability of the deformation in both space and time can explain the SW-directed concave curvature of the faults if it is assumed that the faults initiated in the SE and propagated towards the NW. These kinematic interpretations suggest that the early Moncton Sub-basin deformed in an oblique-extension tectonic environment (N – S directed extension), different from previous work that suggested major strike-slip movement. Although identifying the 3-dimensional geometries of faults and folds within sedimentary basins is crucial for resource exploration and exploitation, understanding the fault kinematics may be similarly important. Predictions such

as flow paths for hydrocarbons, connectedness of reservoirs across faults, and how fault-related depositional patterns changed through time, can only be made with a clear understanding of the fault kinematics. Research on comparable sub-basins within the Maritimes Basin and other strike slip basins elsewhere should take into account the transtensional complexities that have been highlighted here.

3.6. References

Allen, M.B., Macdonald, D.I., Xun, Z., Vincent, S.J., and Brouet-Menzies, C., 1998, Transtensional deformation in the evolution of the Bohai Basin, northern China: Geological Society, London, Special Publications, v. 135, p. 215–229.

Davydov, V.I., Korn, D., Schmitz, M.D., Gradstein, F.M., and Hammer, O., 2012, The Carboniferous Period, *in* Gradstein, F.M., Ogg, J.G., Schmidtz, M., and Ogg, G. eds., The Geologic Time Scale 2012, Elsevier, p. 603–651.

Dewey, J.F., Holdsworth, R.E., and Strachan, R.A., 1998, Transpression and transtension zones, *in* Dewey, J.F., Holdsworth, R.E., and Strachan, R.A. eds., Continental Transpressional and Transtensional Tectonics, Geological Society of London Special Publication 135, p. 1–14.

Durling, P., and Martel, A.T., 2003, The McCully gas field: A proven resource with high exploration potential: Geological Society of America Abstracts with programs, v. 35, p. 81.

Fossen, H., 2016, Structural Geology: Cambridge University Press, 510 p.

Fossen, H., and Tikoff, B., 1998, Extended models of transpression and transtension, and application to tectonic settings, *in* Holdsworth, R.E., Strachan, R.A., and Dewey, J.F. eds., Continental transpressional and transtensional tectonics, Geological Society of London Special Publication 135, p. 15–33.

Garfunkel, Z., and Ron, H., 1985, Block rotation and deformation by strike-slip faults: Journal of

Geophysical Research, v. 90, p. 8589–8602.

Gibling, M.R., Culshaw, N., Rygel, M.C., and Pascucci, V., 2009, The Maritimes Basin of Atlantic Canada: Basin Creation and Destruction in the Collisional Zone of Pangea, *in* Miall, A. ed., Sedimentary Basins of the World 5, p. 211–244.

Greiner, H.R., 1962, Facies and sedimentary environments of Albert shale, New Brunswick: The American Association of Petroleum Geologists Bulletin, v. 46, p. 219–234.

Harding, T.P., 1974, Petroleum traps associated with wrench faults: American Association of Petroleum Geologists Bulletin, v. 58, p. 1290–1304.

Hibbard, J., and Waldron, J.W.F., 2009, Truncation and translation of Appalachian promontories: Mid-Paleozoic strike-slip tectonics and basin initiation: Geology, v. 37, p. 497–490.

Hinds, S., 2008a, Geology of the Apohaqui area (NTS 21 H/12h), Kings County, New Brunswick: New Brunswick Department of Natural Resources: Minerals, Policy, and Planning Division.

Hinds, S., 2008b, Geology of the Cedar Camp area (NTS 21 H/11f), Kings County, New Brunswick: New Brunswick Department of Natural Resources: Minerals, Policy, and Planning Division.

Hinds, S., 2008c, Geology of the Crockets Corner area (NTS 21 H/14c), Kings County, New Brunswick: New Brunswick Department of Natural Resources: Minerals, Policy, and Planning Division.

Hinds, S., 2008d, Geology of the Jordan Mountain area (NTS 21 H/14d), Kings County, New Brunswick: New Brunswick Department of Natural Resources: Minerals, Policy, and Planning Division.

Hinds, S., 2008e, Geology of the Sussex Corner area (NTS 21 H/11e), Kings County, New Brunswick: New Brunswick Department of Natural Resources: Minerals, Policy, and Planning Division.

Hinds, S., and St. Peter, C.J., 2008, Geology of the Summerfield area (NTS 21 H/13a), Kings County, New Brunswick: New Brunswick Department of Natural Resources: Minerals, Policy, and Planning Division.

Howie, R.D., and Barss, M.S., 1975, Upper Paleozoic rocks of the Atlantic provinces, Gulf of St. Lawrence, and adjacent continental shelf, *in* Van Der Linden, W.J.M. and Wade, J.A. eds., Offshore geology of eastern Canada, Volume 2 - Regional Geology, Geological Survey of Canada, Paper, v. 74–30, p. 35–50.

Keighley, D., 2008, A lacustrine shoreface succession in the Albert Formation, Moncton Basin, New Brunswick: Bulletin of Canadian Petroleum Geology, v. 56, p. 235–258.

Roliff, W.A., 1962, The Maritimes Carboniferous Basin of Eastern Canada: Geological Association of Canadian Proceedings, v. 14, p. 21–44.

St. Peter, C.J., 1993, Maritimes Basin evolution: key geologic and seismic evidence from the Moncton Subbasin of New Brunswick: Atlantic Geology, v. 29, p. 233–270.

St. Peter, C.J., and Johnson, S.C., 2009, Stratigraphy and structural history of the late Paleozoic Maritimes Basin in southeastern New Brunswick, Canada: New Brunswick Department of Natural Resources, Memoir, v. 3, 348 p.

Sylvester, A.G., 1988, Strike-slip faults: Geological Society of America Bulletin, v. 100, p. 1666–1703.

Tikoff, B., and Fossen, H., 1993, Simultaneous pure and simple shear: the unifying deformation matrix: Tectonophysics, v. 217, p. 267–283.

Waldron, J.W.F., 2005, Extensional fault arrays in strike-slip and transtension: Journal of Structural Geology, v. 27, p. 23–34.

Waldron, J.W.F., Barr, S.M., Park, A.F., White, C.E., and Hibbard, J.P., 2015, Late Paleozoic

strike-slip faults in Maritime Canada and their role in the reconfiguration of the northern Appalachian orogen: Tectonics, v. 34, p. 1661–1684, doi: 10.1002/2015TC003882.

Waldron, J.W.F., Rygel, M.C., Gibling, M.R., and Calder, J.H., 2013, Evaporite tectonics and the late Paleozoic stratigraphic development of the Cumberland basin, Appalachians of Atlantic Canada: Geological Society of America Bulletin, v. 125, p. 945–960.

Wilcox, R.E., Harding, T.P., and Seely, D.R., 1973, Basic wrench tectonics: 1PG Bulletin, v. 57, p. 74–96.

Williams, E.P., 1974, Geology and petroleum possibilities in and around Gulf of St. Lawrence: AAPG Bulletin, v. 58, p. 1137–1155.

Wilson, P., 2005, Stratigraphy, structural geology, and tectonic history of the McCully area, Moncton Subbasin, southeastern New Brunswick: New Brunswick Department of Natural Resources; Minerals, Policy and Planning Division, v. Mineral Resource Report 2005-5, p. 104.

Wilson, P., and White, J.C., 2006, Tectonic evolution of the Moncton Basin, New Brunswick, Eastern Canada; new evidence from field and sub-surface data: Bulletin of Canadian Petroleum Geology, v. 54, p. 319–336, doi: 10.2113/gscpgbull.54.4.319.

Wilson, P., White, J.C., and Roulston, B.V., 2006, Structural geology of the Penobsquis salt structure: late Bashkirian inversion tectonics in the Moncton Basin, New Brunswick, eastern Canada: Canadian Journal of Earth Sciences, v. 43, p. 405–419, doi: 10.1139/e05-116.

Chapter 4: Conclusion and recommendations

The transtensional Moncton Sub-basin, in southern New Brunswick, contains complex structural geometries on both seismic and outcrop scales. This sub-basin is a part of the Maritimes Basin, which covers majority of the Maritime Provinces in Canada. The upper Albert Formation of the Late Devonian to Early Mississippian (Tournaisian) Horton Group was studied in both the sub-surface and at surface in the Sussex area of southern New Brunswick.

Sedimentary basins that developed in transtensional settings contain complex extensional and contractional features making interpretation of kinematic histories difficult. In addition to the intricate relationship between typical extensional (e.g. normal faults) and contractional features (e.g. reverse faults, folds), the rotation of structures through progressive deformation makes it difficult to use observations of present-day orientations and offsets to explain the basin kinematics.

An advanced method of mapping that incorporates both detailed outcrop logging and 3D geometric outcrop modelling was used on four roadcuts located along Highway 1, ~3 km SW of the City of Sussex, New Brunswick (Figure 4.1). Observations including sandstone dykes that follow fault planes, convolute laminae confined to single beds, and an unconformity surface that truncates fault planes imply that deformation occurred early in the basin history. The relative orientations of the observed extensional faults, contractional faults, and fold axes suggest that the sedimentary rocks of the Albert Formation experienced dextral strike slip deformation which resulted in major clockwise rotation of the structures. It is estimated that the extensional faults initiated with WNW – ESE strikes but rotated upwards of 60°.

Industry-generated 2- and 3-dimensional seismic reflection data accompanied by wellbore information were used to map the Frederick Brook shale horizon at the McCully gas field. Here, the Frederick Brook member is folded and offset by numerous faults (Figure 4.2). Apparent stretch (S^*) and shortening (S') measurements were combined with fault orientations relative to

the shear zone boundary (θ') to make estimates of the angle of divergence (α) and the amount of fault rotation. The bulk strain at McCully indicates that the extension direction for the early Moncton Sub-basin was very close to N – S (Figure 4.3), different from directions suggested in previous work that estimated NE – SW extension. Variations in S^* and θ' across the shear zone have implications for the origin of the SW-directed concave curvature of the faults. This curvature likely formed due to a combination of rotation and asynchronous fault propagation, variable strain magnitude and direction across the shear zone, and variable deformation through time. The variability in the estimated kinematic parameters in Chapter 3 implies that the sub-basin deformed heterogeneously in space, due to estimates of decreasing α and increasing fault rotation to the SE, and time, due to differences in estimates of α using finite strain (high α) and instantaneous strain (low α); a result that questions how uniform the deformation between sub-basins within the greater Maritimes Basin actually was, let alone within a single basin.

Recommended future work includes:

1) Microscopic-scale investigation into the deformation at the roadcuts.

2) Broadening the kinematic analysis of the roadcuts to include transtensional possibilities.

3) A tectonic wedge is present in the McCully area. Investigating the composition and timing of emplacement of this wedge, combined with observations from the SE portion of the Moncton Sub-basin, will lead to a better understanding of how the basin developed through time.

4) Mapping of the Windsor stratigraphy can be done at McCully to better understand how halokinesis might be linked to the tectonic wedge emplacement and how salt movement may have created subsidence for the deposition of the Cumberland and Pictou groups.

5) Apply the kinematic model developed for the subsurface data to studies of

reservoir compartmentalization, timing of faulting and trap formation, burial history, lateral extension and integrity or breaching of seals.

A strong understanding of the tectonic environment in which a basin was formed and deformed is critical to successful resource exploration. Linking the sedimentology with a kinematic deformation model can strengthen depositional models and improve the recognition of facies patterns of reservoir rocks. Furthermore, identifying the geometry of faults in 3-dimensions can help determine flow paths for hydrocarbons and the connectedness of reservoirs across faults at present day. Also, understanding the kinematics of the basin can help make predictions about how these factors changed through time, because it is expected that fault tip locations and orientations of the faults change with progressive deformation.

Figure 4.1. Geologic map of four roadcuts along Highway 1, roughly 3 km SW of the City of Sussex, New Brunswick.

See pocket.

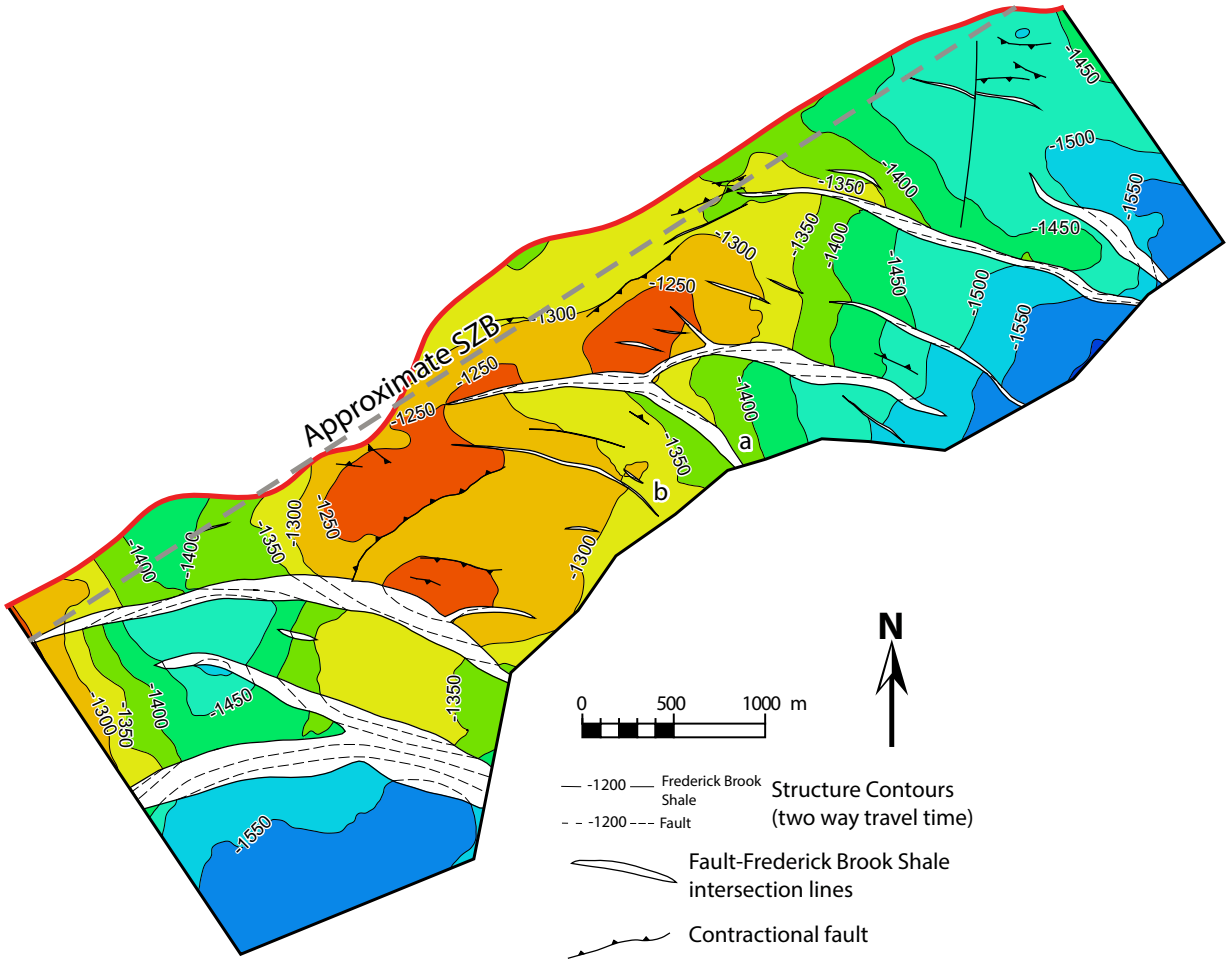

Figure 4.2. Subsurface time structure contour map of the Fredrick Brook shale horizon.

Structure contours are displayed in two-way travel time and have an interval of 50ms.

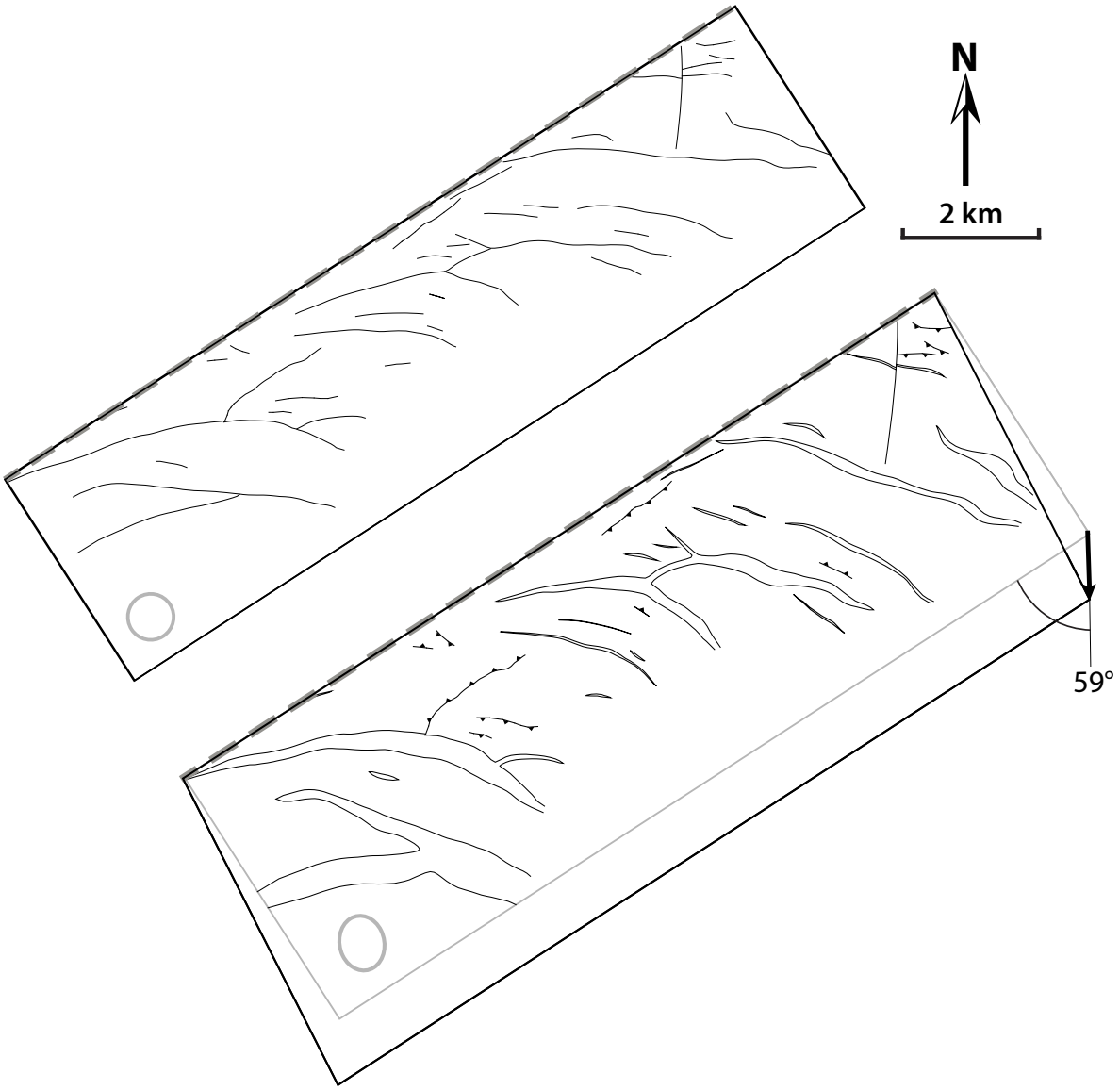

Figure 4.3. Reconstruction of the Frederick Brook shale-fault intersection lines.

(a) Schematic retro-deformed map of the Frederick Brook shale. (b) Present-day Frederick Brook shale-fault intersection lines. The ellipse displays the required strain needed to produce the present-day geometry of the faults. The arrow indicates the divergence of 59° from the shear zone boundary (grey dashed line).

Bibliography

Allen, M.B., Macdonald, D.I., Xun, Z., Vincent, S.J., Brouet-Menzies, C., 1998. Transtensional deformation in the evolution of the Bohai Basin, northern China. Geological Society, London, Special Publications 135, 215–229.

Alsop, G.I., Marco, S., 2011. Soft-sediment deformation within seismogenic slumps of the Dead Sea Basin. Journal of Structural Geology 33, 433–457.

Aydin, A., Nur, A., 1985. The types and role of stepovers in strike-slip tectonics. In: Biddle, K.T., Christie-Blick, N. (Eds.), Strike-Slip Deformation, Basin Formation, and Sedimentation, Society of Economic Paleontologists and Mineralogists Special Publication. 35–44.

Aydin, A., Nur, A., 1982. Evolution of pull-apart basins and their scale independence. Tectonics 1, 91–105.

Barr, S.M., White, C.E., 1999. Field relations, petrology and structure of Neoproterozoic rocks in the Caledonia Highlands, southern New Brunswick. Geologic Survey of Canada Natural Resources Canada.

Belt, E.S., 1968. Post-Acadian rifts and related facies, eastern Canada. In: Zen, E., White, W.S., Hadley, J.. (Eds.), Studies of Appalachian Geology, Northern and Maritime. Wiley Interscience, New York, 95–113.

Bradley, D.C., 1982. Subsidence in late Paleozoic basins in the northern Appalachians. Tectonics 1, 107–123.

Carter, D.C., Pickerill, R.K., 1985. Lithostratigraphy of the Late Devonian–Early Carboniferous Horton Group of the Moncton Subbasin, southern New Brunswick. Maritime Sediments and Atlantic Geology 21, 11–24.

Claerbout, J.F., 1985. Imaging the Earth's Interior. Blackwell Sci. Publ., London.

Davydov, V.I., Korn, D., Schmitz, M.D., Gradstein, F.M., Hammer, O., 2012. The Carboniferous Period. In: Gradstein, F.M., Ogg, J.G., Schmidtz, M., Ogg, G. (Eds.), The Geologic Time Scale 2012. Elsevier, 603–651.

Dewey, J.F., Holdsworth, R.E., Strachan, R.A., 1998. Transpression and transtension zones. In: Dewey, J.F., Holdsworth, R.E., Strachan, R.A. (Eds.), Continental Transpressional and Transtensional Tectonics, Geological Society of London Special Publication. 1–14.

Durling, P., Martel, A.T., 2003. The McCully gas field: A proven resource with high exploration potential. Geological Society of America Abstracts with Programs 35, 81.

Fossen, H., 2016. Structural Geology, 2nd ed. Cambridge University Press.

Fossen, H., Tikoff, B., 1998. Extended models of transpression and transtension, and application to tectonic settings. In: Holdsworth, R.E., Strachan, R.A., Dewey, J.F. (Eds.), Continental

Transpressional and Transtensional Tectonics, Geological Society of London Special Publication. 15–33.

Fossen, H., Tikoff, B., Teyssier, C.T., 1994. Strain modelling of transpressional and transtensional deformation. Norsk Geologisk Tidsskrift 74, 134–145.

Fyffe, L.R., Johnson, S.C., van Staal, C.R., 2011. A review of Proterozoic to Early Paleozoic lithotectonic terranes in the northeastern Appalachian orogen of New Brunswick, Canada, and their tectonic evolution during Penobscot, Taconic, Salinic, and Acadian orogenesis. Atlantic Geology 47, 211–248.

Garfunkel, Z., Ron, H., 1985. Block rotation and deformation by strike-slip faults. Journal of Geophysical Research 90, 8589–8602.

Gibling, M.R., Calder, J.H., Ryan, R., Van de Poll, H.W., Yeo, G.M., 1992. Late Carboniferous and early Permian drainage patterns in Atlantic Canada. Canadian Journal of Earth Sciences 29, 338–352.

Gibling, M.R., Culshaw, N., Rygel, M.C., Pascucci, V., 2009. The Maritimes Basin of Atlantic Canada: Basin Creation and Destruction in the Collisional Zone of Pangea. In: Miall, A. (Ed.), Sedimentary Basins of the World. 211–244.

Giles, P.S., 1981. Major Transgressive-Regressive Cycles in Middle to Late Visean Rocks of Nova Scotia, Nova Scotia Department of Mines and Energy Branch, Paper.

Greiner, H.R., 1962. Facies and sedimentary environments of Albert shale, New Brunswick. The American Association of Petroleum Geologists Bulletin 46, 219–234.

Gussow, W.C., 1953. Carboniferous stratigraphy and structural geology of New Brunswick, Canada. The American Association of Petroleum Geologists Bulletin 37, 1713–1816.

Harding, T.P., 1974. Petroleum traps associated with wrench faults. American Association of Petroleum Geologists Bulletin 58, 1290–1304.

Hibbard, J., Waldron, J.W.F., 2009. Truncation and translation of Appalachian promontories: Mid-Paleozoic strike-slip tectonics and basin initiation. Geology 37, 497–490.

Hibbard, J., Waldron, J.W.F., 2009. Truncation and translation of Appalachian Promontories: Mid-Paleozoic strike-slip tectonics and basin initiation. Geology 37, 487–490. https://doi.org/10.1130/G25614A.1

Hinds, S., 2008a. Geology of the Apohaqui area (NTS 21 H/12h), Kings County, New Brunswick., New Brunswick Department of Natural Resources: Minerals, Policy, and Planning Division, Plate 2008-10 (revised 2009). ed.

Hinds, S., 2008b. Geology of the Cedar Camp area (NTS 21 H/11f), Kings County, New Brunswick., New Brunswick Department of Natural Resources: Minerals, Policy, and

Planning Division, Plate 2008-08 (revised 2009). ed.

Hinds, S., 2008c. Geology of the Crockets Corner area (NTS 21 H/14c), Kings County, New Brunswick., New Brunswick Department of Natural Resources: Minerals, Policy, and Planning Division, Plate 2008-12 (revised (2009). ed.

Hinds, S., 2008d. Geology of the Jordan Mountain area (NTS 21 H/14d), Kings County, New Brunswick., New Brunswick Department of Natural Resources: Minerals, Policy, and Planning Division, Plate 2008-13 (revised 2009). ed.

Hinds, S., 2008e. Geology of the Sussex Corner area (NTS 21 H/11e), Kings County, New Brunswick., New Brunswick Department of Natural Resources: Minerals, Policy, and Planning Division, Plate 2008-7 (revised 2009). ed.

Hinds, S., St. Peter, C.J., 2008. Geology of the Summerfield area (NTS 21 H/13a), Kings County, New Brunswick., New Brunswick Department of Natural Resources: Minerals, Policy, and Planning Division, Plate 2008-11 (revised 2009). ed.

Hinds, S.J., Park, A.F., 2009. Structural and stratigraphic relationships between the Horton and Sussex groups (Tournaisian: Lower Carboniferous) around Elgin, southern New Brunswick 2009. In: Merlini, S.A.A. (Ed.), Exploration, Mining and Petroleum New Brunswick, Abstracts. 13–14.

Hinds, S., St. Peter, C., 2005. The McCully gas field project. New Brunswick Department of Natural Resources: Geological surveys division.

Howie, R.D., Barss, M.S., 1975. Upper Paleozoic rocks of the Atlantic provinces, Gulf of St. Lawrence, and adjacent continental shelf. In: Van Der Linden, W.J.M., Wade, J.A. (Eds.), Offshore Geology of Eastern Canada, Volume 2 - Regional Geology, Geological Survey of Canada, Paper. 35–50.

James, M.R., Robson, S., 2014. Straightforward reconstruction of 3D surfaces and topography with a camera: accuracy and geoscience application. Journal of Geophysical Research, Earth Surface 117, 1–17.

Jolly, R.J.H., Lonergan, L., 2002. Mechanisms and controls on the formation of sand intrusions. Journal of the Geological Society, London 159, 605–617.

Keighley, D., 2008. A lacustrine shoreface succession in the Albert Formation, Moncton Basin, New Brunswick. Bulletin of Canadian Petroleum Geology 56, 235–258.

McCutcheon, S.R., 1981. Stratigraphy and paleogeography of the Windsor Group in southern New Brunswick. New Brunswick Department of Natural Resources; Mineral Resources Branch Open File Report 81-31, 210.

McCutcheon, S.R., Robinson, P.T., 1987. Geological constraints on the genesis of the Maritimes Basin, Atlantic Canada. In: Beaumont, C., Tankard, A.J. (Eds.), Sedimentary Basins and

Basin-Forming Mechanism, Canadian Society of Petroleum Geologists, Memoir. 287–297.

Murphy, J.B., Waldron, J.W.F., Kontak, D., Pe-Piper, G., Piper, D.J.W., 2011. Minas Fault Zone: Late Paleozoic history of an intra-continental orogenic transform fault in the Canadian Appalachians. Journal of Structural Geology 33, 312–328.

Nilsen, T.H., Sylvester, A.G., 1995. Strike-slip basins. Tectonics of Sedimentary Basins 425–457.

Oldenburg, D.W., Scheuer, T., Levy, S., 1983. Recovery of acoustic impedance from reflection seismology. Geophysics 48, 1318–1337.

Park, A.F., St. Peter, C.J., 2009. Stratigraphy and structure of the Indian Mountain Deformed Zone, Maritimes Basin, Westmorland County, Southeastern New Brunswick, New Brunswick Department of Natural Resources; Minerals, Policy and Planning Division, Mineral Resources Report.

Park, A.F., St. Peter, C.J., 2005. Deformation of Lower Carboniferous rocks in the Rosevale to Saint-Joseph area, Albert and Westmorland counties, southeastern New Brunswick. In: Martin, G.L. (Ed.), Geological Investigations in New Brunswick for 2004, New Brunswick Department of Natural Resources; Minerals, Policy and Planning Division, Mineral Resources Report. 45–98.

Park, A.F., St. Peter, C.J., Keighley, D., Wilson, P., 2010. Overstep and imbrication along a side-wall ramp and its relationship to a hydrocarbon play in Tournaisian rocks of the Moncton Basin: the Peck Creek section, Albert Mines area, southeastern New Brunswick. Bulletin of Canadian Petroleum Geology 58, 268–282.

Park, A.F., St. Peter, C.J., Keighley, D.G., 2007. Structural styles in Late Devonian – early Carboniferous rocks along the southern margin of the Moncton Subbasin: Caledonia Mountain to Elgin, southeastern New Brunswick. In: Martin, G.L. (Ed.), Geological Investigations in New Brunswick for 2006, New Brunswick Department of Natural Resources, Mineral Resources Report. 87–125.

Ramsay, J.G., Huber, M.I., 1983. The Techniques of Modern Structural Geology. Volume 1: Strain Analysis. Academic Press, London.

Roliff, W.A., 1962. The Maritimes Carboniferous Basin of Eastern Canada. Geological Association of Canadian Proceedings 14, 21–44.

Sanderson, D.J., Marchini, W.R.D., 1984. Transpression. Journal of Structural Geology 6, 449–458.

Schenk, P.E., 1969. Carbonate-sulfate-redbed facies and cyclic sedimentation of the Windsorian Stage (middle Carboniferous), Maritime Provinces. Canadian Journal of Earth Sciences 6, 1037–1066.

St. Peter, C.J., 2006. Geological relationship between the Cocagne Subbasin and the Indian Mountain deformed zone, Maritimes basin, New Brunswick. In: Martin, G.L. (Ed.), Geological Investigations in New Brunswick for 2005, New Brunswick Department of Natural Resources, Mineral Resources Report. 103–183.

St. Peter, C.J., 2002. Bedrock geology of the McCully natural gas field area, Moncton Subbasin (parts of 21 H/11, 12, 13 and 14), New Brunswick., New Brunswick Department of Natural Resources and Energy; Minerals and Energy Division, Plate 2002-33 (revised 2004). ed.

St. Peter, C.J., 2001. Petroleum geology in the Carboniferous of southeastern New Brunswick. In: Guidebook to Field Trips in New Brunswick and western Maine, R.K. Pickerill and D.R. Lentz (editors). New England Intercollegiate Geological Conference, 93rd Annual Meeting.

St. Peter, C.J., 1993. Maritimes Basin evolution: key geologic and seismic evidence from the Moncton Subbasin of New Brunswick. Atlantic Geology 29, 233–270.

St. Peter, C.J., Johnson, S.C., 2009. Stratigraphy and structural history of the late Paleozoic Maritimes Basin in southeastern New Brunswick, Canada, New Brunswick Department of Natural Resources, Memoir.

Sylvester, A.G., 1988. Strike-slip faults. Geological Society of America Bulletin 100, 1666–1703.

Tikoff, B., Fossen, H., 1993. Simultaneous pure and simple shear: the unifying deformation matrix. Tectonophysics 217, 267–283.

Tikoff, B., Teyssier, C., 1994. Strain modeling of displacement-field partitioning in transpressional orogens. Journal of Structural Geology 16, 1575–1588.

Utting, J., Giles, P.S., 2004. Biostratigraphical implications of new palynological data from the Mississippian of Newfoundland and Nova Scotia, Canada. Memoirs of the Association of Australasian Palaeontologists. 115–160.

Vestrum, R., Gittins, J., 2009. Technologies from foothills seismic imaging: replacements or complements? First Break 27, 61–66.

Waldron, J.W.F., 2005. Extensional fault arrays in strike-slip and transtension. Journal of Structural Geology 27, 23–34.

Waldron, J.W.F., Barr, S.M., Park, A.F., White, C.E., Hibbard, J.P., 2015. Late Paleozoic strike-slip faults in Maritime Canada and their role in the reconfiguration of the northern Appalachian orogen. Tectonics 34, 1661–1684. https://doi.org/10.1002/2015TC003882

Waldron, J.W.F., Rygel, M.C., 2005. Role of evaporite withdrawal in the preservation of a unique coal-bearing succession: Pennsylvanian Joggins Formation, Nova Scotia. Geology 33,

337–340.

Waldron, J.W.F., Rygel, M.C., Gibling, M.R., Calder, J.H., 2013. Evaporite tectonics and the late Paleozoic stratigraphic development of the Cumberland basin, Appalachians of Atlantic Canada. Geological Society of America Bulletin 125, 945–960.

Wilcox, R.E., Harding, T.P., Seely, D.R., 1973. Basic wrench tectonics. AAPG Bulletin 57, 74–96.

Williams, E.P., 1974. Geology and petroleum possibilities in and around Gulf of St. Lawrence. AAPG Bulletin 58, 1137–1155.

Wilson, P., 2005. Stratigraphy, structural geology, and tectonic history of the McCully area, Moncton Subbasin, southeastern New Brunswick. New Brunswick Department of Natural Resources; Minerals, Policy and Planning Division Mineral Resource Report 2005-5, 104.

Wilson, P., White, J.C., 2006. Tectonic evolution of the Moncton Basin, New Brunswick, Eastern Canada; new evidence from field and sub-surface data. Bulletin of Canadian Petroleum Geology 54, 319–336. https://doi.org/10.2113/gscpgbull.54.4.319

Wilson, P., White, J.C., Roulston, B.V., 2006. Structural geology of the Penobsquis salt structure: late Bashkirian inversion tectonics in the Moncton Basin, New Brunswick, eastern Canada. Canadian Journal of Earth Sciences 43, 405–419. https://doi.org/10.1139/e05-116

Yilmaz, O., 2001. Seismic Data Analysis, Investigations in Geophysics. Society of Exploration Geophysicists.

Appendix A: Orthophotographs and interpretations of road outcrops along Highway 1

(a) Northern road outcrop. (b) North face of highway median. (c) South face of highway median.

(d) Southern road outcrop.

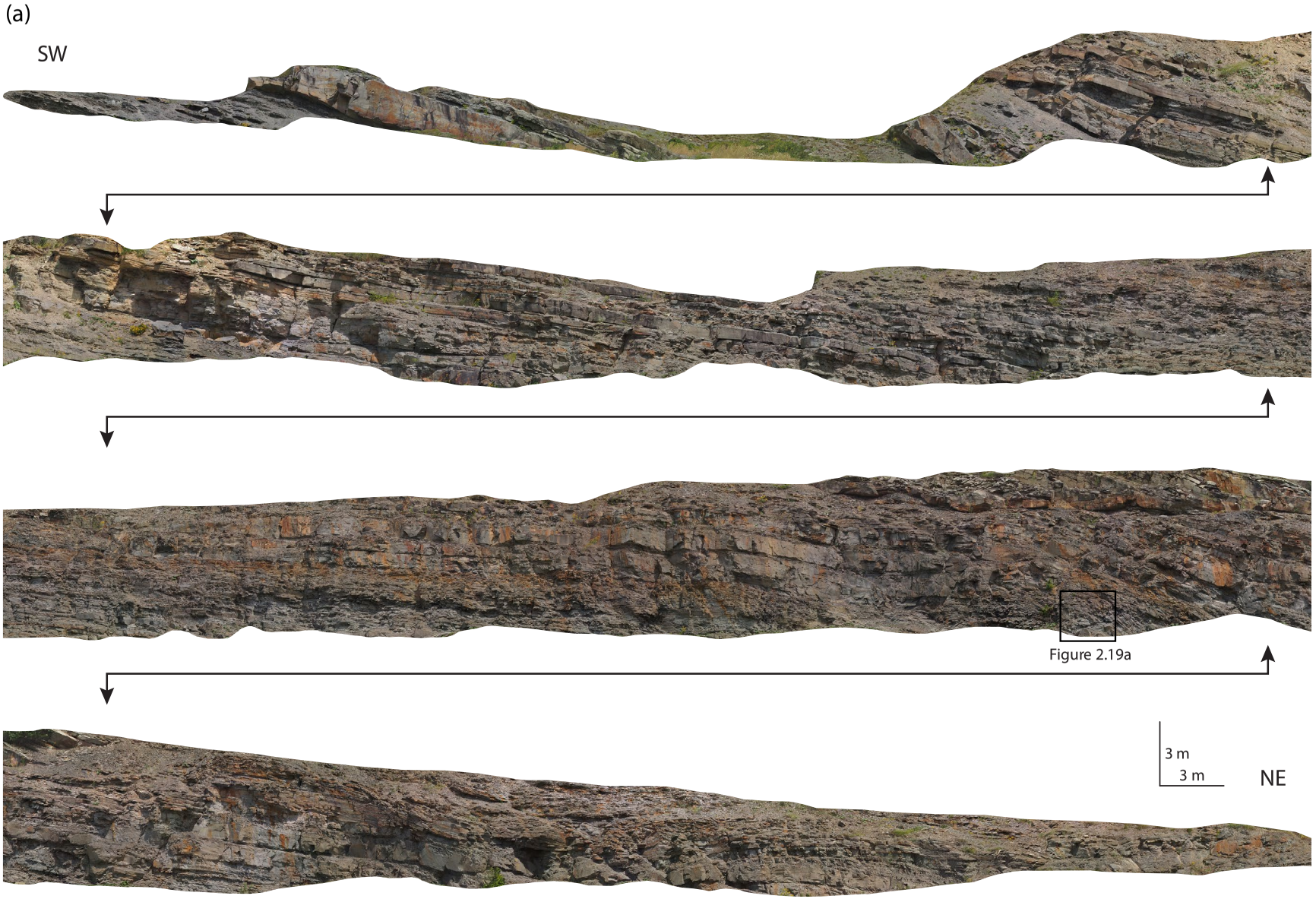
(a)
SW
Figure 2.19a
3 m
3 m
NE

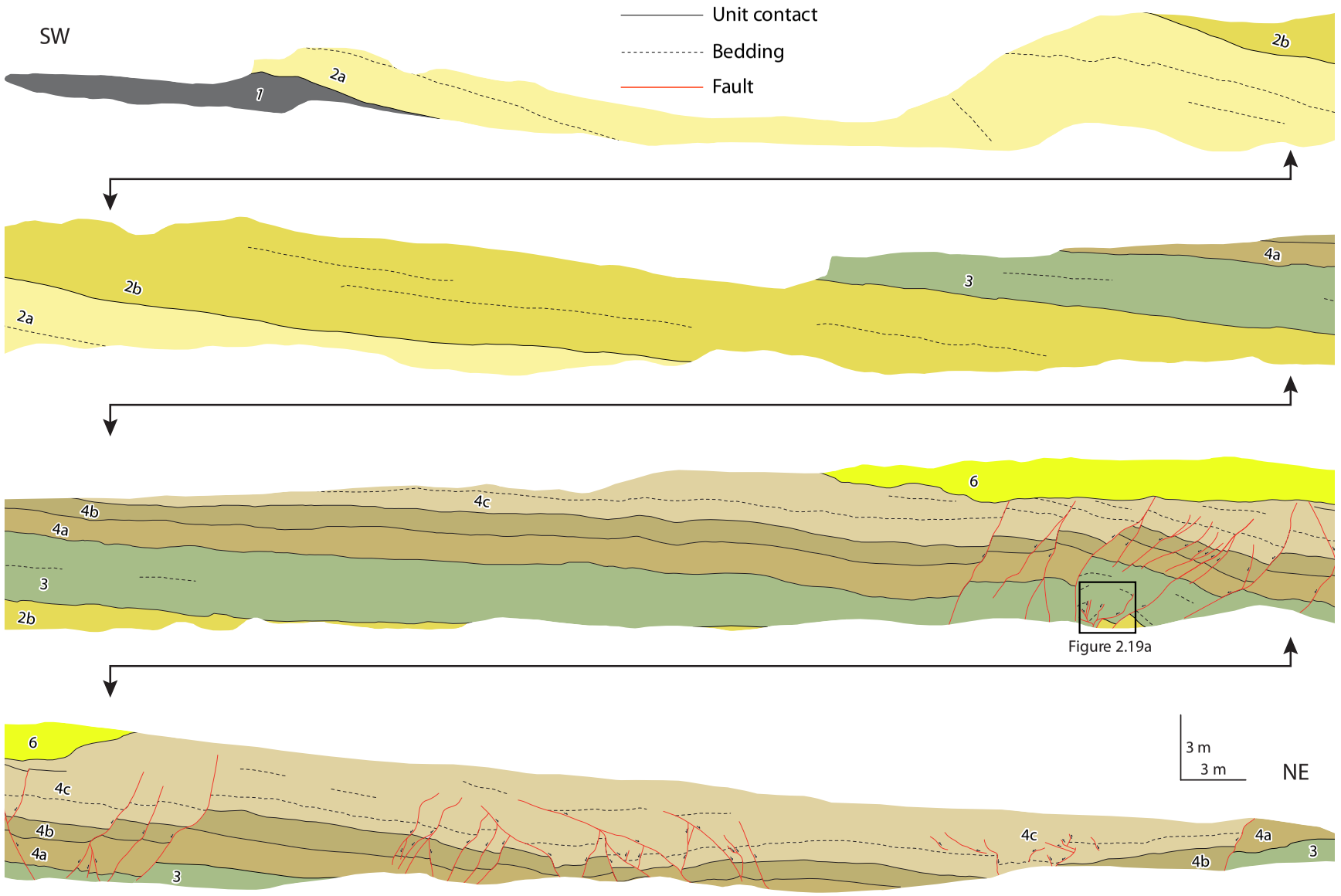
SW
Unit contact
Bedding
Fault
1
2a
2b
3
4a
4b
4c
6
Figure 2.19a
3 m
3 m
NE

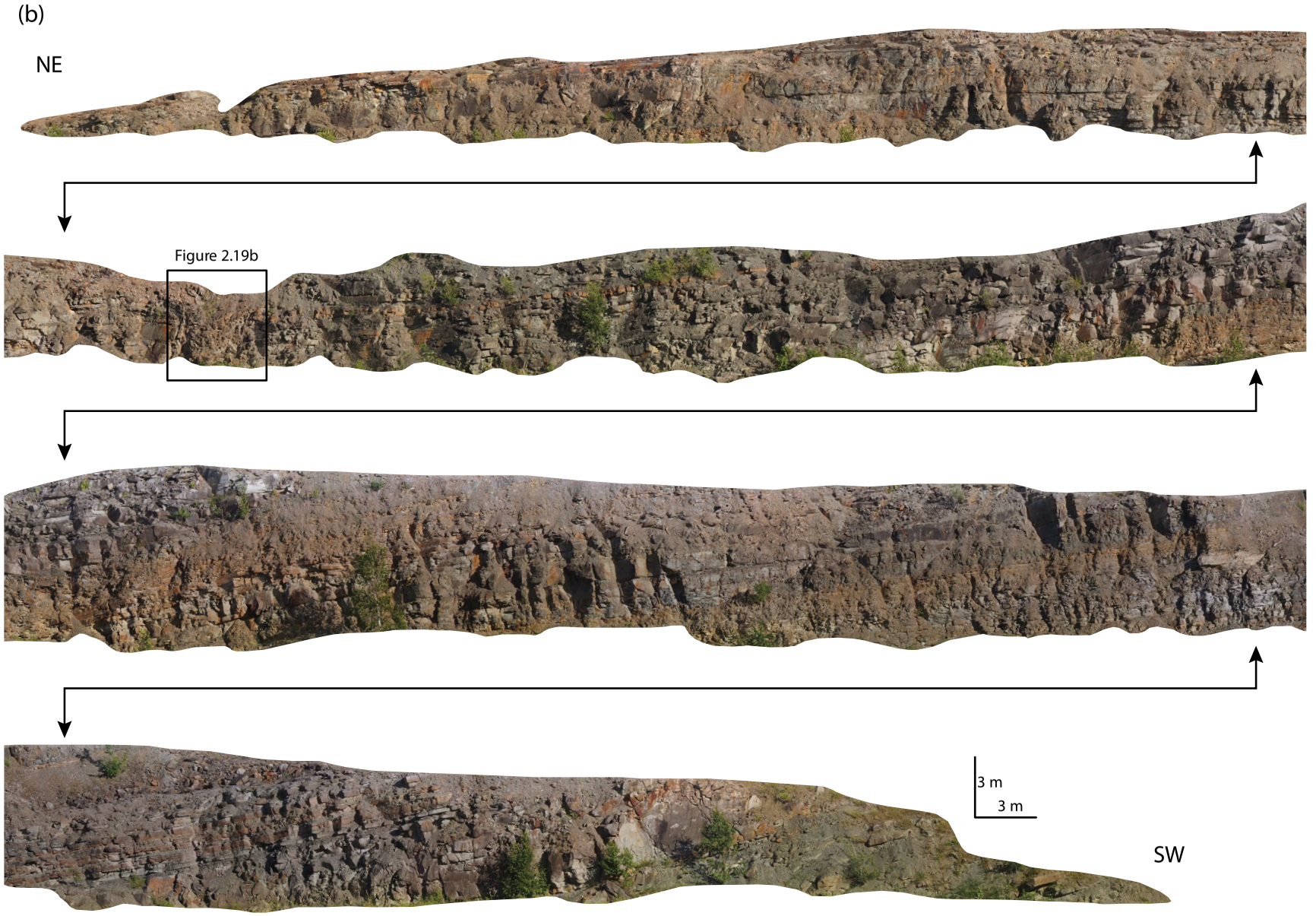
(b)
NE
Figure 2.19b
3 m
3 m
SW

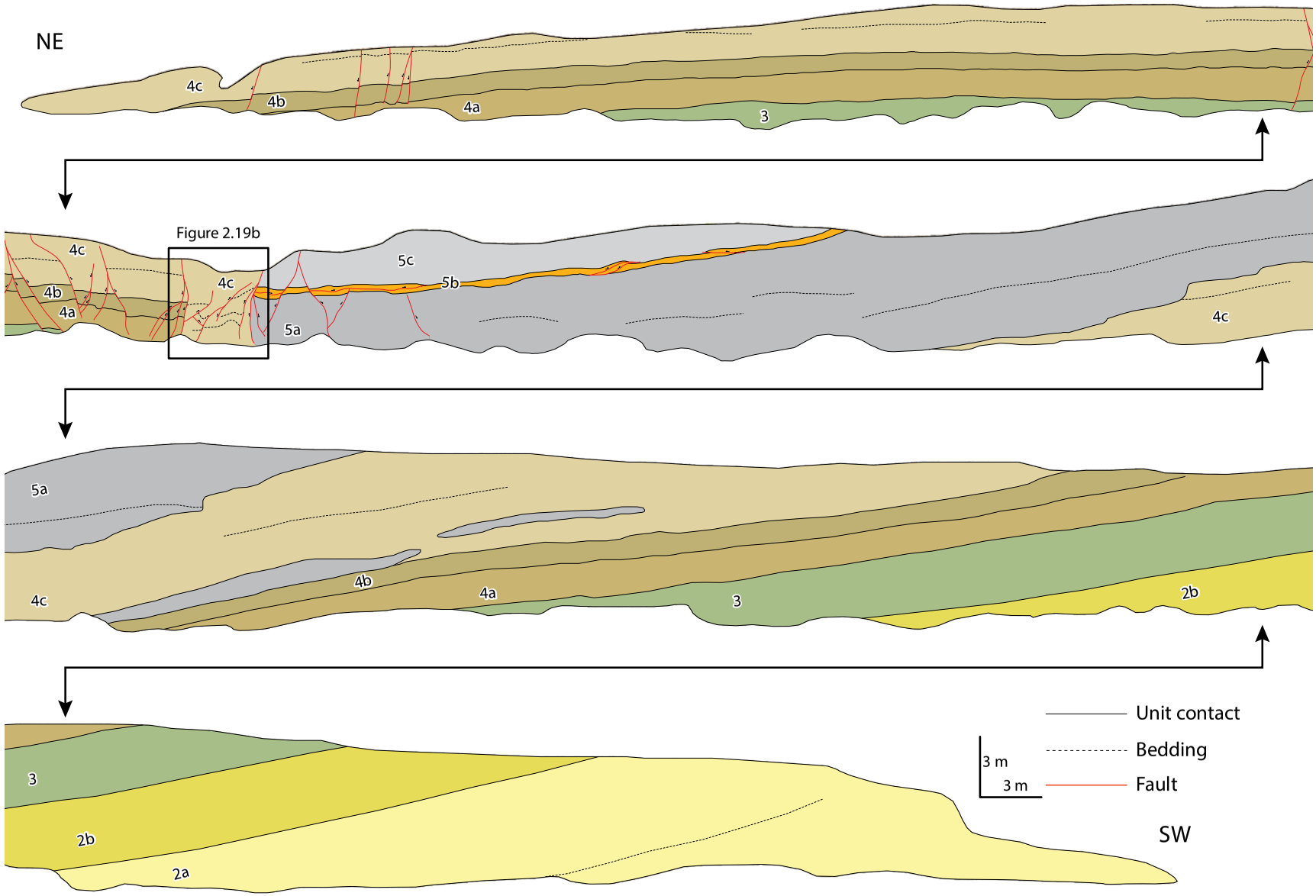
NE
4c
4b
4a
3
Figure 2.19b
4c
4b
4a
4c
5c
5b
5a
4c
5a
4c
4b
4a
3
2b
3
2b
2a
Unit contact
Bedding
Fault
3 m
3 m
SW


(c)
SW
Figure 2.19c
3 m
3 m
NE

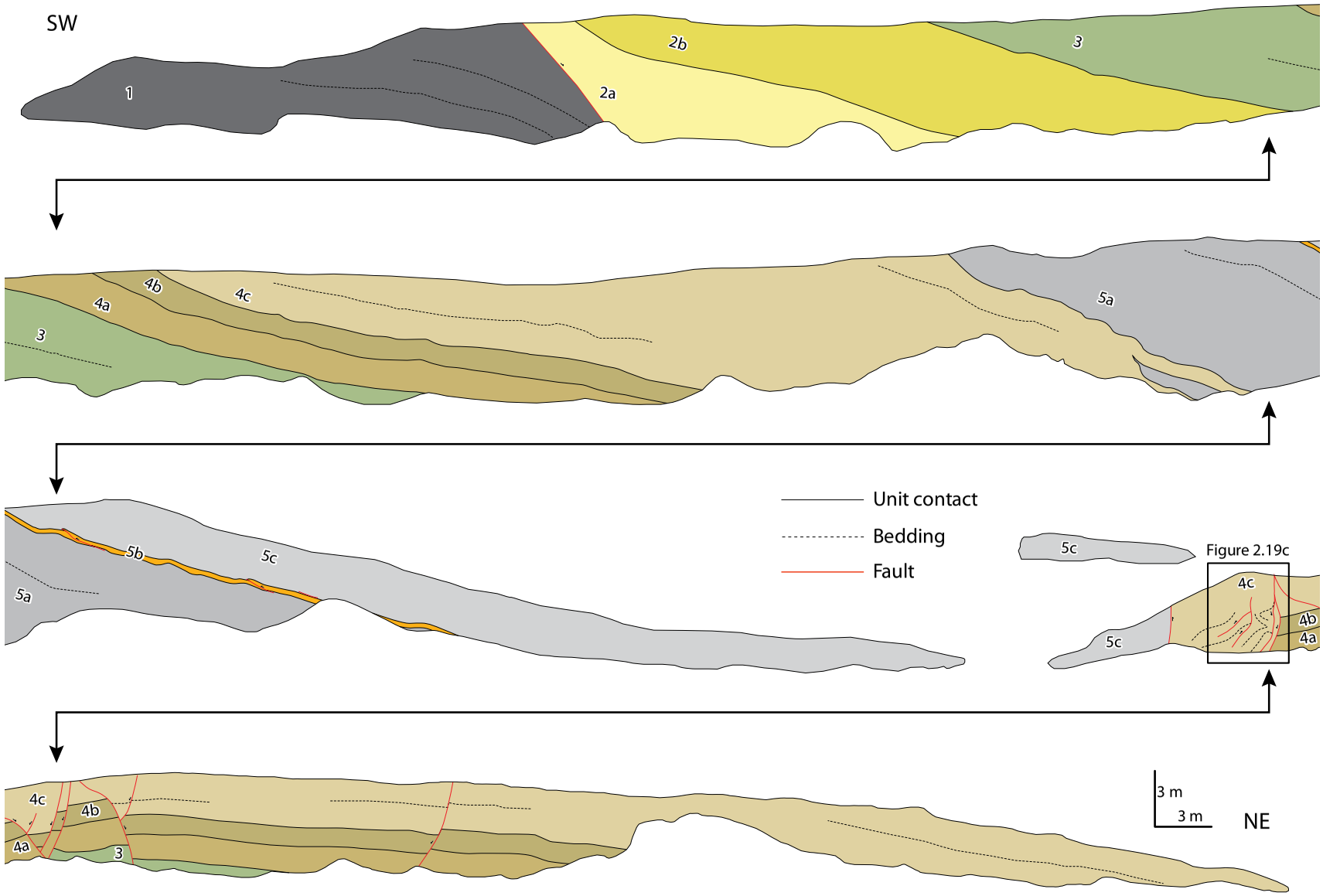
SW
1
2a
2b
3
4a
4b
4c
5a
5b
5c
Unit contact
Bedding
Fault
Figure 2.19c
3 m
3 m
NE


(d)
NE
3 m
3 m
SW

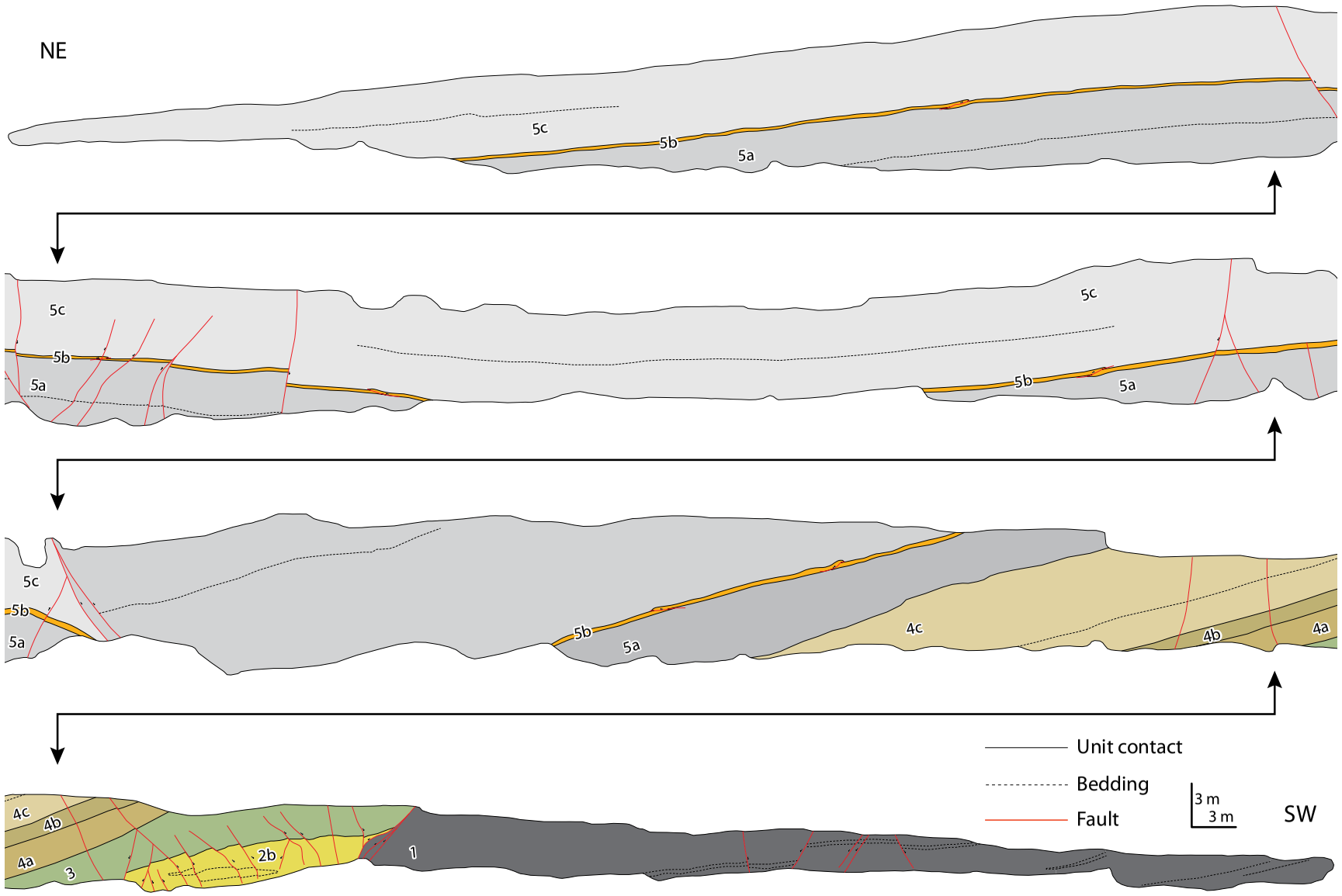
NE
5c
5b
5a
5c
5b
5a
5c
5b
5a
5c
5b
5a
4c
4b
4a
5c
5b
5a
4c
4b
4a
3
2b
1
Unit contact
Bedding
Fault
3 m
3 m
SW